SCREENING OF SYNTHESIZED NANOPARTICLE AND ANTINEOPLASTICS CYTOTOXICITY AGAINST DRUG-RESISTANT BREAST CANCER CELLS

JASON DARMADI

DISSERTATION SUBMITTED IN FULFILMENT OF THE REQUIREMENTS FOR THE DEGREE OF MASTER OF SCIENCE IN LIFE SCIENCE

SCHOOL MEDICAL AND LIFE SCIENCES

SUNWAY UNIVERSITY

MALAYSIA

2024

ORIGINAL LITERARY WORK DECLARATION

Name of Candidate : Jason Darmadi

Student ID : 20055638

Name of Degree : M.Sc. in Life Science

Title of Project Paper/Research Report/Dissertation/Thesis ("this Work"):

Screening of Synthesized Nanoparticle and Antineoplastics Cytotoxicity against Drug-Resistant Breast Cancer Cells

I do solemnly and sincerely declare that:

1. I am the sole author/writer of this Work;

2. This Work is original;

3. Any use of any work in which copyright exists was done by way of fair dealing and for permitted purposes and any excerpt or extract from, or reference to or reproduction of any copyright work has been disclosed expressly and sufficiently and the title of the Work and its authorship have been acknowledged in this Work;

4. I do not have any actual knowledge nor do I ought reasonably to know that the making of this work constitutes an infringement of any copyright work;

5. I hereby assign all and every right in the copyright to this Work to the Sunway University (SunU), who henceforth shall be owner of the copyright in this Work and that any reproduction or use in any form or by any means whatsoever is prohibited without the written consent of Sunway University having been first had and obtained;

6. I am fully aware that if in the course of making this Work I have infringed any copyright whether intentionally or otherwise, I may be subject to legal action or any other action as may be determined by Sunway University.

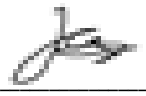

Candidate's Signature Date: 27.05.2024

Subscribed and solemnly declared before,

Witness's Signature Date: 28/05/2024

Name : Ayaz Anwar
Designation : Associate Professor / Main Supervisor

**Witness will be the supervisor*

(This form to be attached together with the final hardbound thesis)

SCREENING OF SYNTHESIZED NANOPARTICLE AND ANTINEOPLASTICS CYTOTOXICITY AGAINST DRUG-RESISTANT BREAST CANCER CELLS

ABSTRACT

Breast cancer is regarded as a major global health issue due to its high incidence and mortality rate. They are also becoming harder to treat due to the emergence of multi-drug resistance (MDR), rendering anticancer drugs less sensitive than ever. Therapeutic nanoparticles and novel bio-derived drugs can be used as a potential replacement for chemo-drug-resistant breast cancer. This study was performed to investigate resistance of breast cancer cells against a multitude of drugs as well as to evaluate whether certain nanoparticles could induce cytotoxicity. Four antineoplastic agents Cisplatin (CDDP), Paclitaxel (PTX), Alpha-Mangostin (A-MG), and Andrographolide (Andr-G), as well as three nanoparticles synthesized gold nanoparticles (AuNPs), synthesized silver nanoparticles (AgNPs), and graphene oxide (GO) were investigated for cytotoxicity against non-chemo-resistant breast cancer MCF-7, chemo-resistant MCF-7-CR, and MDR MDA-MB-231 cell lines. AuNPs and AgNPs were synthesized via chemical reduction using reducing agents $NaBH_4$ and ascorbic acid, where they were further characterized. Treatment of GO was coupled with UV-B irradiation to determine the influence on cytotoxicity against breast cancer cells. It was found that PTX was the most potent yet easiest to be desensitized among all four drugs, whereas A-MG and Andr-G were less prone to be desensitized in longer duration treatment, with 25 µM of A-MG resulted in about 20% cell viability. Ascorbic acid-reduced AuNPs were found to be spherical with size 170 nm, zeta potential -36 mV, and polydispersity index of about 17%. $NaBH_4$-reduced AgNPs were also characterized to have irregular shapes at around 680 nm size and zeta potential -21 mV. AgNPs and AuNPs were less potent against drug-

resistant breast cancer cells. In MCF-7 cells, ascorbic acid-reduced AgNPs and $NaBH_4$-reduced AuNPs caused 50% and 25% cell death using 10 µM, respectively. GO was observed to be toxic to both MCF-7 and MDA-MB-231 with viability observed at 70% on MCF-7 for 100 µg/mL GO. UV-B irradiation influenced cytotoxicity in MCF-7 by increasing potency from 80% to 50% cell viability after 3h GO incubation and 10 mJ/cm^2 exposure. GO was more toxic on MCF-7 and MDA-MB-231 cells, whereas MCF-7-CR was more susceptible to both AgNPs and AuNPs. Further studies on the mechanism of action between nanoparticles, drugs, and cancer cells are necessary. The inclusion of different drug-resistant breast cancer as well as normal cells is also necessary to further compound the potential therapeutic importance of the study.

Keywords – Monolayer Breast Cancer Model, Chemo-Drug Resistance, Antineoplastic Agents Desensitization, Gold and Silver Nanoparticles, Graphene Oxide

(386 words)

ACKNOWLEDGEMENTS

The author is deeply grateful to the assigned supervisors at Sunway University, **Assoc. Prof. Dr. Ayaz Anwar** from Department of Biological Science (DBS) and **Prof. Mohammad Khalid** from Sunway Center for Electrochemical Energy and Sustainable Technology for their support until the completion of this research. The author would also like to thank **Prof. Jeff Tan Kuan Onn and his team** from DBS for providing help with resources via the research grant project number FRGS/1/2020/SKK06/SYUC/01/1 and guidance throughout the author's Master's Degree research. Without all of these people, the research would not be realized.

The author would like to acknowledge the help from **Prof. Saidur Rahman and his team** from the Research Center for Nano-Materials and Energy Technology (RCNMET) for the characterization of certain nanoparticles. The author would also like to acknowledge the **lab officers, research colleagues, and DBS staff** at Sunway University for their support on the practical side of research as well as administration-related issues. The author would also like to thank the Sunway University for funding throughout the author's study timeframe via Sunway University Scholarship program.

Finally, the author is very grateful for all the support their family has given during the pandemic and throughout the author's studentship at Sunway University.

TABLE OF CONTENTS

LIST OF FIGURES

LIST OF TABLES

LIST OF SYMBOLS AND ABBREVIATIONS

µg/mL	microgram per milliliter concentration
µM	micromolar concentration
2D	two-dimensional
3D	three-dimensional
AFM	Atomic force microscopy
$AgNO_3$	Silver nitrate
AgNPs	Silver nanoparticles
A-MG	Alpha-Mangostin
Andr-G	Andrographolide
AuNPs	Gold nanoparticles
CDDP	Cisplatin
CL	Claudin-low
cm^{-1}	Reciprocal wavelength centimeter
CYP	Cytochrome P450
DI H_2O	Deionized water
DLS	Dynamic light scattering
DMEM	Dulbecco's Modified Eagle Medium
DMF	Dimethylformamide
DMSO	Dimethyl sulfoxide
EMT	Epithelial-mesenchymal transition

EPR	Enhanced permeability and retention
ER	Endoplasmic reticulum
ER	Estrogen receptor
FBS	Fetal bovine serum
FDA	Food and Drug Agency
FTIR	Fourier transform infrared
GO or GONP	Graphene oxide or graphene oxide nanoparticles
h	hourly duration unit
$HAuCl_4$	Chloroauric acid
HCl	Hydrochloric acid
HER2	Human Epidermal Growth Factor Receptor 2
HNO_3	Nitric acid
IC_{50}	Inhibition concentration where viability reached 50%
IR	Infrared
KCl	Potassium chloride
KH_2PO_4	Potassium dihydrogen phosphate
LbL	Layer-by-layer
MDR	Multi-drug resistant
MDR1	Multidrug resistance protein 1
mJ/cm^2	millijoules of UV intensity dose per square centimeter covered

MOMP	Mitochondrial outer membrane permeabilization
MS	Mass spectrometry
MTT	Thiazolyl Blue Tetrazolium Bromide
mV	millivolt zeta potential
MW	Molecular weight
Na_2HPO_4	Disodium hydrogen phosphate
$NaBH_4$	Sodium borohydride
NaCl	Sodium chloride
NaOH	Sodium hydroxide
NEAA	Non-essential amino acid
nm	nanometers diameter or length
NMR	Nuclear magnetic resonance
oncomiRs	Oncogenic microRNAs
PBS	Phosphate-buffered saline
pDNA	plasmid DNA
PEG	polyethylene glycol
PenStrep	Penicillin-Streptomycin antibiotic cocktail
PLL	Poly-L-Lysine
PR	Progesterone receptor
PTT/PDT	Photothermal / photodynamic therapy
PTX	Paclitaxel

PVP	polyvinvylpyrrolidone
rGO	Reduced GO
ROS	Radical oxygen species
RPM	revolutions per minute
SEM	Scanning electron microscopy
SERS	Surface-enhanced Raman scattering
siRNA	Small interfering RNAs
SPR	Surface plasmon resonance
ssNMR	Solid-state NMR
TEM	Transmission electron microscopy
TGA	Thermogravimetric analysis
TNBC	Triple-negative breast cancer
TSG	Tumor-suppressing genes
UV	Ultraviolet
UV-vis	UV-visible
VEGF	Vascular endothelial growth factors
XRD	X-ray diffraction
XPS	X-ray photoelectron spectroscopy

LIST OF APPENDICES

CHAPTER 1 - INTRODUCTION

1.1.Background

In most Asian nations, including Malaysia, breast cancer is known as a major health problem as it has a high incidence and mortality rate, even among other cancer cases (Sung *et al.*, 2021; The Global Cancer Observatory, 2021). Cancer cells, including breast cancer cells, are malignant cells that have accumulated numerous genetic, physiological, and metabolic disorders (Hanahan and Weinberg, 2017). Careful prognoses for breast cancer types and appropriate treatment plans need to be devised to reduce the risk of breast cancer recurrence or further health complications (Lukasiewicz *et al.*, 2021).

The accumulation of the aforementioned disorder and other factors results in breast cells acquiring detrimental characteristics like uncontrollable replication, metastasis, and immortality. These cancerous characteristics can also be found in almost all cancer types and are categorized as the key hallmarks of cancer (Hanahan and Weinberg, 2017; Hanahan, 2022). As most of these hallmarks stem from specific biochemical signaling in cancer cells, they are extensively studied as potential diagnostic and therapeutic targets. In one instance, the cancer hallmark in breast cancer cells called ‘cell death resistance’ was studied as the target for a specific anticancer agent to trigger programmed cell death by activating pro-apoptotic proteins (Simon *et al.*, 2022).

Anticancer drugs or antineoplastic agents are compounds used as a means to treat cancer, either as adjuvant or neoadjuvant therapy. Most anticancer drugs target certain or multiple cancer hallmarks to inhibit cancer growth, while some can interfere with the cellular pathways to kill cells (Hanahan and Weinberg, 2017; Masui *et al.*, 2013). To help the selection of appropriate drugs and targeting specific breast cancer hallmarks, antineoplastic agents are classified based on their mechanism of action as well as their structure or derived source (Espinosa *et al.*, 2003; Taskin-Tok and Gowder, 2014). There

has been an increase in clinical approval for novel antineoplastic drugs that target specific hallmarks (LiverTox, 2021), however, the efficacy of these drugs against intrinsically and drug-acquiring chemo-drug-resistant cancer cells is still yet to be determined. Four antineoplastic drugs were tested in this study to compare the cytotoxicity of current FDA-approved drugs used for metastatic breast cancer treatment Cisplatin (CDDP) and Paclitaxel (PTX) (Wang *et al.*, 2021) with novel antineoplastic agents reported to exhibit cytotoxicity against drug-resistant breast cancer cells (Alpha-Mangostin/A-MG and Andrographolide/Andr-G) (Simon *et al*., 2022; Li *et al*., 2021).

Multi-drug resistance (MDR) is a major problem in cancer chemotherapy as it makes administering single or multiple drugs harder. While some cancer cells are intrinsically resistant to therapeutic compounds due to gene expression, the presence of specific membrane receptors, as well as enhanced metabolism, some cancer cells may acquire resistance against such antineoplastic agents due to selective pressure as well as factors such as accumulating detrimental genetic mutations and nongenetic alterations, quite similar to MDR development in bacteria (War, 2018; Lei *et al*., 2020). Depending on their protein expression profile and cell surface morphology, MDR phenotype cells can expel drugs from their system as the mechanism of action in their drug chemoresistance (Rathore *et al.*, 2017; Wang *et al.*, 2017). Aside from drug efflux from cells, MDR phenotype is also attributed to other mechanisms such as DNA damage repair, epithelial-mesenchymal transition (EMT), metabolism and growth factor enhancement, drug inactivation, and cell death inhibition (Bukowski *et al.*, 2020; Housman *et al.*, 2014). One way to overcome MDR cancer cells is by targeting key hallmarks related to cell death resistance, such as forcefully inducing programmed cell death or apoptotic pathways. This could be done by introducing foreign agents such as nanoparticles to trigger cells to generate oxidative stresses which cause further DNA damage (Yesilot and Aydin, 2019; Schaeublin *et al.*, 2011; Ou *et al.*, 2016).

Nanoparticles have been used in cancer therapy for drug delivery, diagnosis, monitoring, and cancer treatment. Nanoparticles are also documented to induce toxicity and apoptosis, thereby making them potential therapeutics against MDR cancer cells (Martinelli and Biglietti, 2020). Three nanoparticles are discussed and tested against cancer cells, which are silver nanoparticles (AgNPs), gold nanoparticles (AuNPs), and graphene oxide nanoparticles (GO or GONPs). Both AgNPs and AuNPs can be synthesized by different methods, with the most versatile and conventional method being the chemical reduction of nanoparticle ions into individual nanoparticle grains (Iriarte-Mesa *et al.*, 2020); whereas GO can be synthesized by graphite oxidation and further exfoliated into individual GO sheets (Rhazouani *et al.*, 2021). Besides its chemical composition, nanoparticle toxicity may also be attributed to the underlying morphology as well as other physical characteristics (Zhang **B** *et al.*, 2016). Thus, to determine the resulting physicochemical properties of synthesized nanoparticles, AuNPs, AgNPs, and GO can be characterized using optoelectronic measurements as well as chemical composition analysis (Gomes *et al.*, 2021).

Initially, four monolayer breast cancer cell models were supposed to be selected for studying cytotoxicity of antineoplastic agents and nanoparticles, namely Luminal A subtype MCF-7 breast cancer, the chemo-drug-resistant CDDP-resistant MCF-7-CR, the chemo-drug-resistant PTX-resistant MCF-7-PTR, and triple-negative breast cancer (TNBC) MDA-MB-231 cells. MCF-7 cells are known to be intrinsically resistant to hormonal drugs and genetically unstable which results in diverse cancer heterogeneity and phenotype variants (Comșa *et al*., 2015; Lee *et al*., 2015); PTX and CDDP were selected for drug-acquiring chemo-drug-resistant model on MCF-7 as they are known to be common FDA-approved drugs and have been used in breast cancer treatment regimen (Wang *et al*., 2021; Zhu and Chen, 2019; Al-Taweel *et al*., 2014; Zhang *et al*., 2015); whereas MDA-MB-231 cells are intrinsically resistant to hormonal drugs and other

chemotherapeutics due to their lack of hormone receptors, poor prognoses, as well as other MDR hallmarks such as EMT and drug effluxion (Chavez *et al*., 2010; Huang *et al*., 2020; Li *et al.*, 2020; Han *et al*., 2019; Alkaraki *et al*., 2020). However, only MCF-7, MCF-7-CR, and MDA-MB-231 were finally used in the study due to limitations related to time and resources.

1.2.Aims and Objectives

The objectives of this study are:

- To investigate the cytotoxic effects of four antineoplastic agents Cisplatin (CDDP), Paclitaxel (PTX), Alpha-Mangostin (A-MG), Andrographolide (Andr-G) against non-chemo-drug-resistant breast cancer cell MCF-7, chemo-drug-resistant breast cancer cell MCF-7-CR, and MDR breast cancer cell MDA-MB-231
- To synthesize, characterize, and evaluate the cytotoxic activity of metallic nanoparticles (AgNPs and AuNPs) when treated to non-chemo-resistant breast cancer cell MCF-7, chemo-drug-resistant breast cancer cell MCF-7-CR, and MDR breast cancer cell MDA-MB-231
- To evaluate the cytotoxic activity from graphene oxide (GO) nanoparticles on MCF-7, MCF-7-CR, and MDA-MB-231 as well as to evaluate the presence of synergistic cytotoxic activity with UV-B radiation against MCF-7

1.3.Research Questions

#Q1: What is the cytotoxicity trend in antineoplastic agents CDDP, PTX, A-MG, and Andr-G against non-chemo-drug-resistant breast cancer cell MCF-7, chemo-drug-resistant breast cancer cell MCF-7-CR, and MDR breast cancer cell MDA-MB-231?

#Q2: Among synthesized metallic nanoparticles AgNPs and AuNPs, which were the strongest in exhibiting cytotoxicity activity non-chemo-drug-resistant breast cancer cell

MCF-7, chemo-drug-resistant breast cancer cell MCF-7-CR, and MDR breast cancer cell MDA-MB-231?

#Q3: Would GO nanoparticles result in the reduction of breast cancer cell viability with or without exposure to UV-B radiation as a means of integrating synergistic cytotoxicity?

1.4.Research Scope of Study

The purposes of this study are to compare chemo-drug sensitivity between different cancer cell lines and chemo-drug-resistant breast cell lines in several treatments and to synthesize metallic nanoparticles while evaluating their cytotoxicity effects alongside one already studied organic nanoparticle to treat breast cancer cells, including MDR cancer cell. Several cancer cell models were used to test chemo-drug sensitization which are: non-chemo-drug-resistant MCF-7 breast cancer, chemo-drug-resistant model MCF-7-CR cisplatin-resistant breast cancer, and multi-drug resistant (MDR) model MDA-MB-231 triple-negative breast cancer. Antineoplastic agents used to investigate chemo-drug resistance of cancer cells were Cisplatin (CDDP), Paclitaxel (PTX), Alpha-Mangostin (A-MG), and Andrographolide (Andr-G); one of which was tested to be effective against MCF-7-CR and MCF-7 based on studies done by Simon *et al.* (2021). Two types of synthesized metallic nanoparticles were used for treatment: silver nanoparticles (AgNPs) and gold nanoparticles (AuNPs); whereas one organic nanoparticle was used for treatment: graphene oxide (GO). This study is not an extensive study on different MDR cancer cell lines as well as other groups of nanoparticles such as polymers, hybridized nanoparticles, and other metallic or organic nanoparticles. This study is limited to studying breast cancer model cells including two types of drug-resistant cell models which are drug-specific resistant as well as MDR cancer cells.

1.5.Research Thesis Structure

The contents of this research thesis are broken down into several chapters: Introduction, Literature Review, Methodology, Results, Discussion, and Conclusion. In the first chapter, the author discussed the research background and objectives as well as the scope surrounding the study. In the second chapter, the author reviewed topics related to the background of this study. The topics reviewed are general key hallmarks of cancer cells, the emergence of MDR cancer cells, the overview of breast cancer in research and as a health problem, antineoplastic agent classifications, nanoparticles such as AuNPs, AgNPs, and GO in terms of structure, synthesis and modification method, toxicity, physicochemical properties, and characterization. In the third chapter, materials used for reagents and samples were mentioned; while experimental plans and procedures used throughout the designed research were discussed. In the fourth chapter, results for antineoplastic agent treatment, nanoparticle synthesis, nanoparticle characterization, as well as nanoparticle treatment of various cancer cell models were shown. In addition, another separate chapter titled Discussion discussed and analyzed the results and interpretation from the previous chapter. In the final chapter, the main body of the research (from the first chapter until the fifth chapter) was summarized and future research outlooks and recommendations were briefly outlined.

CHAPTER 2 – LITERATURE REVIEW

2.1.Key hallmarks of cancer cells

Essentially, cell malignancy and the emergence of cancer cells are caused by disorders in the immune, metabolic, and genetic levels (Hanahan and Weinberg, 2017). However, cancers are most commonly caused by accumulations of mutations and other alterations in the genome which affects cell metabolism and structure as a whole. Aside from the internal disorders, cancer formation may also be induced externally by carcinogenic chemicals, radioactive agents, or even oncogenic viruses that can disrupt genes both directly or indirectly (Weinberg, 2013). By silencing and interfering with genes associated with cell cycle arrest and related repair genes, cancer cells are capable of proliferating uncontrollably and may invade other normal-functioning tissues (Weinberg, 2013).

The acquired replicative immortality properties as well as other acquired characteristics, are categorized into 10 key hallmarks of cancer. These 10 characteristics revolve around certain aspects of cancer cells, which are uncontrollable growth (sustaining proliferative signaling, resisting cell death, enabling replicative immortality), disruption of nearby cells (deregulating cellular metabolism), malignancy propagation (tumor-promoting inflammation, activating invasion and metastasis, inducing or accessing vasculature), evasiveness (evading growth suppressors, avoiding immune destruction), and oncogenic mutation (genome instability and mutation) (Hanahan and Weinberg, 2017). There has also been an update that increased the key hallmark numbers to 14 hallmarks, with the new four proposed hallmarks known as unlocking phenotypic plasticity, nonmutational epigenetic programming, polymorphic microbiomes, and senescent cells (Figure 2.1). Unlocking phenotypic plasticity refers to cancer's capability of disrupting cellular differentiation resulting in dedifferentiation to more potent progenitor or stem cells,

blocking and silencing differentiation pathways, and transdifferentiation to non-related cancer line which leads to the acquisition of unwanted characteristics. Nonmutational epigenetic programming refers to genomic reprogramming due to stress and mitotic-driven epigenetic mechanisms that regulate oncogenes and silence specific chromatin regions housing tumor-suppressing genes (TSG). Polymorphic microbiomes refer to the systemic and local site-modulating interactions between tumor niche and gut, intratumoral, and other microbiota. Senescent cells refer to malignancy progression caused by aging cells (Hanahan, 2022).

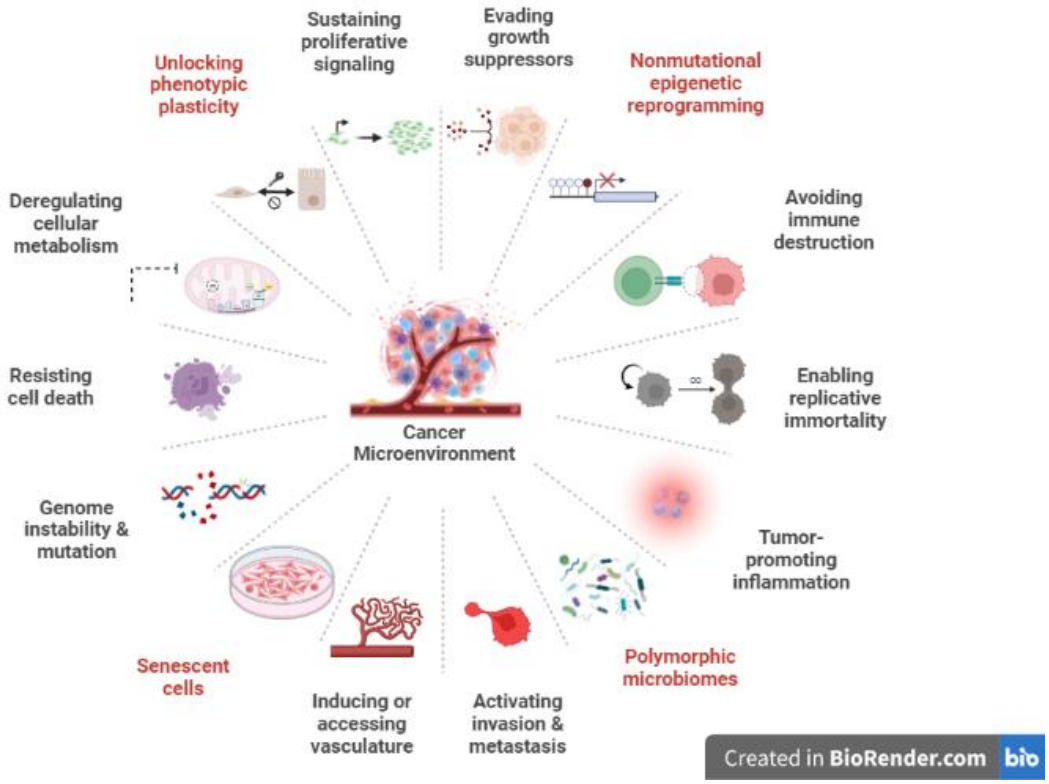

Figure 2.1 10 canonical key hallmarks of cancer, with 4 newly proposed additions, adapted from Hanahan (2022). The image was created with BioRender.com

All of the aforementioned hallmarks also have potential for diagnostic and therapeutic targets, for instance downregulating certain growth factors to reduce angiogenesis in cancer sites. Certain inhibitors such as telomerase inhibitors and vascular endothelial growth factors (VEGF) could be used to suppress genome replication and prevent

vasculature from forming, thereby suppressing cancer immortality and angiogenesis as well as invasion to occur respectively. Cell death could also be forcefully induced by introducing pro-apoptotic compounds such as antineoplastic drugs and pro-apoptotic proteins, which target at least two hallmarks such as resisting cell death and genome instability (Hanahan and Weinberg, 2017).

Cancer hallmark identification is also necessary for determining how certain cancer types behave as well as the appropriate treatments to be used (Hanahan and Weinberg, 2017), as in the case of classifying key hallmarks in breast cancer. The well-observed breast cancer hallmarks stem from genomic and chromosomal instability, resulting in gene silencing and oncogenic overexpression. Derivative hallmarks that are enabled by such instability include cell death resisting in the form of apoptosis, heightened form of replication and proliferation, metastatic invasion, angiogenesis, and detrimental immunomodulation (Castellanos *et al.*, 2022; Lukasiewicz *et al.*, 2021). These hallmarks were reported by Saha *et al.* (2021) to be extensively studied for therapeutic targets from 1968 until 2021 using targeted therapy, with a recent focus on anti-metastasis.

Despite many possibilities for hallmark targeting as well as extensive research on treatments, cancer is still deemed a large medical problem. This has to do with how besides promoting activation of oncogenes and TSG related to cell cycle arrest and genome repair mechanism, multiple different key hallmark pathways can occur at the same time, further reducing treatment instances (Weinberg, 2013). While combinational approaches are becoming more mainstream such as in most adjuvant therapies to target multiple hallmarks, most of these are considered invasive to the patient's body and are generally non-specific, thus causing side effects and other major health complications. For example, surgical intervention is not curative enough in that the risk of cancer relapse would not be reduced even after tumor removal due to its high invasiveness. While most radiotherapy is non-invasive, their lack of cell selectivity may do more harm to the nearby

cells (Ferreira *et al.*, 2020). This is also the case, especially in the usage of chemotherapeutic agents. Most commercially available anticancer drugs are documented to have side effects involving systemic and local toxicity on vital organs such as the liver, kidneys, and heart, as well as nerve damage due to their non-specificity and biodistribution limitations (Iqbal *et al.*, 2017).

2.2.Multi-drug resistance (MDR) and drug sensitivity in cancer cells

Multi-drug resistance (MDR) is the ability of cancer cells to become resistant to many fundamentally different anticancer drugs, which has become a large cause of the recent spike in cancer-related mortality (Li *et al.*, 2017). Cancer can develop the aforementioned drug resistance through various mechanisms, which include enhanced drug efflux in cells, genetic alterations, growth factors, increased DNA repair capacity, elevated metabolism of xenobiotics (Bukowski *et al.*, 2020), cell death pathway inhibition, drug target alterations, cancer cell heterogeneity in tumoral site, and epithelial-to-mesenchymal transition (EMT) properties in cancer cells (Housman *et al.*, 2014); all of which are attributed to specific cancer hallmarks.

Drug efflux in MDR cancer cells is known to be associated with the overexpression of ATPase-type proteins such as multidrug resistance protein 1 (MDR1) (Housman *et al.*, 2014). These proteins reduce the amount of intracellular active drugs by increasing xenobiotic drug transports outside the cells, thereby decreasing cellular cytotoxicity (War, 2018). In addition, MDR cancer cells are also known to have genetic alternations, including gene mutations and abnormal epigenetics that lead to the silencing of tumor suppressors genes (TSGs), defective DNA repairs, and apoptosis signaling mechanisms in the cancer cells (Salehan and Morse, 2013; Rathore *et al.*, 2017). TSGs are genes found throughout most cells and attributed to various cellular activities such as DNA damage detection and repair, cell-cycle regulation, as well as cell death activation (Sherr, 2004). As most tumor suppression genes are recessive and highly susceptible to mutation, their

activity is mostly attenuated in tumor cells, more so in MDR cancer cells (Morris and Chan, 2015).

MDR cancer cells could also regulate the expression of enzymes that can inhibit anticancer drugs or other xenobiotics after receptors corresponding to the drugs are activated, thereby promoting increased metabolic sensitivity and further effluxion (Omiecinski *et al.*, 2011; Bukowski *et al.*, 2020). One example of xenobiotic-based suppression is Cytochrome P450 (CYP) system protein expression in cancer cells that results in suppression and alteration of specific target proteins and genes, such as DNA-coiling regulation enzymes topoisomerase II. This results in cancer cells that are impervious to DNA damage as well as topoisomerase II inhibitor drugs (Housman *et al.*, 2014).

Aside from genomic instability and apoptosis evasion, other cancer hallmarks involved in the emergence of MDR phenotypes are EMT or stem cell-like traits as well as growth factor abuse which increases proliferation, metastasis, and self-renewal. By simultaneously alternating their morphology and surface receptor composition, MDR cancer cells could increase tolerance against most antineoplastic agents and also make them nearly undetectable by nanoparticle carriers or the immune system. The ever-changing morphology trait of cancer cells would lead to the diversification of cell types in certain cancer niches, further heightening MDR phenotypes in the tumor microenvironment (Housman *et al.*, 2014). In one study, cancer-associated fibroblasts secreted exosomes filled with oncogenic microRNAs (oncomiRs) miR-92a-3p which promoted heightened invasiveness, EMT, and downregulation of key pro-apoptotic protein, the emergence of cancer stem cells, and eventual MDR phenotype in multiple colorectal cancer cell lines (Hu *et al.*, 2019).

2.3.Overview of breast cancer in clinical studies

2.3.1. Epidemiology

In recent years, breast cancer has become a major contributor to emerging cancer cases in women worldwide with 24.5% of accounted cases from the year 2020 being breast cancer-related, and recorded mortality from female breast cancer reached just almost 685,000 deaths (Sung *et al.*, 2021). Even in the United States, breast cancer cases have become the highest cancer incidence in women at 31% of cases in 2023 and were estimated to be the second highest cause of cancer death in women aside from lung-related cancer (Siegel *et al.*, 2023). Compared to other regions, while breast cancer incidence throughout the Asian region was not as high as in Northern America, Latin America as well as the Caribbean, Europe, and Oceania; mortality rates were a lot higher, reaching second-third place just behind Africa. Socioeconomic- and population-wise, however, Asian regions reached the highest for both incidence and mortality (The Global Cancer Observatory, 2020). In Malaysia alone, breast cancer has become the most common cancer case in 2020 and contributed to the highest cancer-related mortality at 20.7% when compared to other common cases such as colorectal and lung cancer (The Global Cancer Observatory, 2021).

2.3.2. Risk Factors

Similar to how other cancer types emerge, breast cancer can be acquired due to some risk factors related to age, health complications, dietary reasons or lifestyle, genetic mutation, and inheritance, as well as foreign agents such as excessive sex-related hormones, harmful radiation, and carcinogens. In particular, several well-known oncogenic genes such as *BRCA1* and *BRCA2* can be detected in carriers and are mutated in breast cancer patients. Some types of breast cancer cells are also more commonly found in older patients, however, senescence in general is known to be a major proponent in cancer emergence (Lukasiewicz *et al.*, 2021).

2.3.3. Clinical Treatment

Depending on the cell subtype, tumor stage severity, and complication, treatments for breast cancer can be varied. There are several types of breast cancer treatment strategies, which include: surgical intervention or tumor resection, chemotherapy, radiation therapy, endocrine or hormonal therapy, immunotherapy, and targeted therapy. Surgery is divided into two major types: breast-conserving surgery which involves the removal of tumoral tissue alongside plastic surgery for breast reconstruction, and mastectomy or complete breast removal which also involves breast reconstruction. Surgical intervention is used for lighter-stage tumors and non-invasive cancer due to its need to fully remove large tissue regions (Lukasiewicz *et al.*, 2021).

For chemotherapy, a combination of several drugs is used based on the subtype or tumor severity, for example, the drug cocktail of Gemtacitabine-Dodetaxel alongside an additional cocktail of Capecitabine-Dodetaxel is used in advanced breast cancer cases. In most cases, chemotherapy is used as a neoadjuvant (chemotherapy for reducing tumor size before surgical intervention) or adjuvant (chemotherapy for reducing the risk of tumor recurrence after certain primary treatments such as surgery). However, chemotherapy is highly prone to causing side effects which can lead to further health complications (Lukasiewicz *et al.*, 2021).

Radiotherapy is usually performed as an adjuvant or advanced treatment to reduce the risk of recurrence or to combat metastatic instances. However, similar to chemotherapy, radiotherapy is also prone to side effects as radiation may damage nearby cells. Endocrinal or hormonal therapy uses hormone receptor blocker drugs to block certain receptors such as ERs in Luminal-subtype cells, such as the use of Tamoxifen. Thus, hormonal therapy is mostly used as either a neoadjuvant or adjuvant therapy for combating recurrence and reducing certain Luminal subtype-based tissue. However, hormonal therapy is not viable for long-term treatment as hormone receptor-positive cells

will become increasingly resistant to hormone receptor blockers. Immunotherapy, or specifically Trastuzumab and other monoclonal antibodies is considered to intersect with targeted therapy due to its use in targeting HER2 receptors. Similar to chemotherapy, immunotherapy is a neoadjuvant as well as an adjuvant therapy due to its use in lowering recurrence risk and also for inhibiting angiogenesis. Other targeted therapies are usually experimental or still in the study due to the use of specific inhibitor agents that target certain cancer characteristics, or key hallmarks (Lukasiewicz *et al.*, 2021).

2.3.4. Subtype Classification

In the microenvironment of breast cancer tissues, different breast cancer cells and/or stem cells exist which resulted in the difficulty of providing the exact treatment regimen. To help the study, prognosis, and treatment of patients, breast cancer cells have been classified according to the cells' specific hormone receptor expression. These are known to be estrogen receptor (ER), progesterone receptor (PR), and human epidermal growth factor 2 receptor (HER2) (Orrantia-Borunda *et al.*, 2022). From this receptor expression criterion, four breast cancer subtypes are classified: Luminal A, Luminal B, HER2-positive ($HER2^+$), and triple-negative (TNBC). TNBC may also be divided into 2 more subtypes which are basal and claudin-low (CL), based on their claudin protein expression (Holliday and Speirs, 2011). In terms of estimated composition as well as the rarity in breast cancer cases in the world, Luminal breast cancer for A and B combined reached up to 70% cases, $HER2^+$ breast cancer cases make up to 10-15%, Basal-like breast cancer cases make up to about 20%, and finally, 7-14% of tumor cells are CL subtypes which are the least treated due to poor prognosis (Lukasiewicz *et al.*, 2021).

Luminal A breast cancers (e.g. MCF-7) can be treated with hormonal or chemotherapy and are characterized to have a lack of major oncogene biomarkers. Luminal A breast cancers also have ER and PR expressions but no HER2 expression (ER^+, PR^+, $HER2^-$) as well as some instances of Ki67 expression, resulting in an overall good prognosis.

Luminal B breast cancers (e.g. BT474) are characterized to express oncogenic mutation *BRCA2,* high ER expression, some instances of PR, lack of HER2 expression, and some instances of Ki67 expression (ER^{+}, $PR^{+/-}$, $HER2^{-}$). They are regarded as having a middle prognosis and can be treated with hormonal, immuno-, or chemotherapy. $HER2^{+}$ breast cancer (e.g. SKBR3) is characterized to express high instances of HER2 and Ki67, low instances of ER and PR ($ER^{+/-}$, $PR^{+/-}$, $HER2^{+}$). HER2 subtype cells also express easily mutated *p53,* have a middle-to-bad prognosis, and can be treated with immunotherapy in the form of monoclonal antibody Herceptin or trastuzumab. Basal-like and CL are characterized to not express any of the receptors (ER^{-}, PR^{-}, $HER2^{-}$), express a high degree of Ki67, and contain oncogenic biomarkers *p53* and *BRCA1.* Basal-like breast cancers (e.g. MDA-MB-468) are further profiled to express additional receptors called epidermal growth factor receptors ($EGFR^{+}$) and are also known to be resistant to immuno- or hormonal therapy but quite responsive to chemotherapy. Whereas CL breast cancer cells (e.g. MDA-MB-231) are highly resistant to immune- or chemotherapy and are overall regarded as having a bad prognosis (Holliday and Speirs, 2011; Orrantia-Borunda *et al.*, 2022).

2.4.Breast cancer cell models

In cancer research, there are numerous breast cancer models used depending on their applications. Generally, cancer cell models range from *in vitro* (experiments performed outside of a living organism), *in silico* (experiments performed within computers and computation), and *in vivo* (experiments performed within or on a living organism). *In silico* studies use computational models to study cancer mechanisms via molecular docking and to identify cancer biomarkers ranging from metabolites, oncoproteins in cancer pathways, and genomic identifiers such as single-nucleotide polymorphisms. *In vivo* studies use animal models that are genetically altered or are transplanted with tumor-inducing agents as well as cancer cells. In cancer research, *in vivo* models are

predominantly used for pre-clinical studies with commonly used animals including mice, fruit flies, zebra fishes, and pigs (Sajjad *et al.*, 2021; Boix-Montesinos *et al.*, 2021).

In vitro models can be differentiated into 2D traditional models, 3D advanced models, as well as more sophisticated lab-on-a-chip models. 2D *in* vitro models use a monolayer cell culture model for experiments on non-complex singular cancer cell lines as well as a co-culture model to represent tumor microenvironment and overall interactions between different 2D cell lines (Boix-Montesinos *et al.*, 2021). 3D models used 3D spheroid model to study intercellular interactions as well as 3D tumor characteristics, 3D organoid models to further understand cancer impact on small-scale organ structures made from derived pluripotent stem cells, and near-2D or 3D patient-derived xenografts taken from biopsies to further study personalized medicine and specific cancer variants or phenotypes. Lab-on-a-chip-related models are an emerging model type that uses microfluidics and precise biologics printing for specialized tissue or organ fabrication and high-throughput drug or biomarker screening (Boix-Montesinos *et al.*, 2021; Fröhlich *et al.*, 2023).

In this study, monolayer cell culture was selected for studying toxicity of breast cancer cells as it was an inexpensive and simple model that can be easily modified without specific treatment like 3D spheroid as well as co-culture models. Three breast cancer cell lines were selected for the monolayer cell models, which were the subtype Luminal A MCF-7 cancer cell, the drug-resistant derivative of MCF-7 called MCF-7-CR, and subtype CL from the TNBC family called MDA-MB-231 cells.

2.4.1. MCF-7 breast cancer cell

MCF-7 is an epithelial breast cancer cell line or adenocarcinoma generated by the Michigan Cancer Foundation and isolated from the pleural effusion of a metastatic female patient named Helen Marion. MCF-7 cell line has been used for cancer research, specifically for estrogen receptors, hormonal drug resistance, and cancer cell gene cloning

studies (Lee *et al.,* 2015). This cell line is characterized to highly express estrogen, progesterone, and glucocorticoid receptors (Camarillo et al, 2014). Morphologically, monolayer-grown MCF-7 cells have the classic cobblestone shape and low invasiveness, resulting in more pronounced cell-cell adherence (Holliday and Speirs, 2011). MCF-7 cells are classified as Luminal A cancer cells, which are endocrine and chemotherapeutic responsive. MCF-7 cells also have multiple different phenotypes due to diverse levels of expressed receptor and biomarker proteins. However, while they have different levels of expressed proteins, overall MCF-7 phenotypes express similar levels of ER^+, PR^+, $HER2^-$, and low Ki67 (Lukasiewicz *et al*., 2021; Orrantia-Borunda *et al.,* 2022). The amount of MCF-7 cell phenotype and genotype variation results in a high degree of heterogeneity even in a single tumor microenvironment. Genetic instability was also seen throughout the cell variants, as there are more than 100 subclone variants of MCF-7 cells observed and characterized (Comşa *et al.,* 2015; Lee *et al.,* 2015).

2.4.2. MCF-7-CR breast cancer cell

MCF-7-CR is an artificially-derived MCF-7 subclone made by treating antineoplastic agent cisplatin for 7 cycles of 24h low-dose incubation (Watson *et al.,* 2007). MCF-7-CR was first established as a means of studying the dosage and resistance of chemotherapy regimens for breast metastasis that used a combination of cisplatin/docetaxel. As had been briefly touched on in Subsection 2.4.1., MCF-7 cells are genetically unstable, therefore short-term treatment of cisplatin was reported to increase desensitization in MCF-7 cells after multiple exposures. Despite this, it was also reported that cisplatin resistance emerged independently from were seen on proteins associated with MDR phenotype such as MDR1 and p53 (Watson *et al.*, 2007). Expression of GSTπ protein was also observed in MCF-7-CR cells, indicating that epigenetic alterations via chromosomal hypomethylation had occurred to genes associated with apoptosis, estrogen metabolism, and metastasis (Chekhun *et al*., 2007). In a recent study by Ruiz-Silvestre *et al*. (2024), it

was revealed that cisplatin resistance was associated with the expression of numerous long non-coding RNAs (lncRNAs) such as *NEAT1* and *MALAT1* which were also associated with cisplatin sensitivity in lung and ovarian cancer.

2.4.3. MDA-MB-231 breast cancer cell

MDA-MB-231 is an epithelial-like metastatic breast cancer cell or an adenocarcinoma generated by the M.D. Anderson Cancer Center and isolated from the pleural effusion of a mammary metastatic female patient. MDA-MB-231 cell line is used in cancer research mainly for studying breast-to-brain metastasis, hormonal and chemotherapy resistance, cancer stem cell mechanism, cell line heterogeneity, co-culture studies, and targeted therapy for MDR cancer cell lines (Lu *et al.*, 2009). In addition to being metastatic, MDA-MB-231 are classified as CL subtypes due to not expressing ER, PR, or HER2 receptors, as well as detected low levels of Ki67 proliferation markers; resulting in poor prognosis among the other TNBCs (Chavez *et al*., 2010). Morphologically, MDA-MB-231 monolayer cell models are seen to be rather fibroblastic and have less cell-cell contact with each other compared to the cobblestone-like MCF-7. MDA-MB-231 cells may also form synaptic-like junctions between the ends of each cell (Franchi *et al.*, 2020). MDA-MB-231 cells can bypass cytotoxic antineoplastic agents by various mechanisms such as EMT morphological regulation (Huang *et al.*, 2020), transporter protein MDR1 expression, *BRCA1/BRCA2* DNA repair mechanism, epigenetic and genomic alterations (Li *et al.*, 2020; Han *et al.*, 2019), and increased pro-survival and pro-growth gene upregulation (Kwon *et al*., 2015; Wang *et al*., 2017; Alkaraki *et al*., 2020).

2.5.Anticancer drugs and drug classification

Antineoplastic agents commonly referred to as anticancer drugs are used to disrupt mechanisms that enable the hallmarks of cancer to occur, such as uncontrollable self-replication and resisting cell death (Hanahan and Weinberg, 2017). Because of the large

diversity of chemicals and the emerging need to identify the best drug for each treatment, drugs can be divided into two groups according to their selectivity, which are cytotoxic drugs that could damage normal healthy cells and targeted antineoplastic drugs that work by blocking several targeted pathways in cancer cells to stop their growth and replication (Masui *et al.*, 2013). Antineoplastic agents can also be broadly categorized into four major groups depending on their targeted therapeutic use, which are chemotherapy, immunotherapy, hormonal therapy, and biologics therapy (which includes gene and protein-based drugs). These four groups can be further classified into eleven large categories based on their mechanism of action or specific properties (Figure 2.2). These categories are alkylating agents, antimetabolites, antibiotics, topoisomerase inhibitors, taxanes along with vinca alkaloids which make up mitosis disruptors, histone deacetylase, inhibitors hormonal therapy, targeted therapy, immunotherapeutics, bio-derived products, as well as miscellaneous group (LiverTox, 2021; Espinosa *et al.*, 2003; Taskin-Tok and Gowder, 2014; Iqbal *et al.*, 2017).

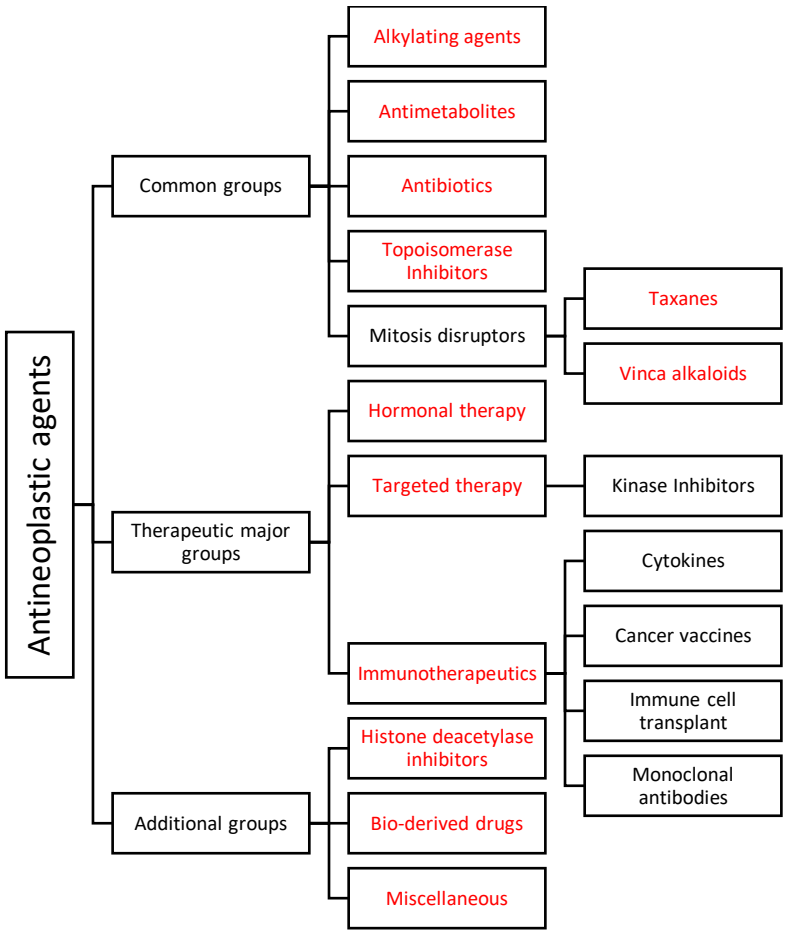

Figure 2.2 Classification of antineoplastic agents, with red-labeled groups as the eleven major groups.

Of the eleven major categories, six of them are regarded as common groups. Alkylating agents are drugs that can damage and mutate DNAs by alkylating onto the nitrogen bases (e.g. **Cisplatin/CDDP**, Cyclophosphamide). Antimetabolites inhibit macromolecules essential in peptide and nucleic acid pathways (e.g. Capecitabine, Gemcitabine). Different types of antibiotics are also known to be capable of cytotoxic and antitumor activity such as Doxorubicin and Mitomycin. Topoisomerase inhibitors are drugs that can interfere with the winding and unwinding of chromatin DNAs (e.g. Etoposide, Camptothecin). Mitosis disruptors are naturally derived drugs that can interfere with cell division by inhibiting the microtubules. Mitosis disruptors can be further differentiated into taxanes which prevent microtubule disassembly (e.g. Docetaxel, **Paclitaxel/PTX**), and vinca

alkaloids which prevent microtubule assembly (e.g. Vincristine, Vinorelbine). (LiverTox, 2021; Espinosa *et al.*, 2003).

Besides the common six major groups of chemotherapeutics, three classes of antineoplastic agents are broad groups that are related to specific therapies which are immunotherapy, hormonal therapy, and biologics or targeted therapy. Hormonal therapy-based antagonists can disrupt hormonal pathways that are used for cancer growth (e.g. anti-estrogenic Tamoxifen, anti-androgenic Cyproterone). In targeted therapy, the therapeutics used have specific functions that allow the inhibition of overexpressed oncoproteins or other antigens. From targeted therapeutics, this major group can be further differentiated into a certain group subset that works as protein kinase pathway inhibitors (e.g. Afatinib, Vandetanib). In immunotherapy, multiple types of immunotherapeutics are used. These are cytokines (e.g. Aldesleukin IL-2, Interferon Gamma), cancer vaccines, immune cell transplant, and monoclonal antibodies (e.g. Bevacizumab, Trastuzumab). (LiverTox, 2021; Taşkin-Tok and Gowder, 2014).

Three additional groups are added to the six common groups and three major therapeutics, which are histone deacetylase inhibitors, miscellaneous, as well as bio-derived. Histone deacetylase inhibitors are similar to alkylators; however, they induce acetyls in histones to prompt cell cycle arrest (e.g. Belinostat, Vorinostat). Miscellaneous are other antineoplastic agents that are grouped into a single miscellaneous category due to their unique traits (e.g. Venetoclax, Thalidomide) as well as emerging new compounds that could not quite fit with the rest of the classification groups such as therapeutic nanoparticles. (LiverTox, 2021; Espinosa *et al.*, 2003). Recently, another largely considered type as an emerging antineoplastic agent group is bio-derived drugs, more commonly known as natural products which overlap with other groups due to their historic nature. Natural products, especially anticancer phytochemicals (e.g. Curcumin, Resveratrol), could serve as an alternative to chemotherapeutics as many anticancer drugs

are well known to cause direct hepatotoxicity as well as local tissue-to-organ failure (Taşkin-Tok and Gowder, 2014; Iqbal *et al.,* 2017). Two naturally-derived compounds, called **alpha-mangostin (A-MG)** and **andrographolide (Andr-G)** were reported to exhibit cytotoxic activity by inducing apoptosis pathways (Li *et al.,* 2014; Simon *et al.,* 2022; Xuan *et al.,* 2022; Gao *et al.,* 2021; Yan *et al.,* 2012).

Due to their specific classification criteria, some of the compounds classified in the three additional groups tend to overlap with the rest of the groups. For instance: the case for paclitaxel or PTX. PTX originally was a phytochemically-extracted antineoplastic compound, however, the extract and further isolated single compound were then discovered to induce mitotic disruption in cancer cells among other mechanisms of action (Zhu and Chen, 2019). Another example is the broad category of silver nanoparticles (AgNPs) under the miscellaneous group. The reason for such compounds' classification was due to their diverse range of physicochemical properties with different mechanisms of action observed in cancer cells related to targeted therapy against key hallmarks such as apoptosis (Talarska *et al.,* 2021), anti-angiogenesis (Zhang **A** *et al.,* 2016; Yang *et al.,* 2016), autophagy (Chakraborty *et al.,* 2016), and DNA damage (Kovács *et al.,* 2022).

2.5.1. Cisplatin (CDDP)

CDDP ($Pt(NH_3)_2Cl_2$, MW = 301.1 g/mol) is a platinum-based, FDA-approved anticancer drug that works as an alkylating agent in cells. CDDP binds to the nitrogen bases on DNAs, specifically purines, resulting in interference in DNA repair as well as oncogene expression (Dasari and Tchounwou, 2014). The inhibition CDDP concentration necessary to get 50% breast cancer cell MCF-7 viability (cell viability IC_{50}) after 24h CDDP treatment was recorded to be at the range of below 10 µM, specifically around 5.8 µM (Suberu *et al.,* 2014). In a study done by Al-Taweel *et al.* (2014), 52% of cisplatin-resistant breast cancer cells MCF-7-CR were found to be more desensitized and did not respond to 10 µM CDDP while only 23% of MCF-7 cells were responsive to drug

exposure and disrupted Ca^{2+} concentration. In another study, it was found that the IC_{50} of triple-negative breast cancer cell MDA-MB-231 for 72h exposure was at around 7.8 µM while IC_{50} for 24h exposure could not be measured due to the highest CDDP concentration of 30 µM only resulted in 80% cell death (Yin *et al.*, 2018).

2.5.2. Paclitaxel (PTX)

PTX ($C_{47}H_{51}NO_{14}$, MW = 853.9 g/mol) is a tetracyclic diterpenoid compound isolated from the bark of *Taxus breviolia*, which has been used as an FDA-approved anticancer drug. PTX works as a mitotic inhibitor in cancer cells, where the compound interferes with the binding of microtubules by preventing microtubule dissociation in the cell replication phase (Zhu and Chen, 2019). In one study, IC_{50} of PTX treated for 24h on MCF-7 and MDA-MB-231 were reported to be 3.5 µM and 0.3 µM, respectively (Haghnavaz *et al.*, 2017). In another study, IC_{50} of PTX treated for 24h in MCF-7 was found to be at 20 nM, while paclitaxel-resistant MCF-7/PTX were far higher at 2291 nM (Zhang *et al.*, 2015).

2.5.3. Alpha-Mangostin (A-MG)

A-MG ($C_{24}H_{26}O_6$, MW = 410.5 g/mol) is a xanthone-class natural product that can be isolated from *Garcinia mangostana L.*, specifically found in pericarp extracts. As a member of the xanthone family of natural products, A-MG contains phenolic groups and an aromatic ether. Studies have shown that A-MG exhibits multiple biological activities, including antioxidant, antibacterial, anti-inflammatory, as well as anticancer activities. There are multiple pathways proposed for the A-MG mechanism of action against cancer cells, with some of the mechanisms found to be associated with apoptotic signaling (National Center for Biotechnology Information **B**, 2023). In a study done by Li *et al.* (2014), breast cancer MCF-7 and triple-negative breast cancer MDA-MB-231 cells were treated with A-MG. After treatment of A-MG, the inhibition concentration necessary to

get 50% cell viability (cell viability IC_{50}) of A-MG on MCF-7 was found to be 3.57 µM for 24h treatment and 2.74 µM for 48h treatment; whereas cell viability IC_{50} of A-MG on MDA-MB-231 for treatments 24h and 48h were 3.35 µM and 2.60 µM respectively. Cells treated in A-MG were found to have elevated expression of Bax and downregulation of Bcl-2, suggesting apoptosis occurrence by A-MG. In another study, the presence of A-MG increased MOAP-1 expression in MCF-7, leading to caspase-dependent and mitochondrial-mediated apoptosis. MDR phenotype-conferring oncoprotein Bcl-xL was also found to be highly downregulated in MCF-7 cells treated with 20 µM of A-MG. Besides apoptotic induction, A-MG was potent in treating MDR cancer cells such as Cisplatin-resistant MCF-7 cancer cell MCF-7-CR, where 24h treatment of A-MG resulted in cell viability IC_{50} to be 2.534 ± 1.363 µM (Simon *et al.*, 2022).

2.5.4. Andrographolide (Andr-G)

Andr-G ($C_{20}H_{30}O_5$, MW = 350.4 g/mol) is a labdane diterpenoid lactone, a compound found in the terpenoid-class natural product. and can be isolated from *Andrographis paniculata*. Andr-G has been documented as an anti-inflammatory and anti-platelet aggregation drug, with some potential indications of anticancer activity (National Center for Biotechnology Information **C**, 2023). As its mechanism of action, Andr-G can induce apoptosis as well as several other pathways including cell cycle arrest (Yan *et al.*, 2011). Andr-G was able to inhibit the growth, proliferation, and migration of bladder cancer T24 and 5637 while also promoting apoptosis. Expression of anti-apoptotic and pro-migration-related proteins such as NF-κB was downregulated after treatment in Andr-G (Xuan *et al.*, 2011). In gastric cancer SGC7901, treatment of Andr-G resulted in the downregulation of Mdm-2 and increased expression of p53 proteins, which are one of the core proteins in apoptotic pathways (Gao *et al.*, 2021). It was also found that treatment in MCF-7 for 48h resulted in IC_{50} of 70 µM, where cell migration and invasion were inhibited due upregulation of PDCD4 proteins (Li *et al.*, 2021).

2.6.Introduction to therapeutic nanoparticles

Generally, nanoparticles are particles produced in the nanoscale from materials such as metals, organic polymers, as well as ceramics which showed different arrays of emergent physicochemical properties ranging from optical to magnetic properties (Khan *et al.*, 2019). Nanoparticles are categorized into several types depending on their chemical compositions, which are: liposomes or lipid bilayer-based nano-vesicles, living bacteria or viral vectors, solid lipid nanoparticles, artificially-made and natural polymer nanoparticles, dendrimers and aptamers, silica-and ceramic-based porous nanoparticles, as well as metal-based nanoparticles (Amreddy *et al.*, 2018; Roacho-Perez *et al.*, 2017). Besides the type of materials, synthesis methods and post-synthesis modification also results in differing characteristics that can be utilized for biomedical research in various cases, such as bioimaging, biomarker detection as well as targeting, molecular vehicles, and therapeutics (Wang and Wang, 2015). For example, liposomes can carry hydrophilic, hydrophobic, and amphiphilic molecules and can be easily manipulated in their fabrication process. Most metallic and inorganic nanoparticles are used for inducing toxicity in cells as well as monitoring using radiation-, light-, thermal-, or acoustic-based imaging (Martinelli and Biglietti, 2020). Artificially made polymeric nanoparticles are easily modified or functionalized and are toxic to cells, while natural polymeric nanoparticles are more biodegradable and biocompatible in various microenvironments (Sung and Kim, 2019; Lu *et al.*, 2016). Viral vectors and bacteria could be used to induce toxicity in target cells as well as biologics-type interventions such as delivering genes to cells, but are more prone to triggering immunogenic responses and could result in health complications (Goklany *et al.*, 2019).

As briefly described in Subsection 2.5., therapeutic nanoparticles are classified under miscellaneous antineoplastic agent due to their wide range of base compound forms and modification, as well as diverse mechanisms of action depending on their properties. In

terms of therapeutics, nanoparticles have been studied for their delivery capabilities as well as inherent toxicity to cells. Due to their morphology and material, endocytosed nanoparticles and disintegrated nanoparticles in cells can promote cell death-associated cellular pathways such as the production of reactive oxygen species (ROS) that leads to morphological and physiological breakdown (Shang *et al.*, 2014). While the inherent toxicity of nanoparticles can be utilized for the treatment of diseased cells such as cancer, toxicity may also occur in healthy cells and can lead to organ-scale as well as systemic toxicity (Yang *et al.*, 2021). Hence, studies were done to determine whether nanoparticles could be used to treat primarily cancer cells and not target normal cells. In one study, biosynthesized gold nanoparticles (AuNPs) were found to be toxic against breast cancer MCF-7 after exposure under 72h while no cell death was seen on normal kidney fibroblast Vero cells (Pechyen *et al.*, 2022). In another study, modified AuNPs were able to selectively induce apoptotic-associated cell death in breast cancer cells MCF-7 rather than other cell lines such as lung cancer A549, noting further that nanoparticles could target specific cells by fabricating nanoparticles in different synthesis and modification methods (Repotente Jr *et al.*, 2022). Pre-clinical trials have also been conducted on cancer-based nanoparticle therapeutics, with most metallic nanoparticles coated in biocompatible molecules to further increase internalization instances to cancer cells (Zhang *et al.*, 2008).

2.7.Silver nanoparticles (AgNPs)

Silver nanoparticles (AgNPs) are small-sized silver solid particles (~1-100 nm), usually in the form of powder solids or suspended as a colloid. On a nano-solid scale, most nanomaterials including colloidal AgNPs have different properties when compared to their larger macroscopic counterpart. This has to do with how the atomic to sub-micron level where particle size affects mechanical and optical properties. Surface silver atoms have lesser bonds compared to multiple grains of silver crystallites, causing differences in thermodynamic-based properties such as instability. Moreover, at a quantum level,

nanoparticle clusters exhibit magnetic and semiconductor properties by sharing their outer electron band shell, whereas condensed solids are more inert due to their high energy stability (Roduner, 2006). Due to this, AgNPs have unique characteristics that can be utilized in a diverse range of applications such as in physics for their conductivity and optical properties or in the industrial sector for their catalytic activity and photothermal energy conversion (Galatage *et al.*, 2020).

AgNPs are becoming increasingly applicable as a nano-sized material in cancer research. Aside from their versatility in customization, AgNPs can be uptaken by cells through endocytosis, enabling the delivery of contrasting or therapeutic agents to cancer cells (Gomes *et al.*, 2021). In addition to being used as nanocarriers, AgNPs are capable of directly treating cancer cells as they possess inherent cytotoxic properties. This is related to the promotion of apoptosis pathways as well as ROS production that causes mitochondrial and genetic damage to cells (Yesilot and Aydin, 2019). Thus, AgNPs open the way for interesting and novel therapeutic methods against cancer cells, through the delivery of both therapeutic agents as well as the exhibition of synergistic activity in targeting tumorigenic pathway-related hallmarks.

2.7.1. AgNPs synthesis and modification

AgNPs can be synthesized or modified to tune inherent metallic properties and emergent colloid properties such as surface plasmonic resonance (SPR), thermal conductivity, size-shape morphology, zeta potential, and dispersion rate. AgNPs can be synthesized using a physical, chemical, or biological method (Vlasceanu *et al.*, 2016). The physical method uses mainly laser-ablation and temperature-based methods to separate silver solids into smaller nanoparticles or by condensing and evaporating dissolved silver ions into colloids. While there is minimal use of hazardous chemicals and the resulting size and shape could be customized by just modifying temperature, solvent used, or laser parameters, the lack

of uniformity, low AgNPs yield, and ineffective heat energy conversion make it ineffective for mass production (Zhang **B** *et al.*, 2016; Galatage *et al.*, 2020).

Chemical synthesis uses mainly redox reactions to convert metal ions into solid nanoparticles. In chemical synthesis, there are three components needed to form AgNPs which are: metallic precursors such as silver nitrate ($AgNO_3$) or silver citrate to form the metallic base, reducing agent to initiate reduction reaction on the solvent-dissolved metallic precursors, as well as stabilizing agent to cap and stabilize the formation of silver solids from degrading back into ions and unwanted products (Gamboa *et al.*, 2019). By combining all three components, both silver ions and small silver solid crystals will be reduced and nucleated into grains of silver solids which will grow by absorbing nearby silver ions (Figure 2.3). The advantages of using chemical synthesis are having a high yield and ease of synthesis compared to the other methods. On the other hand, most reducing and stabilizing agents used are toxic and may have adverse effects (Zhang **B** *et al.*, 2016; Vlasceanu *et al.*, 2016).

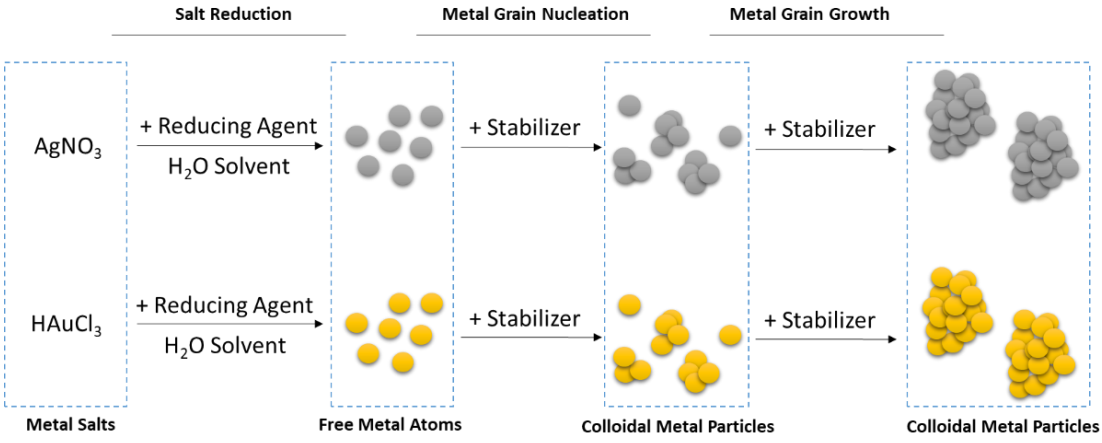

Figure 2.3 General mechanism of metallic nanoparticle synthesis from salt reduction, nucleation, and nanoparticle growth, adapted from Gamboa *et al.* (2019).

Capping agents, stabilizing agents, and reducing agents are studied for their ability to stabilize adequate morphological growth and AgNPs dispersal while exhibiting enough nanoparticle toxicity to target certain sites such as cancer cells (Javed *et al.*, 2020; El-

Nour *et al.*, 2010). Well-known reduction agents, such as sodium borohydride ($NaBH_4$), trisodium citrate, ascorbic acid, and hydrazine hydrate, as well as the presence of stabilizers such as polyvinylpyrrolidone (PVP), polyethylene glycol (PEG), and starch, can be used to customize AgNPs size and shapes. A combination of ascorbic acid as a reductant and sodium citrate for stabilizing nanoparticle synthesis was documented to result in near-spherical AgNPs with additional size tunability of nanoparticles by changing the pH of the reduction reaction (Qin *et al.*, 2010). By combining a very strong yet easily degradable hydrazine hydrate with stabilizer PVP, Gurusamy *et al.* (2016) were able to prepare stable biologically active AgNPs colloid. In another study, it was found by using the Turkevich Method where nanoparticles are formed using citrate reduction at around 100°C, increasing the reaction temperature to above 90-100°C resulted in a higher instance of ~60nm rod-shaped nanoparticles, compared to 60-80°C where most AgNPs formed were 30nm and spherical or irregular-like (Mazzonello *et al.*, 2017). The use of strong reducing agent $NaBH_4$ resulted in 4nm nanospheres and can be further supplemented with ascorbic acid and additional $AgNO_3$ to form nanowires or nanobars depending on their concentration and temperature (Gamboa *et al.*, 2019). However, $NaBH_4$ is also known to be highly toxic and can produce unwanted side effects due to its inherent strong reducing capability (Banne *et al.*, 2017; Zhang **B** *et al.*, 2016).

Biological synthesis uses biological system-mediated synthesis to synthesize AgNPs from silver precursors. Specifically, silver precursors are reduced in reactions within organisms such as bacteria, fungi, or plants (Galatage *et al.*, 2020). Another subset of biological synthesis called ‘green’ chemistry is by reducing silver or other metals in extracted biological-based metabolites, which sometimes are also considered to be under chemical synthesis. By utilizing ‘green’ chemistry, natural products can also be conjugated to AgNPs, with their biological activity incorporated into the nanoparticle for medicinal or therapeutic purposes. Another advantage of a ‘green’ chemistry-based

nanoparticle is its low-pollutant, eco-friendly process of producing AgNPs while resulting in a similar yield as conventional chemical synthesis (Zhang **B** *et al.*, 2016). In one study, extracted proteins from cyanobacterium *Oscillatoria limnetica* were able to synthesize spherical AgNPs from $AgNO_3$, with size distribution recorded to be around 3-17 nm (Hamouda *et al.*, 2019). Changes in extract pH, metal precursor-extract concentration, and reaction time greatly influenced the size and shape of the aforementioned nanoparticles. Hamouda *et al.* also noted that the resulting diversity was due to the electrochemical reaction occurring between each nanoparticle component.

Besides synthesis, modification to the AgNPs structure can be done to allow extrinsic properties such as low toxicity and drug loading capabilities to be appended. Such modifications include: changing the chemical composition in AgNPs, altering the physical structure of the nanoparticle, or attaching various other functional molecules that give specific activities (Zhang **B** *et al.*, 2016). By performing surface functionalization, synthesized and ready-made AgNPs could be designed to be biocompatible and nontoxic (Vlasceanu *et al.*, 2016). By conjugating fibronectin to the surface of AgNPs, Hung *et al.* (2021) showed biocompatible nanoparticles capable of facilitating growth, proliferation, and endothelial cell differentiation of Wharton's jelly-derived mesenchymal stem cells.

Surface functionalization also enables the fabrication of drug-delivering AgNPs by modification of their physical structure and chemical composition. Drugs or other cargo can be loaded to AgNPs by direct chemical conjugation to its surface, conjugation to its attached linker and coating agents, or encapsulation in nanoshell-like AgNPs. Anticancer drugs as well as other theranostic compounds can also be coupled to AgNPs during the synthesis of AgNP by conjugation in the presence of reducing and capping agents, which allows interaction between cargo with AgNPs, thus fully stabilizing the formation of drug-conjugated AgNPs solids as a drug delivery-capable nanocarrier (Gomes *et al.*, 2021).

2.7.2. AgNPs physicochemical properties and characterization

Synthesized and modified AgNPs are characterized in various parameters to determine the specification and features of each nanoparticle. Among the available characterization selection, AgNPs used for drug delivery can be characterized according to their morphology, electromagnetic properties and spectrum, surface-chemical composition, degradation rate, biocompatibility, polydispersity, and particle size distribution, as well as drug loading-release (Ivanova *et al.*, 2018; Gomes *et al.*, 2021).

Size-shape morphology is important for AgNPs as they can influence the toxicity and biodistribution of nanoparticles within organisms (Gomes *et al.*, 2021). The size and shape of each nanoparticle can be visualized by transmission electron microscopy (TEM) to view the structure and integrity of each particle while scanning electron microscopy (SEM) is used to visualize the surface of nanoparticles. In one study, TEM was used to determine the effect of pH on the size and shape of AgNPs formation where the particle size of quasi-spherical AgNPs was documented at a range of around 30-70 nm (Qin *et al.*, 2010); while another study reported size variation of 30 to 100 nm in SEM after synthesis using Burst method with sodium borohydride reduction agent (Banne *et al.*, 2017). Another piece of equipment that allows size-shape morphology characterization is atomic force microscopy (AFM) where the full 2D or 3D topography of viewed nanoparticles can be used for particle size distribution and uniformity determination. Visual results from TEM/SEM and AFM can also be complemented with characterization using dynamic light scattering (DLS) to determine the hydrodynamic size distribution of AgNPs suspended in colloids. By focusing light on the colloidal AgNPs, DLS can indirectly measure the dispersion rate of the nanoparticle as well as the uniformity of particle size in colloids (Gamboa *et al.*, 2019).

AgNPs surface properties must be characterized to determine the effectiveness of AgNPs delivery as well as the composition as well as confirmation of synthesized target

nanoparticles. Among some surface properties, several important properties used in the biomedical field are surface charge potential which is measured with zeta potential, surface chemical composition analyzed using multiple different characterizations, and binding structure or functional group. Surface charge potential relates to the stability of AgNPs in dispersed colloidal form, where the surface electrical charge contributes to repelling or attracting nanoparticles. The surface chemical composition of AgNP can be analyzed using X-ray diffraction (XRD), X-ray photoelectron spectroscopy (XPS), nuclear magnetic resonance (NMR), and mass spectrometry (MS). XRD is used to identify the crystalline phase in AgNPs, with sharp Bragg's peaks indicating crystalline structure while broad peaks indicating amorphous structure. XPS is used to identify elemental silver and other compounds, where pure silver elements can be detected under 368.2 eV binding energy at region Ag3d (Gamboa *et al.*, 2019). Surface chemical binding and functional group conjugation can be analyzed using Fourier transform infrared (FTIR) spectroscopy and surface-enhanced resonance Raman scattering (SERS) or Raman spectroscopy. Both FTIR and Raman spectroscopy detect absorbed or emitted IR radiation which tells the molecular vibration of a nanoparticle, with FTIR measuring changes in dipolar moments, whereas Raman measures polarizable moments (Gamboa *et al.*, 2019). Functional groups of AgNPs and binding molecules can be scanned broadly in FTIR from 4000-500 cm^{-1}, whereas functional groups of AgNPs can be scanned broadly in Raman spectroscopy from 2000-800 cm^{-1} Raman shift (Matsumoto *et al.*, 2022).

Another important characteristic notable for metallic nanoparticles especially AgNPs is in the form of optical and electronic properties which forms a phenomenon called surface plasmon resonance (SPR). In principle, due to the energy state of the dispersed AgNPs, their electrons could oscillate in resonance when excited externally, primarily by light. The radiation would be partially absorbed by the electron shells and could be inverted into a different energy or the radiation could be redirected (Roduner, 2006). As a result,

colloidal AgNPs would exhibit unique color and differing light-absorbing capabilities depending on their customizations like size (Agnihotri *et al.*, 2014), concentration, surface functionalization, and reaction time (Fu *et al.*, 2021) as well as various external environments such as pH (Anigol *et al.*, 2017). SPR can be characterized using UV-visible (UV-vis) spectroscopy broadly around wavelength 300-800 nm, with AgNP presence-associated peak found generally at 400-450 nm.

2.7.3. AgNPs toxicity and mechanism of action in cancer cells

The mechanism of action of the cytotoxic activity of AgNPs is not yet fully understood, but it is widely known that AgNPs can produce oxidative stresses in cells as well as inhibit multiple carcinogenic-associated pathways (Zhang **B** *et al.*, 2016). Besides the generation of ROS and subsequent DNA as well as organelle damage, AgNPs are also known to cause cell membrane leakage by chemically altering its structure and permeability, which has been documented to occur in some bacterial cells (Lee and Jun *et al.*, 2019) (Figure 2.4).

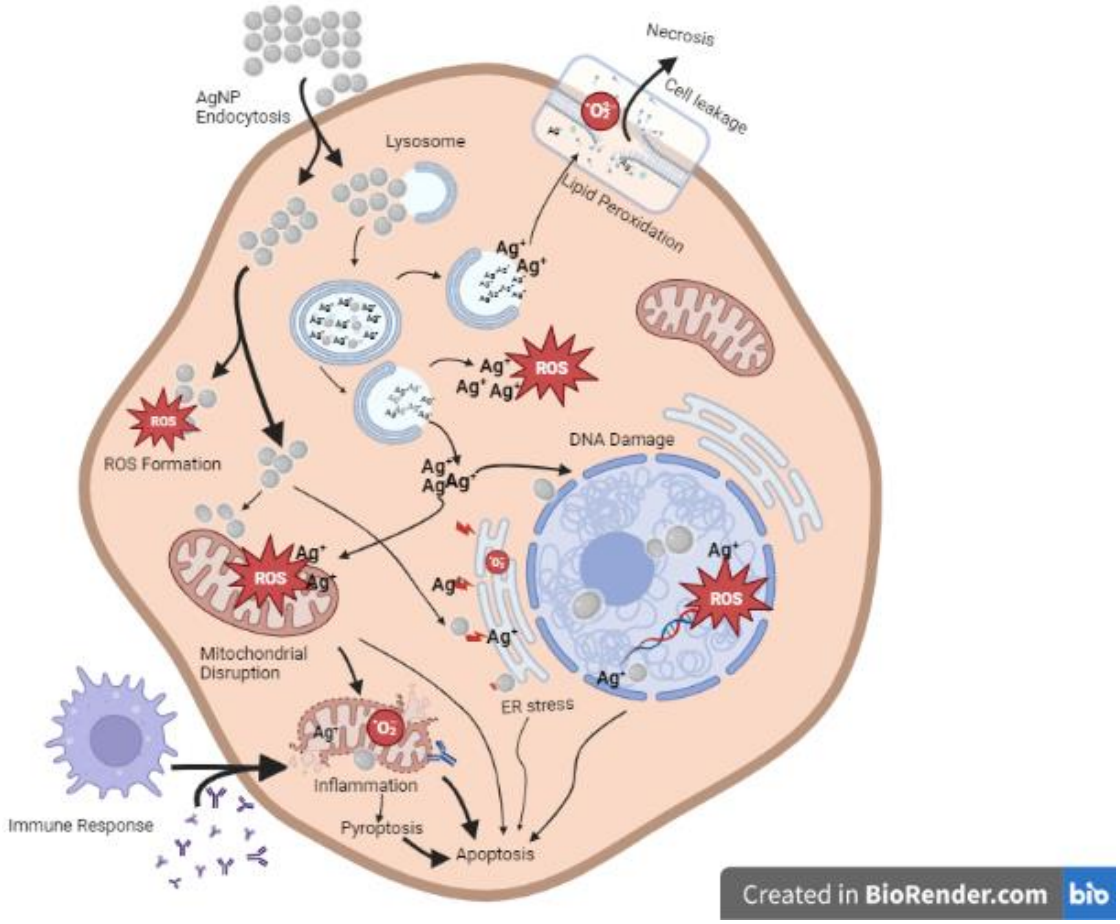

Figure 2.4 Possible mechanisms of AgNP-induced cytotoxicity in cancer cells, adapted from Zhang **B** *et al.* (2016); Lee and Jun (2019); and Yesilot and Aydin (2019). The image was created with BioRender.com

Passively and actively targeting AgNPs are first taken up by cells which would then lyse the cells from within, causing the mechanism of cellular uptake of AgNPs to be referred to as a "Trojan-horse" type mechanism (Kovács *et al.*, 2022). AgNPs can be internalized via endocytosis or direct penetration, which are then localized in the cytoplasm or nearby vital organelles such as mitochondrial and endoplasmic reticulum (ER). The AgNPs would then inhibit ER and mitochondrial-localized enzymes and growth factors associated with anti-apoptosis, angiogenesis, and cell proliferation (Zhang **A** *et al.*, 2016). Yang *et al.* (2016) reported downregulation of VEGF-A and GLUT-1 protein in HUVEC and MCF-7 cells after being treated with 100 µg/mL AgNPs, suggesting anti-angiogenesis and antiproliferation activity.

Related to apoptosis pathway cascade and oxidative stresses, another cytotoxic mechanism associated with AgNPs is cell cycle arrest and DNA damage. Internalized AgNPs by endocytosis are directed to lysosomes to be degraded, causing dispersion into reactive Ag^+ ions which increases ROS amount in cells resulting in DNA damage (Kovács *et al.*, 2022). The reactive ions are localized in mitochondria disrupting the electron transport chain in metabolism which results in mitochondrial respiration failure, generating free oxygen radicals that are reactive and damaging to surrounding proteins and DNAs. The resulting oxidative stresses would spread to nearby organelles and eventually trigger a cascade of pro-apoptotic proteins (Talarska *et al.*, 2021). In one study, AgNPs increased the upregulation of pro-apoptotic protein Bax as well as an increase of detected LDH in rat neural stem cells, resulting in increased generation of ROS and apoptosis instances in cells (Liu *et al.*, 2015).

It was recently found that intact endocytosed AgNPs which were unable to be lysed and directly entering AgNPs would enter a different cytotoxic pathway compared to its reactive cation Ag^+. In one study, silver ions were verified to mediate apoptosis and ROS generation in the form of H_2O_2, whereas cytotoxicity in non-degraded AgNPs was more attributed to necrosis and lipid peroxidation. Both silver products were also found to induce proteotoxicity, with protein oxidation in multiple organelles found after treatment (Rohde *et al.*, 2021). This indicates that one of the main modalities of AgNPs' cytotoxicity stems from its reactive oxidation and lipid peroxidation, which can cause both necrotic and apoptotic cell death simultaneously depending on the degradation rate of AgNPs.

Aside from initiating apoptotic and necrotic pathways, AgNP-induced oxidative stresses also contributed to immunomodulation, in the form of inflammatory protein markers activation. Pyroptosis pathways are induced by the activation of caspase-1 as well as the activation of inflammasome complexes and several cytokines (Zhang **A** *et al.*, 2016). In one study, spherical albumin-coated AgNPs were able to stimulate increased levels of

multiple white blood cells in LACA albino mice, with around 5x fold significant increase of leucocytes, lymphocytes, and granulocytes at 9-10 mg/kg dose due to toxicity. Necrosis spots were seen in liver, spleen, and kidney cells exposed to albumin-AgNPs with 9 and 10 mg/kg doses, while little to no detrimental effects were seen in cells exposed to AgNP doses lower than 9 mg/kg. Fibrosarcoma tumor tissues in mice were found to generate twice the ROS when administered 4 mg/kg albumin-AgNP and levels of tumor-associated cytokines in tissues such as IL-6, IL-1β, and TNF-α were also found to be significantly reduced (Chakraborty *et al.*, 2016).

Physicochemical properties as well as changes also contribute to cytotoxic modulation in AgNPs against cancer cells, as demonstrated by Hamouda *et al.*, (2019). They reported that the spherical AgNPs synthesized using proteins from *O. limnetica* resulted in strong anticancer activity against MCF-7 breast cancer cells as well as antibacterial activity against MDR bacteria.

Despite the apparent anticancer-associated activity exhibited, due to its non-specificity in targeting pathways and cells, a large dose of AgNPs can cause systemic toxicity and off-targeting (Kovács *et al.*, 2022). In addition, the size of AgNPs also affects the apoptosis-inducing capability of nanoparticles, leading to variations in biodistribution and local toxicity in vital excretory organs (Talarska *et al.*, 2021).

2.8.Gold nanoparticles (AuNPs)

Gold nanoparticles (AuNPs) are 1-100 nm-sized metallic nanoparticles made from gold that can be used for imaging, diagnostics, as well as for therapy in the biomedical field due to their properties and versatility (Carvalho *et al.*, 2019). Similar to AgNPs, AuNPs exhibit several emergent properties due to their size, in the form of optical, magnetic, and electronic properties (Roduner, 2006). Because of this, AuNPs are capable of being used as a colorimetric analytical assay (Iriarte-Mesa *et al.*, 2020), radio imaging, photoacoustic

monitoring (Her *et al.*, 2017; Dreaden *et al.*, 2014), and photothermal as well as photodynamic therapy (PTT/PDT), in which AuNPs absorb focused light at a certain wavelength range and heat cancer cells to denature them or cause ROS generation which can damage DNAs (Ahmad *et al.*, 2020).

2.8.1. AuNPs synthesis and surface modification

As in the case of AgNPs, AuNPs can be categorized into physical, chemical, and biological or 'green' synthesis. In physical synthesis, AuNPs can be fabricated using external forces such as ultrasonic waves, laser ablation, and microwaves to transform bulk gold into nanopowders (Sztandera *et al.*, 2019. Besides, AuNPs can be made by the reduction of Au ions into AuNPs using photochemistry in UV and IR or electrochemistry (Sani *et al.*, 2021).

One of the most common chemical synthesis methods used and studied, aside from 'green' chemistry, is a reduction chemical synthesis (Figure 3) called the Turkevich method, in which chloroauric acid ($HAuCl_4$) or other gold-bearing salts are reduced by reducing and stabilizing agents, usually trisodium citrate in water-boiling temperature (Sztandera *et al.*, 2019). Another method called the Brust method uses organic solvents and water as the phase-transferring medium for gold salts, with tetraoctylammonium bromide used as the catalyst as well as $NaBH_4$ as a reducing agent. The dissolved gold ions would be transferred from water to the organic solvent which results in catalysis and reduction of AuNPs (Iriarte-Mesa *et al.*, 2020). Another method called seed-mediated growth is more advanced in that it is used to grow nucleate seeds from irregular or spherical into different geometrical shapes such as elongated rods (Amina and Guo, 2020). Several parameters such as concentration of reducing agents, presence of stabilizing agents, and environmental conditions can be changed to produce AuNPs with different sizes and shapes (Sani *et al.*, 2021).

Recently, ‘green chemistry’ as well as the biological synthesis of AuNPs have been studied to produce environmentally friendly and non-toxic AuNPs, by using natural products as reducing and stabilizing agents or introducing gold salts to organisms for jump-starting reduction reactions respectively (Sztandera *et al.*, 2019). Algae and bacterial microbes, fungi, as well as plants have been documented to mediate AuNPs synthesis (Sani *et al.*, 2021). In one study, AuNPs were biosynthesized in mycorrhizal fungus *Tricholoma crassum* extract which resulted in spherical, extract protein-capped AuNPs which was used for delivering genes to Sarcoma180 cells (Basu *et al.*, 2018).

Size-shape morphology, as well as the surface charge of AuNPs, have been shown to affect AuNP toxicity, thus modification can be done to increase or reduce the toxicity of AuNPs (Wozniak *et al.*, 2017). Surface modification can be done to apply various beneficial properties, such as using hyaluronic acid as an organic surface coating to increase biocompatibility by reducing thrombosis or functionalizing PVP to nanoparticles to increase hydrophilicity (Wyman, 2012). The surface of most nanoparticles could be functionalized by different types of polymer linkers, hybridized DNAs, proteins, cell membranes, or inorganic chemicals such as metals and ceramic coatings (Pinelli *et al.*, 2020). While coating agents and linkers are used interchangeably due to both being functionalized or modified to nanoparticles, linkers are more used as a surface modification to bridge or link between carrier nanoparticles and their target ligands, either as cargo in passive targeting or as a tracking agent for active targeting (Rahme and Dagher, 2019).

For metal-based nanoparticles, these surface modifications are mostly used to increase targeting efficacy, the overall stability of the colloid or solid system, biocompatibility of nanoparticles, improve mechanical properties like toughness and yield strength, as well as to provide spaces for ligands to anchor themselves to the vehicle (Umut, 2013). For AuNPs, functionalization could be done to tone down the cytotoxicity of some shapes,

for instance, large nanospheres as well as to increase nanoparticle circulation time in the bloodstream using coating agents and linkers made of biocompatible and biodegradable polymers (Guo *et al.*, 2015; Mohd-Zahid *et al.*, 2020). While gold particles are naturally inert and have a relatively good permeability due to their chemical composition, they can be further functionalized with biocompatible molecules and cell penetrants to increase the probability of cancer cell internalization, especially on MDR cancers (Martinelli and Biglietti, 2020; Madani *et al.*, 2011).

Aside from direct therapy and diagnostic lab assays, AuNPs can be used as a vehicle to deliver therapeutics or contrast agents for imaging and biomarker diagnosis. By taking advantage of the inherent 'stealth-like attribute, researchers could fabricate an effect called enhanced permeability and retention (EPR) which is primarily used as a mechanism for most passive targeting in drug delivery systems (Pinelli *et al.*, 2020). A hybrid delivery system in the form of encapsulation in another nanoparticle may also be done as a means of protection for both cargo and the primary vehicle (Rhim *et al.*, 2008). By encapsulating the AuNP-pDNA complex in liposomes, system stability, and transfection efficiency increased despite higher concentrations of lipid layer to lower its cytotoxicity. Other polymers may also be used to coat the AuNPs in a method called Layer-by-layer (LbL), in which differently charged polymers coat the surface of a particle in thin films several times to create layers and load drugs or genes to the gap between each layer (Guo *et al.*, 2010; Lee *et al.*, 2011). By adding multiple layers of poly-L-lysine (PLL) known to be highly degradable, Lee *et al.* (2011) were able to fabricate a progressively degrading nanoparticle to gradually trigger the release of siRNA.

For drug delivery, one well-known method for AuNPs functionalization due to its simplicity is by conjugating thiol-containing (SH–) chemicals to form partial electrostatic-covalent bonds made out of S-Au, which can allow drug loading and release (Her *et al.*, 2017; Ding *et al.*, 2014; Ajnai *et al.*, 2014). Au-S bonding may also be used

as an anchoring mechanism for different types of polymers for surface coating as well as for carrying target ligands (Umut, 2013). Khutale *et al.* (2017) employed thiolated PEG as a foundational linker to AuNPs for increasing colloidal dispersion stability which could be extended with anticancer drug-carrying dendrimer; while Yeom (2013) utilized thiolated DNA oligonucleotides for conjugating mRNA cargo to spherical AuNPs towards HeLa cells and *in vivo* studies on mice models. In another study, synthesized nanorods were attached with partially thiolated PAMAM dendrimers and further functionalized with tumor-targeting peptide GX1 for a combinational therapy using PTT as well as gene therapy (Ye *et al.*, 2021).

2.8.2. AuNPs physicochemical properties and characterization

As metallic nanoparticles, AuNPs are similar to AgNPs in that they can be uniquely shaped (rods, prisms, spheres). Other important physicochemical properties related to toxicity and drug delivery, besides size-shape morphology, include chemical composition, surface charge and stability, and dispersion rate. Another crucial characteristic that made them useful in diverse fields of study is light-heat conversion in SPR. As a result, colloidal AuNPs would exhibit unique color and differing light-absorbing capabilities depending on their customizations like size (Guo *et al.*, 2015), shape, and surface functionalization (Wang *et al.*, 2020) as well as various external environmental factors such as temperature and pressure (Iriarte-Mesa *et al.*, 2020). Surface plasmonic bands can be read using UV-vis spectroscopy at 500-1600nm, with an absorbance peak corresponding to spherical AuNPs found at ~520 nm, and more advanced size and shape can be found in higher wavelengths (Sztandera *et al.*, 2019).

For morphology and particle size distribution, several characterization methods could be performed, for instance: DLS for colloid dispersibility and hydrodynamic diameter, TEM, as well as SEM visualization. As mentioned earlier, the size of AuNPs could range from ~2 nm to up to 100-200 nm (Bao *et al.*, 2015; Steckiewicz *et al.* 2019). Surface potential

and aggregation or colloidal stability could be characterized in AuNPs using DLS as well as zeta potential measurements (Ke *et al.*, 2017; Ielo *et al.*, 2021).

Other characterization in terms of surface modification and chemical composition can be performed in the same as characterization for AgNPs, which has been written in Subsection 2.7.2. regarding the characterization of AgNPs. For FTIR spectra, AuNPs could be observed and analyzed starting from 400-4000 nm wavenumber (Sobczak-Kupiec *et al.*, 2011). XPS spectroscopy could be performed to view elemental Au under 95-80 eV binding energy at region Au4f (Oliveira *et al.*, 2021; Jiang *et al.*, 2001). Other specific properties related to degradation and composition such as thermal stability, resistance to environmental oxidation, and synthesis purity of AuNPs can also be tested using thermogravimetric analysis (TGA), where AuNPs would be subjected to pyrolysis (Ielo *et al.*, 2021).

2.8.3. AuNPs toxicity and mechanism of action in cancer cells

AuNPs can be considered unique in that they are still able to retain inertness in colloidal nanoparticle form, which made it possible for stealth-like AuNPs to be used for drug delivery. However, some studies are contradictory to this statement, as size and shape can directly affect AuNPs toxicity by increasing cell uptake and biocompatibility. By modifying the AuNPs seeding and synthesis procedures, Woźniak *et al.* (2017) were able to form multiple shapes of AuNPs, including nanospheres, nanorods, nanoflowers, nanostars, and nanoprisms. Each AuNPs shape exhibits varying cytotoxicity levels, with spherical and nanorods showing stronger WST-1 reduction in higher incubation time and concentration compared to other shapes on HeLa and HEK293; while the more anisotropic-shaped AuNPs were more successfully internalized by cells and behaving less toxic. On the contrary, Steckiewicz *et al.* (2019) reported that nanostars at around 200 nm were the most cytotoxic via induction of apoptotic pathways whereas nanospheres at approximately 6 nm were the least cytotoxic. This suggests that shape and size alone

would not be significant enough to modulate AuNPs toxicity, with other factors such as functionalized ligands and coatings also playing an equal or perhaps larger role.

Size has a significant impact on altering the toxicity of AuNPs. Small and ultra-small particles from 1-5 nm were suggested to be highly toxic due to their ability to further penetrate the nucleus and bind with the chromosomes (Bao *et al.*, 2015; Zamora-Justo *et al.*, 2019); while 10-200 nm are more preferable to pass cell membranes (Shah *et al.*, 2014; Dreaden *et al.*, 2014). This was likely due to the low surface area-to-volume ratio in large-sized AuNPs which in turn decreased their surface bioactivity towards cells (Sani *et al.*, 2021). However, in some cases, small AuNPs sizes would be a better alternative for *in vivo* studies as their size enabled longer circulation time on model animals and higher biodistribution in the bloodstream at a cost of localized toxicity to organs related to detoxification and excretion such as spleen, kidneys, liver, and intestines (Schmid *et al.*, 2017; Ajnai *et al.*, 2014).

While the exact mechanisms of AuNPs cytotoxicity are not yet fully understood, there have been reports on AuNPs causing inhibition of angiogenesis, induction of inflammatory responses, genotoxicity, cell cycle arrest and apoptosis, necrosis, as well as autophagy. There was evidence suggesting that one of the main mechanisms of action for AuNPs toxicity, was oxidative stress generation (Figure 2.5). In a study conducted by Daei *et al.* (2021), 20nm citrate-stabilized AuNPs were able to increase ROS production in bladder cancer 5637 cells, with highly elevated expression of Bax proteins and activity of caspase-3 as well as caspase-7, suggesting apoptosis. However, the authors found that the apoptosis state and antiangiogenic activity caused by AuNPs were different in other reported cell lines, thus concluding that cell-type difference might also play a role.

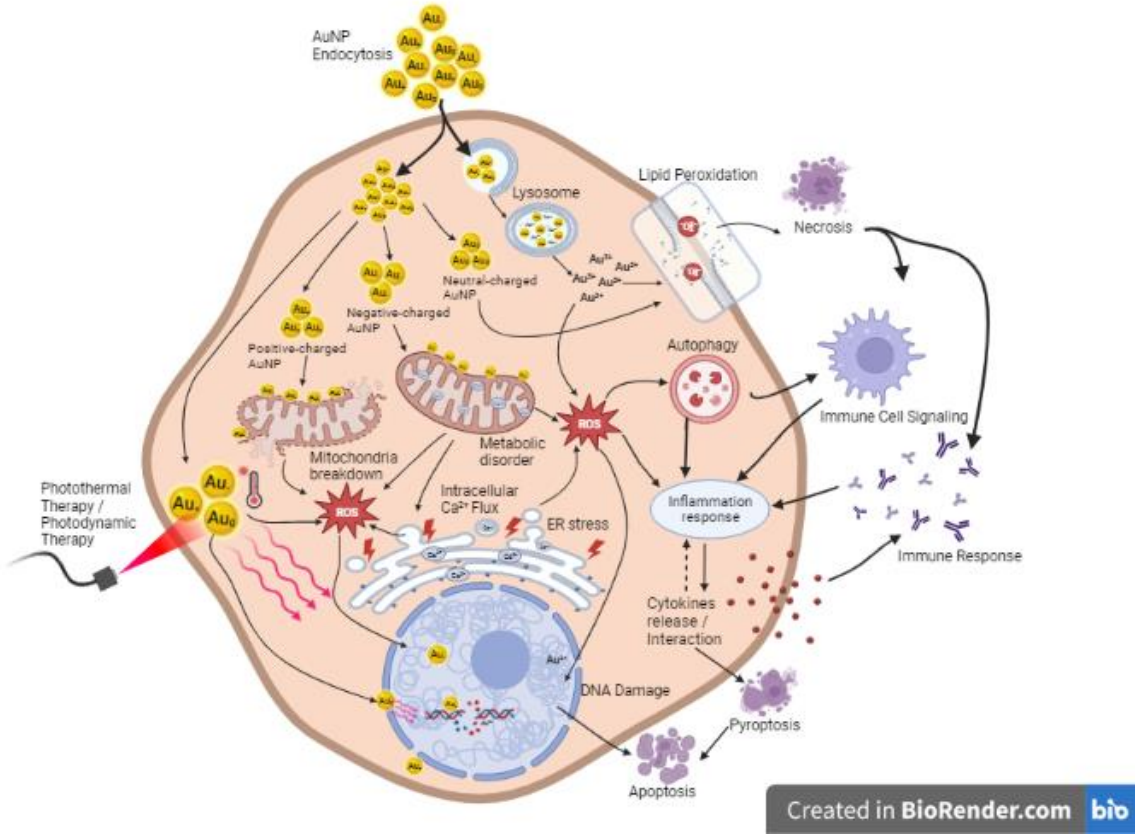

Figure 2.5 Toxicity mechanism of differently-charged AuNPs and Au^{3+} ions in cancer cells, adapted from Schaeublin *et al.* (2011) and Sani *et al.* (2021). The image was created with BioRender.com.

Another possible mechanism of AuNPs toxicity, aside from ROS generation, is protein corona formation. While Au ions can cause ROS production, AuNPs on their own are also a main contributor to free radical formation. AuNPs have some affinity to bind with proteins and DNAs due to their surface charge properties and the affinity of Au as an element towards amines as well as thiol groups (Sani *et al.*, 2021). Small-sized AuNPs could form covalent or partially covalent bonds with DNA, resulting in DNA or protein damage as well as subsequent denaturation and cell cycle arrest, as seen in Figure 2.5. It was suspected that some of the toxicity caused by AuNPs such as angiogenesis inhibition and cytoskeletal disruption was associated with these AuNP-protein interactions, as seen in the binding of AuNPs with VEGFA and heparin-binding VEGF165 growth factor and (Daei *et al.*, 2021; Sztandera *et al.*, 2019).

Surface charge as a physicochemical property also played a role in modulating toxicity as it is related to the affinity of Au towards certain functional groups, thus it is necessary to decide on coating and stabilizing agents for AuNPs, as mentioned before (Umair *et al.*, 2016; Guo *et al.*, 2015). Schaeublin *et al.* (2011) proposed the mechanism of cell death of differently charged AuNPs, where AuNPs were able to bind with the mitochondria through thiol-based surface charge binding. It was proposed that positively charged AuNPs would disrupt the mitochondrial membrane and result in apoptosis by mitochondrial outer membrane permeabilization (MOMP), whereas negatively charged AuNPs disrupted mitochondrial membrane potential which caused effluxion of Ca^{2+} ions and apoptosis induction (Figure 2.5). Interestingly, neutral-charged AuNP did not result in apoptosis but caused necrosis of HaCaT cells.

2.9.Graphene oxide (GO)

Graphene oxide (GO) is a carbon-based material that belongs to the graphene-family nanomaterials, with a size range of around 1-100 nm and a thickness of <10nm (Ou *et al.*, 2016). Structurally, GO is two-dimensional (2D) and made out of single-layered, planar carbon crystals arranged in a honeycombed array, with some presence of oxidized carbon atoms found randomly (Ou *et al.*, 2016). The oxidized functional groups in GO are differentiated according to where in GO the oxidation is occurring, such as epoxides (-O-) and hydroxyls (-OH) on its basal planes as well as carbonyls (C-O) and carboxylic (-COOH) groups decorating the edges of the GO plane, as seen in Figure 2.6 (Munoz *et al.*, 2019). Similar to graphene, GO can form interactions between aromatic hexagonal molecules and π electrons in the hexagonal ring of the GO basal plane. This results in π-π stacking, where GO appears to be conjugated or stacked on top of the other molecules and may lead to larger sandwiching molecules, as in the case of graphite and graphite oxide which are just multi-layered graphene or GO stacked one onto another (Liu *et al.*, 2021). However, due to their strong π-π bonds, graphene tends to conjugate with each

other, causing insolubility in water. On the other hand, GO can form dispersed colloids in water-based solvents because of its high hydrophilicity caused by its mostly polar functional groups, for example, carboxyls and hydroxyls (Munoz *et al.*, 2019).

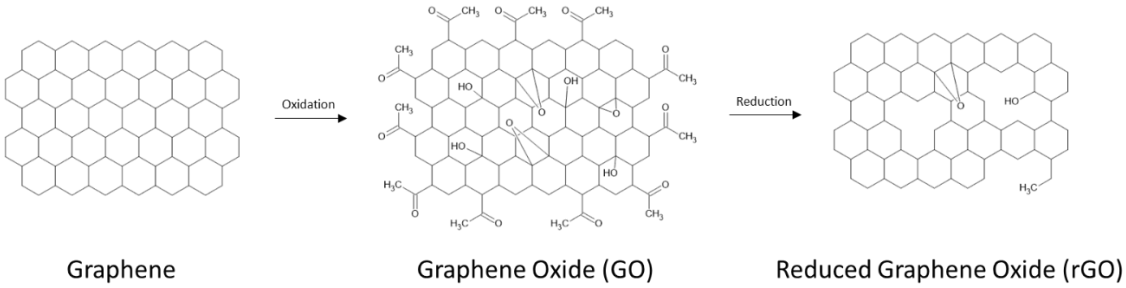

Figure 2.6 Comparison between graphene, graphene oxide (GO), and reduced graphene oxide (rGO), adapted from Munoz *et al.* (2019). In GO, carboxyls are located on the edges while epoxides and hydroxyls are located in the center or basal plane

2.9.1. GO Synthesis and modification

There are broadly speaking two main methods of GO synthesis, which are called 'bottom-up' and 'top-down'. 'Bottom-up' refers to the construction of graphene-based molecules from simple carbon compounds, while 'top-down' refers to the breakdown of multi-layered graphene or similar structures into single layers. As most 'bottom-up' methods such as chemical vapor deposition are known to have low time and yield efficiency, GO is more often produced using 'top-down' methods (Smith *et al.*, 2019). Among the 'top-down' methods, one conventional method is based on Brodie's, Staudenmaier's, and Hummers'-Offeman's methods; where graphite sheets are oxidized using a combination of acids and oxidizing agents to make graphite oxides which would then be separated into single-layered GOs (Rhazouani *et al.*, 2021).

The "Hummers and Offeman" method uses sulfuric acid, sodium nitrate, and potassium permanganate; which would then be added with hydrogen peroxide to oxidize graphite into graphite oxide. The resulting graphite oxides would then be exfoliated using

sonication to fully disperse the layers into individual sheets of GO or GO precursors (Rhazouani *et al.*, 2021; Priyadarsini *et al.*, 2018). The "Hummers and Offeman" method can be further modified for studies according to the functionalization or GO specification, with the resulting method called "Modified or Improved Hummers". The steps of the 'Modified or Improved Hummers' are the same as before, with changes done on the type of protonated solvent or acids (in the form of sulfuric acid, phosphoric acid, or a mixture of both), parameter values such as mixing temperature and duration, presence of sodium nitrate, as well as the used concentration of hydrogen peroxide for metal ion removal (Smith *et al.*, 2019).

Functional groups in GO can be further reduced so that most of its oxygen-based functional groups are taken out. Due to its high surface reactivity from the oxygen functional group in the basal plane, GO sheets can be transformed into reduced GO (rGO) which contain far fewer groups on the edges and basal planes. Transformation to rGO can be done thermally where GO is heated directly or with wave irradiation, chemically where reducing agents such as hydrazine hydrate or $NaBH_4$ is used, or a combination of thermal and chemical methods (Dideikin and Vul, 2019). rGOs are more resilient in terms of mechanical strength and wear, conductivity, and dispersibility in solvents as well as between sheets (Smith *et al.*, 2019).

GO can be functionalized by modification on their basal planes as well as on the edges, where there are oxygen-based moieties present. Some ligands and polymers may bind covalently to the functional groups or other noncovalent functionalization such as Van der Waals forces, ionic bonds, hydrogen bonding, hydrophobic interactions, or London forces. Most molecules are functionalized or loaded to GO by utilizing its strong π-π bonds, usually with polycyclic molecules or aromatics (Munoz *et al.*, 2019). In one study, π-π stacked curcumin-GO was functionalized with polyethylene glycol (PEG) polymer on the carboxyls for biodistribution as well as for pH-controlled drug release (Charmi *et*

al., 2019). In another study, sulfonated nanoscale GO functionalized with folic acid was able to deliver Doxorubicin and Camptothecin to MCF-7 cells by π-π stacking (Zhang *et al.*, 2010).

2.9.2. GO physicochemical properties and characterization

In the biomedical field, GO needs to possess several key properties to be used for drug delivery. Some of these characteristics are related to chemical composition as well as its morphology, while some are directly linked with biocompatibility and toxicity. Properties associated with composition and structure can be characterized using various optical and radiological approaches such as AFM, solid-state nuclear magnetic resonance (ssNMR), and UV-vis spectroscopy to measure GO particle size, specific surface area, hydrophilicity, and presence of functionalization (Rhazouani *et al.*, 2021; Dideikin and Vul, 2019).

Physical properties in GO relevant to biomedical studies, especially drug delivery, are particle size, size distribution, lateral dimension, and thickness. The dimensions of GO sheets can be observed and analyzed using TEM, SEM, DLS, and AFM. Generally, individual GO sheets have 1-10 nm thickness and a lateral size ranging from 500 nm – 50 μm. TEM and SEM are also useful to observe the structure and possible functionalization occurring in the sheet (Rhazouani *et al.*, 2021).

The chemical composition of functionalized GO as well as its structure can be analyzed using Raman spectroscopy, FTIR spectroscopy, ssNMR, XRD, and XPS. Raman spectroscopy can be performed from 1200-3000 cm^{-1} for GO, with two broad peaks found for the D band or the disordered crystal structure phase vibration (carbon sp^3 at ~1350 cm^{-1} Raman shift), G band or ordered crystal structure (carbon sp^2), and 2D band or stacking order of graphene planes(harmonic step from D band) with Raman shift at ~1350 cm^{-1}, ~1580 cm^{-1}, and ~2700 cm^{-1} respectively. In FTIR, functionalized group and their

bonds can be analyzed in GO from wavenumber 4000-400 cm^{-1}. ssNMR of GO can analyze functional groups found in GO from chemical shift 200-0 ppm, with the more apparent peaks found in ~80-60 ppm for C-OH and C-O-C, as well as ~140 ppm for C-C sp^2 (Rhazouani *et al.*, 2021). XPS spectra of GO will yield 2 peaks, which correspond to the O1s element on binding energy ~530-520 eV and C1s on binding energy 300-280 eV (Aliyev *et al.*, 2019).

Other important characteristics of GO include thermal stability as well as SPR. TGA tests the thermal stability of GO as well as the quantity of oxygen-based moieties by pyrolytic degradation, where mass loss percentage over GO would significantly increase over the increase of temperature when compared with graphene as well as low-oxygen functionalized graphene-family nanoparticles which would not lose too much mass (Aliyev *et al.*, 2019; Rhazouani *et al.*, 2021). While SPR in GO is not as pronounced as in AgNP and AuNP, the UV-vis spectrum could be analyzed at wavelength ~200-800 nm, where peak absorbance would occur at ~230-270 nm. Increased oxidation in GO would shift the absorbance peak to a lower wavelength and higher absorbance value, with observed GO colloid color also changing depending on GO dimension as well as oxidation levels (Emiru and Ayele, 2017; Lai *et al.*, 2012).

2.9.3. GO toxicity and mechanism of action in cancer cells

In terms of toxicity, there are contradicting reports on whether GO is toxic. However, some studies have shown that high doses of GO exhibit cytotoxicity and apoptosis induction toward cell models, including cancer cells (Rhazouani *et al.*, 2021). While GO can be used to treat cancer directly or for delivering drugs, GO is considered toxic mostly due to its high oxygen composition, size, as well as their surface charge (Liu *et al.*, 2021). GO and other graphene derivatives can induce acute and chronic toxicity by activating inflammatory responses within the system. GO can also result in hemolysis towards erythrocytes and various white blood cells (Ou *et al.*, 2016).

Several possible mechanisms of GO cytotoxicity have been studied, with the majority of mechanisms related to apoptosis, necrosis, and pyroptosis pathways (Figure 2.7). These mechanisms were largely associated with the size of GO, its functional groups, ionic impurities intercalated within GO such as mutagenic Fe^{2+}, and protein-GO interaction which forms protein corona that interrupts protein function. GO can increase ROS generation within cells, which would lead to mitochondrial damage, DNA damage, and inflammatory responses. By producing oxidative stresses, DNA damage-related cytokines are expressed which triggers further apoptosis signaling as well as inflammatory responses (Rhazouni *et al.*, 2021; Ou *et al.*, 2016). Jaworski *et al.* (2014) found that GO and rGO increased the expression of caspase-3 protein and ROS formation in U87 and U118 cells, suggesting apoptosis induction. However, it was also found that GO was less toxic than rGO as there was no apparent necrosis found in r-GO-treated cells.

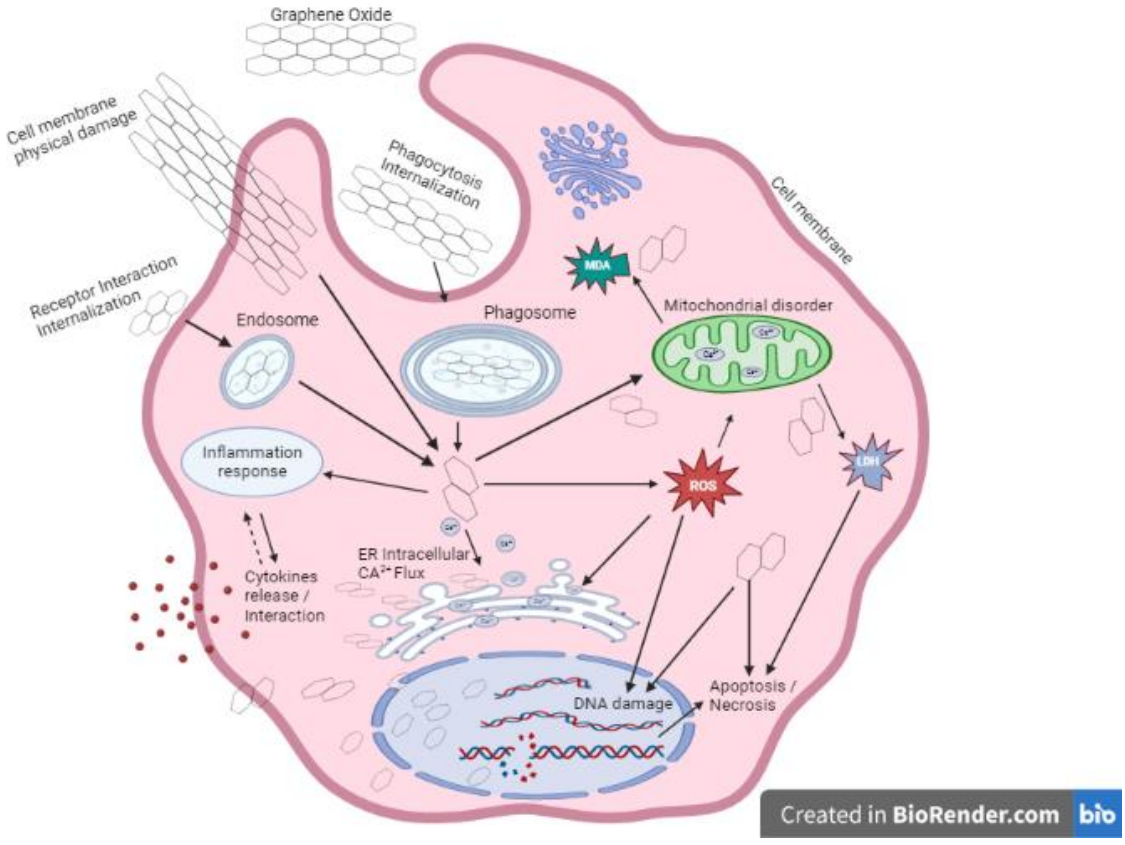

Figure 2.7 A schematic representation of the possible toxicity mechanisms caused by the GO, adapted from Ou *et al.* (2016). The image was created with BioRender.com.

Endocytosed GO can trigger a non-apoptotic cell death in the form of cellular self-degradation, called autophagy. In autophagy, proteins such as Beclin 1 and LC3 activate the autophagosome complex which will degrade organelles within the cell. GO was also documented to elevate the intracellular Ca^{2+} in the cytoplasm and other organelles, which prompts autophagy, LDH leakage, mitochondrial dysfunction, as well as necrosis (Ou *et al.*, 2016). In a study conducted by Shen *et al.* (2022), it was found that GO increased ROS generation which induced apoptosis as well as upregulating expression of AMPK/mTOR/ULK1 proteins, leading to autophagy in HCT116 colorectal cancer cells.

GO toxicity is also associated with epigenetic regulation in cells due to its behavior in enhancing ROS formation. While the exact mechanism is still not well known, GO indirectly triggers gene silencing and also interferes with protein post-translational modification. It was reported that conjugated GO was able to upregulate DNMT3B genes, causing DNA hypermethylation and changing chromatin structure, silencing multiple gene regions (Ou *et al.*, 2016).

Another possible unique mechanism related to the morphology of GO is physical disruption. Due to its physical structure, GO and pristine graphene as anticancer nanomaterial can damage cells using their ‘blade-like single-layer shape by forming hydrophobic interactions with cell membranes. As mentioned earlier, GO can form protein corona with receptor proteins as well as cytoskeletons, enabling GO to direct insertion into the cell membrane. Similar to how it behaves in bacteria, the protein interaction results in cleavage in various membranes as well as organelles, causing intracellular leakage. (Ou *et al.*, 2016).

Due to cytotoxicity in GO being associated with its structure, modulation of cytotoxicity could be performed by GO structure modification (Ou *et al.*, 2016). An example of this was using UV-B irradiation to modify the structure of GO as reported by Simon *et al.* (2021). In their study, UV-B irradiation at 10 minutes in high energy at around 5-50

mJ/cm^2 resulted in a more reduced form of GO where most of the oxygen-containing moieties were gone from the basal plane as well as corners. Since it was also found that UV-B irradiation resulted in apoptotic death in breast cancer cells MCF-7, they compared the combination of GO-UV against single component GO or UV-B toxicity and revealed that synergistic activity was seen throughout UV-B irradiated GO treatment. Another study done by Gallegos-Perez *et al.* (2020) used UV-A irradiation on GO at higher energy irradiance at 37-74 μW/cm^2 for 72h and 120h to evaluate the influence of UV irradiation on structure-associated GO cytotoxicity. The study suggested that the increase in overall cytotoxicity was correlated to multiple factors such as size reduction as well as the increase of sharp edge defects on the structure from GO reduction. While a decrease of oxygen moieties in GO should have resulted in lower cytotoxicity, stable reductions were more present on the basal plane while instances of re-oxidation would occur far more on the edges, resulting the sharp irregular shapes. Interestingly, they also found that the highest UV irradiance and longest UV exposure had resulted in lower cytotoxicity in monocytes which were still unexplained.

CHAPTER 3 – RESEARCH METHODOLOGY

3.1.Materials

3.1.1. Chemical and Reagents Materials

Antineoplastic agents used in the research were cis-diammineplatinum(II) dichloride /Cisplatin (CDDP) (TCI, Japan), Paclitaxel (PTX) (MedChemExpress, USA), Alpha-Mangostin (A-MG) (Chengdu Kanghong Pharmaceutics, China), and Andrographolide (Andr-G) (Chengdu Kanghong Pharmaceutics, China). Silver nitrate ($AgNO_3$) (Systerm Chemicals, Malaysia) and gold (III) chloride trihydrate ($HAuCl_4 \bullet 3H_2O$) (Sigma, USA) were used as metallic nanoparticle precursors for silver nanoparticle (AgNP) and gold nanoparticle (AuNP) synthesis, respectively. Sodium borohydride ($NaBH_4$) (Merck, USA), Hydrazine hydrate 80%, and ascorbic acid (Sigma, USA) were used for reductants in nanoparticle synthesis. Solvents dimethylformamide (DMF) (Sigma, USA), dimethyl sulfoxide (DMSO) (Sigma, USA), and deionized water (DI H_2O) were used for nanoparticle synthesis as well as reagent or buffer preparation. Sodium hydroxide (NaOH) (Sigma, USA) and hydrochloric acid (HCl) (Fisher Scientific, USA) were used for pH control in buffer and reagent preparation. Thiazolyl Blue Tetrazolium Bromide (MTT) (Sigma, USA) was used for the MTT cytotoxicity assay. Graphene oxide (GO) nanoparticle powder was kindly provided by Prof. Mohammed Khalid from the Graphene and Advanced 2D Materials Research Group (GAMRG) at Sunway University, Petaling Jaya, Malaysia. HCl and nitric acid (HNO_3), (Sigma, USA) were used to make aqua regia (1:3 mixture) for washing glassware used in AuNP synthesis.

3.1.2. Cell Culture Materials and Cell Lines

Breast cancer cell models: human breast adenocarcinoma (MCF-7, ATCC-HTB-22™), Cisplatin-resistant human breast adenocarcinoma (MCF-7-CR, ATCC-HTB-22™) (Watson *et al.*, 2007), triple-negative human breast adenocarcinoma (MDA-MB-231,

ATCC-CRM-HTB-26™) were used in the experiments. Cells were cultured in standard Dulbecco's Modified Eagle Medium (DMEM) (Gibco, USA) supplemented with sodium bicarbonate (Sigma, USA), 10% fetal bovine serum (FBS) (Gibco, USA), 1x L-glutamine (Gibco, USA), 1x Penicillin/Streptomycin (PenStrep) antibiotic (Gibco, USA), and 1x non-essential amino acid (NEAA) (Gibco, USA). Dissociation reagents used in cell sub-culturing were 0.05% Trypsin-EDTA (Gibco, USA) for MCF-7 and MCF-7-CR cells as well as TrypLE Express (Gibco, USA) for MDA-MB-231 cell lines. For washing, phosphate buffer saline (PBS) pH 7.4 was made using sodium chloride (NaCl) (Sigma, USA), potassium chloride (KCl) (Sigma, USA), disodium hydrogen phosphate (Na_2HPO_4) (Sigma, USA), and potassium dihydrogen phosphate (KH_2PO_4) (Sigma, USA).

3.2.Research Plan and Design

3.2.1. Evaluation of breast cancer cell drug-resistivity against therapeutics

In the first phase of the research, three different breast cell lines were used to compare and evaluate the drug resistance of each cell. All cell lines were grown in 5% CO_2 at 37°C temperature conditions in CelCulture® CO_2 Incubator Model CCL-170T-8 (Esco, Singapore).

Among the three cell lines, MCF-7 was known to not confer MDR phenotypes and was only resistant to hormonal-related drugs such as tamoxifen (Comşa *et al.*, 2015; Lee *et al.*, 2015), thus was used for cancer cell control in this study as no hormonal drugs were used as samples. MDA-MB-231 was studied extensively for its ability to be resistant to multiple drugs to its poor prognosis, anti-apoptosis, drug effluxion, and EMT (Wang *et al*., 2017; Franchi *et al*., 2020; Huang *et al*., 2020); thus, was used for MDR model of breast cancer cell in this study.

FDA-approved drugs Cisplatin (CDDP) and Paclitaxel (PTX) were supposed to be used for generating two different chemo drug-resistant MCF-7 breast cancer cells that had acquired therapeutic resistance over a short period, as both drugs had been used for advanced metastatic breast cancer treatment regimen (Wang *et al*., 2021; Gupta *et al*., 2019). However, due to resource limitations, only chemo-drug-resistant MCF-7-CR was actualized as the current model.

To compare the drug resistivity of each cell, four antineoplastic agents were used, which were: FDA-approved CDDP from the anti-alkylating agent group, FDA-approved PTX from the taxane group, alpha-mangostin (A-MG) from the naturally derived chemotherapeutic compounds, as well as andrographolide (Andr-G) from the naturally-derived chemotherapeutic compounds. The treatment duration of antineoplastic agents was also investigated to determine whether the drug resistivity of each cell line reduced after a certain amount of time.

3.2.2. Metallic nanoparticles synthesis, characterization, and cytotoxicity determination

In the second phase of the research, two metallic nanoparticles synthesized from gold (AuNPs) and silver (AgNPs) were tested to see how they affect breast cancer cell lines and determine which of the two nanoparticles would reduce cancer cell viability. AuNPs and AgNPs were first synthesized from nanoparticle precursors $HAuCl_4 \bullet 3H_2O$ and $AgNO_3$ in magnetic-stirrer mixing synthesis using three different reducing agents which were sodium borohydride ($NaBH_4$), hydrazine hydrate, and ascorbic acid. The physicochemical properties of the synthesized nanoparticles would be characterized by their surface plasmon resonance (SPR), visual colloidal stability, surface functionalization, size-shape morphology, and zeta potential. The characterization was performed using UV-visible (UV-vis) spectroscopy for SPR, particle analyzer for zeta potential and particle size, FTIR spectroscopy for surface functionalization, and SEM for

size-shape morphology. The synthesized nanoparticles were also taken for treatment to three breast cancer cell lines to compare cell viability reduction, which were: the non-MDR phenotype control breast cancer cell MCF-7, MDR phenotype chemo-drug-resistant cisplatin-resistant breast cancer cell MCF-7-CR, and MDR phenotype triple-negative breast cancer cell MDA-MB-231.

3.2.3. Evaluation of graphene oxide (GO) as pre-synthesized organic nanoparticle as well as UV-B radiation exposure to breast cancer cells for synergistic effects

In the third phase of the research, organic nanoparticle graphene oxide (GO) was tested against breast cancer cells MCF-7, MCF-7-CR, and MDA-MB-231 to compare cytotoxicity activity with metallic nanoparticles AgNPs and AuNPs. GO was treated on breast cancer cells to determine toxicity effects alongside UV-B radiation exposure which was previously studied by Simon *et al.* (2021). Multiple experiments were performed to further study in terms of parameter changes in GO treatment, UV-B exposure, and coupled GO UV-B treatment to investigate their influence on the cytotoxicity against cancer cells. In experimental order, the parameters changed in the GO treatment were: GO solvent treatment, GO treatment duration, and UV-B exposure dose.

In the first experiment, non-chemo-drug-resistant, chemo-drug-resistant, and MDR model cancer cells were screened with GO in different concentrations to determine dose-dependent toxicity effects. The follow-up second and third experiments were conducted to further evaluate treatment differences between solvent and media as well as their impact on the toxicity of GO in cells. Parametric change experiments were also performed in terms of GO treatment duration in addition to UV-B energy exposure.

3.3.Experimental Procedure

3.3.1. Gold nanoparticles (AuNPs) and silver nanoparticles (AgNPs) synthesis and preparation

3.3.1.1. Glassware cleaning by deionized water (DI H_2O) and aqua regia rinsing

Before synthesis, all glassware used for AuNPs synthesis was pre-treated with an acid wash. Glassware, magnetic-stirring rods, and glass pipettes were rinsed with DI H_2O to clean off debris. The glassware was then rinsed in aqua regia (made by slowly adding and mixing one part HNO_3 into three parts HCl). Further, glassware was re-rinsed in DI H_2O to remove excess acid. The glassware was then oven-dried until use.

3.3.1.2. AuNPs and AgNPs magnetic-stirring mixing synthesis for characterization

The metallic nanoparticles were synthesized using a method adapted from Aqeel *et al.* (2016). Reducing agents 20 µL of 5 mM $NaBH_4$ was added dropwise to 20 mL nanoparticle precursor 1 mM $AgNO_3$. Reducing agents 50 µL of 5 mM $NaBH_4$, 100 µL of Hydrazine hydrate 10%, and 500 µL of 5 mg/mL ascorbic acid were added dropwise each to separate Erlenmeyer flasks containing 20 mL nanoparticle precursor 1 mM $AgNO_3$. The reducing agents were also added to three separate flasks containing nanoparticle precursor 1 mM $HAuCl_4 \cdot 3H_2O$. The solutions were then mixed for 10 minutes using magnetic-stirring rods and stirring hotplates (Fisher Scientific, USA) at the dialed speed of 350 RPM for 10 minutes at the standard room temperature of 25°C. 100 µL of the freshly-synthesized AgNP and following synthesis reagents were taken to UV-vis spectroscopic characterization as well as MTT cytotoxicity assay.

3.3.1.3. AuNPs and AgNPs freeze drying for characterization

Freshly synthesized AgNPs and AuNPs colloids were poured into several 50 mL centrifµge tubes in small amounts. The colloid-filled tubes were then put to -80°C to freeze, before placing into the vacuum chamber of -100°C freeze-dryer apparatus ScanVac CoolSafe 110-4 Basic 4lt Freeze Dryer (Labogene, Denmark) and RV5 Rotary

Vane Vacuum Pump (Edwards, Sweden), where the tube caps were replaced with filter paper fastened with rubber bands. The freeze-dryer was turned on for three days, before storing the dried nanoparticle powders and pastes in the dark, at room temperature. The freshly dried nanoparticle powders and pastes were then taken to FTIR, SEM, and DLS characterization.

3.3.2. UV-vis spectroscopy nanoparticle characterization

UV-vis spectroscopy characterization was performed using a method adapted from Aqeel *et al.* (2016). 100 µL of reducing agents of 5 mM $NaBH_4$, Hydrazine hydrate 10%, and 5 mg/mL Ascorbic Acid), nanoparticle precursors (1 mM $AgNO_3$ and 1 mM $HAuCl_4 \bullet 3H_2O$), blank solvent DI H_2O, as well as freshly-made synthesized AuNP and AgNP colloidal samples were loaded to a transparent 96-well plate for analysis. The plate was read using Infinite M Plex plate reader (Tecan, Swiss) with sweeping absorbance ranging from 250-1000 nm wavelength. Plasmonic bands for AgNPs are detected around 400 nm, whereas AuNPs are detected at around 500 nm.

3.3.3. Fourier Transform Infra-Red (FTIR) spectroscopy nanoparticle characterization

FTIR spectroscopy characterization was performed using a method adapted from Simon *et al.* (2021). Spectrum Two FT-IR Spectrometer (Perkin Elmer, USA) was calibrated to reduce background noise. Then freshly freeze-dried synthesized AgNP powders and AuNPs pastes were mounted on top of the FTIR spectrometer detector plate to be read.

3.3.4. Scanning Electron Microscopy (SEM) nanoparticle characterization

SEM characterization was performed using a method adapted from Anwar *et al.* (2019). 50 µL drops of freshly-synthesized AgNPs and AuNPs colloids were placed on top of a microscope slide to be freeze-dried in ScanVac CoolSafe 110-4 Basic 4lt Freeze Dryer (Labogene, Denmark) and RV5 Rotary Vane Vacuum Pump (Edwards, Sweden). The

resulting freeze-dried microscope slides were then ion-sprayed using platinum coating using SPT-20 (Coxem, Korea) for preparation of SEM analysis. The microscope slides were then mounted on Tescan Vega 3 (Tescan, Czech) and observed under 15000x magnification. Images taken were then analyzed using image analyzer ImageJ Software.

3.3.5. Dynamic Light Scattering (DLS) for nanoparticle characterization

DLS characterization was performed using a method adapted from Anwar *et al.* (2019). 1.5 mL of freshly synthesized AgNPs and AuNPs colloids were prepared in two different cuvettes: omega cuvettes and disposable plastic cuvettes. The cuvettes were then taken to particle analyzer LiteSizer 500 (Anton Paar, Germany) for reading, with nanoparticle-filled omega cuvettes for measuring zeta potential while disposable cuvettes were used for measuring particle size.

3.3.6. Cisplatin-resistant MCF-7-CR breast cancer cells preparation

The method to prepare MCF-7-CR cells was adapted from the method described by Watson *et al*. (2007). MCF-7 cells were grown in 10% FBS-completed DMEM and were gradually treated with Cisplatin (CDDP) from 1 µM until the final concentration of 50 µM where surviving cells started to grow back. Concentrations of 50 µM were further used for 7x cycles of 24h. The cells were then re-incubated in untreated media for 30 days to let CDDP-resistant viable cells further proliferate.

3.3.7. MTT cytotoxicity assay for antineoplastic agents and synthesized nanoparticles

Cell culture protocol and MTT cytotoxicity assay were performed using the method adapted from Simon *et al.* (2021). MCF-7, MCF-7-CR, and MDA-MB-231 cell lines at passage p7-p20 were seeded to transparent 96-well plates at a calculated 15000 cell count/well and were left to adhere and grow overnight. Cells were then treated appropriately for 24h or more. Treated cells were then washed in 1x PBS pH 7.4 and

further incubated in 10% FBS completed DMEM media containing 0.5 mg/mL MTT for 2h. The media was then disposed and cells were added with 100 µL of DMSO to dissolve formed formazan crystals. The plates were then read with Infinite M Plex plate reader (Tecan, Swiss) at 570 nm wavelength.

Cytotoxicity of the sample was calculated using the cell viability equation:

$$\%VIability = \frac{A_{Sample}}{A_{control}} \times 100\%$$

where the %viability of each sample was used to plot the %viability vs. concentration graph to determine the correlation of each sample. A_{sample} is the absorbance of the sample after calibrated against blank solvent absorbance, while $A_{control}$ is the absorbance of experiment control (untreated cells).

For experiments related to the influence of antineoplastic agents in Subchapter 3.2.1., 4 different antineoplastic agents were diluted into 1% sample concentration in 10% FBS completed DMEM media and taken for treatment to cells for 24h, 48h, and 72h. Antineoplastic agents used in the experiment were CDDP with final treatment concentrations 0 (solvent control DMF), 1.5625, 3.125, 6.25, 12.5, 25, 50, 100 µM; PTX dissolved in DMSO with final treatment concentrations 0 (solvent control DMSO), 15.625, 31.25, 62.5, 125, 250, 500, and 1000 nM; A-MG with final treatment concentration 0 (solvent control DMSO), 1.5625, 3.125, 6.25, 12.5, 25, 50, 100 µM; and Andr-G with final treatment concentration 0 (solvent control DMSO), 1.5625, 3.125, 6.25, 12.5, 25, 50, 100 µM.

For experiments related to the influence of synthesized AuNPs as well as AgNPs in Subchapter 3.2.2., cells were treated for 24h in two synthesized nanoparticles 1 mM AgNP or 1 mM AuNPs. All instances of samples were diluted with DI H_2O at final

concentrations 0 (solvent control DI H_2O), 2, 4, 6, 8, and 10 µM in 10% FBS completed DMEM media.

3.3.8. MTT cytotoxicity assay for graphene oxide (GO), UV-B exposure, and synergistic effect treatment

Cell culture protocol and MTT cytotoxicity assay were performed using the method adapted from Simon *et al.* (2021). As written in Subchapter 3.3.7., MCF-7, MCF-7-CR, and MDA-MB-231 cell lines at passage p7-p20 were seeded to transparent 96-well plates at a calculated 25000 cell count/well and were left to adhere and grow overnight. Cells were then treated appropriately for 24h. Treated cells were then washed in 1x PBS pH 7.4 and further incubated in 10% FBS completed DMEM media containing 0.5 mg/mL MTT for 2h. The media was then disposed and cells were added with 100 µL of DMSO to dissolve formed formazan crystals. The plates were then read with Infinite M Plex plate reader (Tecan, Swiss) at 570 nm wavelength.

Cytotoxicity of the sample was calculated using the cell viability equation:

$$\%Viability = \frac{A_{Sample}}{A_{control}} \times 100\%$$

where the %viability of each sample was used to plot the %viability vs. concentration graph to determine the correlation of each sample. A_{sample} is the absorbance of the sample after calibrated against blank solvent absorbance, while $A_{control}$ is the absorbance of experiment control (untreated cells).

For the experiment related to screening of GO concentration toxicity in different cancer cell lines and GO dose-dependent toxicity effect in Subchapter 3.2.3., DI H_2O-dissolved 10 µg/mL GO was diluted with 100 µL of 10% FBS completed DMEM media into 0 (solvent control DI H_2O), 25, 50, 75, and 100 µg/mL of media-diluted GO. MCF-7, MCF-7-CR, and MDA-MB-231 cells were treated and incubated for 24h.

For experiments related to GO concentration dose in the presence of PBS in Subchapter 3.2.3., DI H_2O-dissolved 10 µg/mL GO was diluted with 30 µL of 1x PBS pH 7.4 into 0 (solvent control DI H_2O), 25, 50, 75, and 100 µg/mL of PBS-diluted GO. Cells were treated and incubated for 3h before being added with 100 µL of 10% FBS completed DMEM media to be incubated for 24h.

For experiments related to UV-B energy exposure dose in the presence of PBS in Subchapter 3.2.3., DI H_2O-dissolved 10 µg/mL GO was diluted into 30 µL of 1x PBS pH 7.4 in 0, 5, 10, 25, and 50 µg/mL final concentrations of PBS-diluted GO. Cells were treated and incubated for 3h and 6h before being exposed to UV-B energy at energy 0 mJ/cm^2 (non-irradiated), 5 mJ/cm^2, and 10 mJ/cm^2. After irradiation, cells were added with 100 µL of 10% FBS completed DMEM media to be further incubated for 24h.

3.4.Statistical Analysis

Tests were done in three sets of biological replicates, where the data points were calculated and presented in the form of Mean ± Standard Deviation. Statistical analysis for GO results was performed using Student's *t*-test with Type-I error set at 5%, 1%, and 0.5% as the level of significance; where results at p-value ≥ 0.05 are considered as not significant, results at $0.01 \leq$ p-value < 0.05 is considered as partially significant (*), results at $0.01 \leq$ p-value < 0.05 is considered as significant (**), and results at p-value < 0.005 is considered as highly significant (***). All calculations and graphical analyses were performed using Excel software from Microsoft Office.

CHAPTER 4 – RESULTS

4.1.Chemo-resistivity of breast cancer cell lines against various antineoplastic agents

Breast cancer cells MCF-7, Cisplatin (CDDP) -resistant MCF-7-CR, and triple-negative breast cancer MDA-MB-231 cells were treated with different chemotherapeutic agents such as Cisplatin (CDDP), Paclitaxel (PTX), Alpha-mangostin (A-MG), and Andrographolide (Andr-G) to compare the degree of chemo-drug resistance of cells. Cells were exposed to chemotherapeutic agents for 24h, 48h, and 72h incubation with different concentration doses.

4.1.1. Breast cancer cell lines against Cisplatin (CDDP)

CDDP exposure was found to be toxic in MCF-7-CR cells at all incubation times, whereas the drug only resulted in reduced cell viability on MCF-7 and MDA-MB-231 at 48h and 72h incubation (Figures 4.1a, 4.1b, and 4.1c). At 24h incubation, increased concentration of CDDP did not result in MCF-7 viability lower than 100% and most concentrations resulted in high outliers, however, dose-dependent effects were seen at 48h and 72h where the lowest concentration of 1.5625 µM had even resulted in 60% cell viability and 50% cell viability reduction was found to be at the range of 12.5-25 µM (Figure 4.1a). MDA-MB-231 cells were also found to have no viability reduction at 24h and apparent dose-dependent effects on 48h and 72h incubation, where the cell viability reduction was first seen in 1.5625 µM for 48h and 3.125 µM for 72h (Figure 4.1c). For MCF-7-CR, dose-dependent effects were seen in all incubation time instances, where 50% cell viability was reached after 50 µM for 24h, around 25 µM for 48h, and 12.5 µM for 72h (Figure 4.1b). By comparing the starting viability reduction and trend between MCF-7, MCF-7-CR, and MDA-MB-231 cells, CDDP toxicity effects were found to be highly apparent in MCF-7, then MCF-7-CR, and least toxic in MDA-MB-231 cells in 48h and 72h. The results suggested that MDR cancer cells were more resistant to CDDP compared to MCF-7 cells.

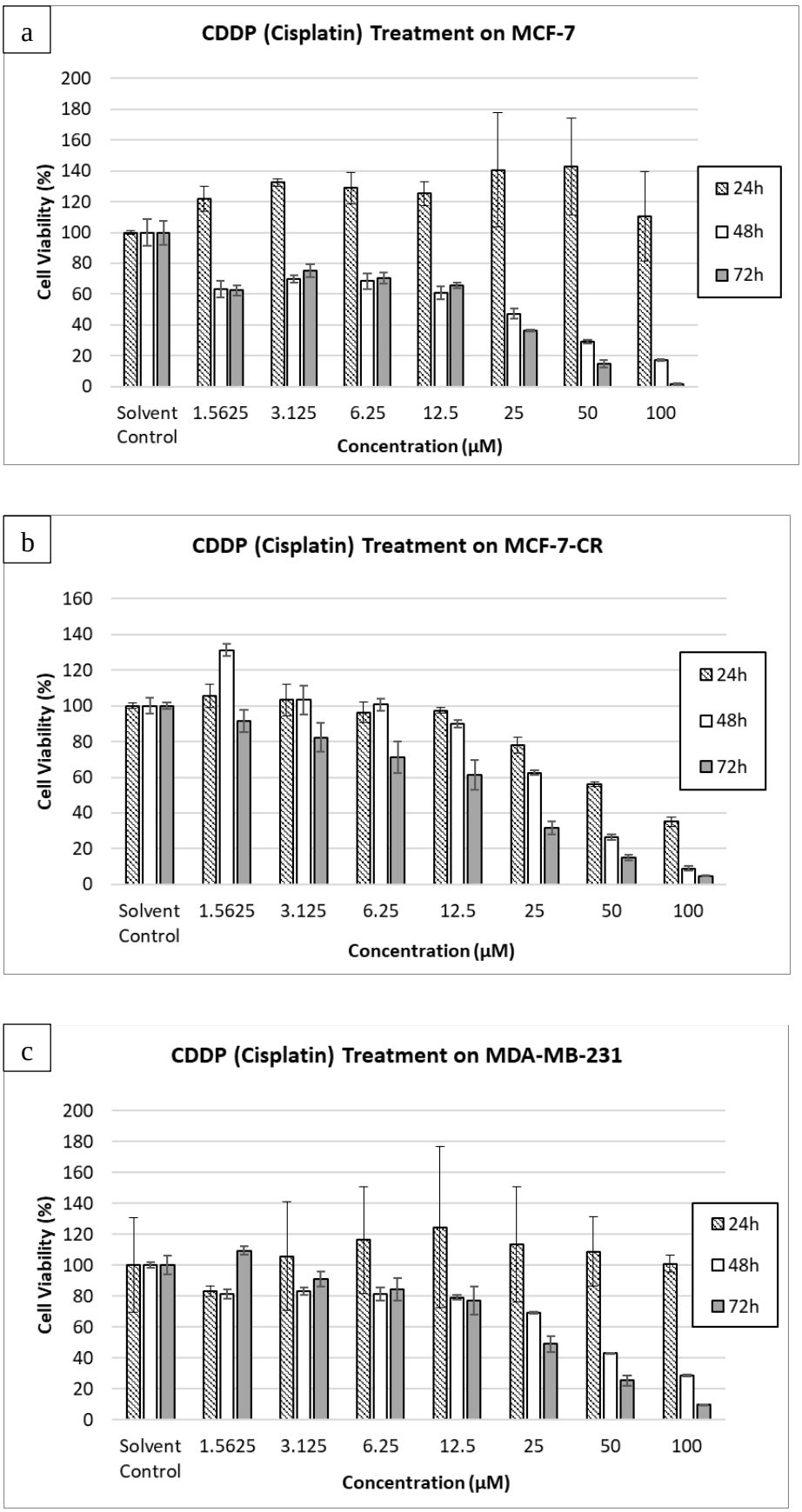

Figure 4.1. Dose-dependent effects of Cisplatin (CDDP) treatment on breast cancer cells (a) MCF-7, (b) MCF-7-CR, and (c) MDA-MB-231 under different exposure times.

4.1.2. Breast cancer cell lines against Paclitaxel (PTX)

Treatments of PTX at 48h and 72h were also found to be toxic in MCF-7, MCF-7-CR, and MDA-MB-231 cells with no toxicity found in both MCF-7 and MDA-MB-231 cells at 24h incubation (Figures 4.2a, 4.2b, and 4.2c) as seen with CDDP treatments (Figures 4.1a, 4.1b, and 4.1c). MCF-7 viability increase was seen for 24h incubation treatment proportional to PTX concentration but higher concentrations had inconsistent results as illustrated by the error bars. While on 48h and 72h incubation, treatments resulted in around 30% cell viability for most concentrations (Figure 4.2a). Despite the high outlier at 62.5 nM concentration for 24h incubation, treatment of MCF-7-CR in all incubation times was found to result in cell death increase proportional to concentration. The lowest cell viability in 24h was seen at 1000 nM, while 50% MCF-7-CR cell viability was seen at 125 nM and below 15.625 nM concentration at 48h and 72h, respectively (Figure 4.2b). PTX resulted in inconsistent and non-cytotoxicity for 24h treatment in MDA-MB-231 yet cell death was seen on both 48h and 72h at about 55% and 30% cell viability respectively. In terms of 48h, cell viability increased slightly proportional to the concentration of PTX from 40% to just below 60% but PTX increased in toxicity for 72h incubation where 40% viability was reduced to 20% from lowest concentration to highest concentration (Figure 4.2c). Based on Figures 4.2a until 4.2c, it was suggested that PTX was most potent against MCF-7 and MDA-MB-231 cells in 48h, but PTX then increased in toxicity against MCF-7-CR for 72h and became desensitized in MDA-MB-231 cells even starting at 48h incubation. The results for Figures 4.1a-c and 4.2a-c suggested that FDA-approved CDDP and PTX became less effective with more prolonged exposure in MDR cancer cells when compared with longer exposure in MCF-7 cells.

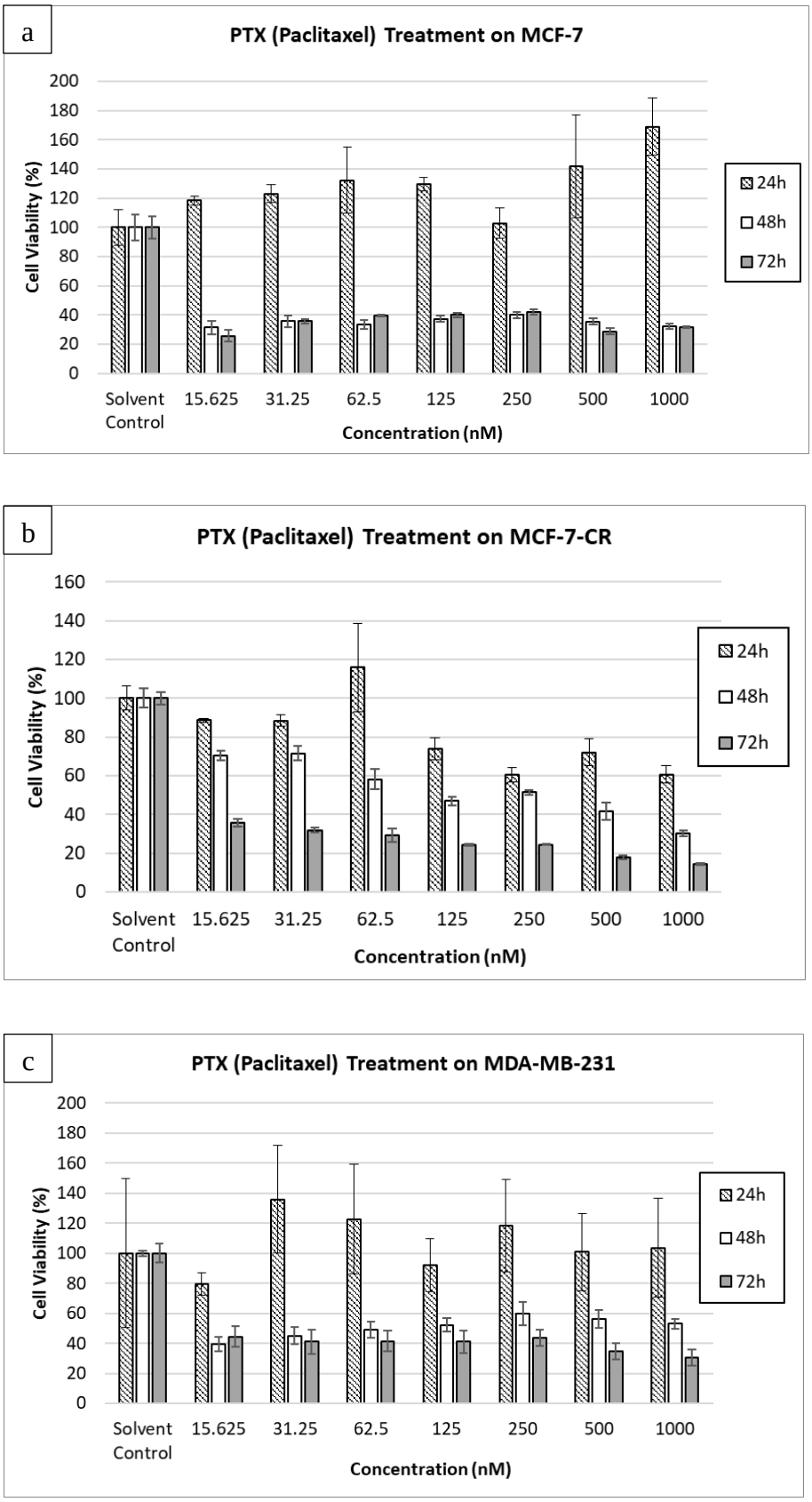

Figure 4.2. Dose-dependent effects of Paclitaxel (PTX) treatment on breast cancer cells (a) MCF-7, (b) MCF-7-CR, and (c) MDA-MB-231 under different exposure times.

4.1.3. Breast cancer cell lines against Alpha-mangostin (A-MG)

A-MG was found to cause cell death on MCF-7, MCF-7-CR, and MDA-MB-231 cells for all incubation time. At concentrations of 25 µM and higher, the viability of all breast cancer cells reached more than 50%, even almost 0% cell viability for MDR cancer cells at 24h, 48h, and 72h (Figures 4.3a, 4.3b, and 4.3c). Interestingly, at very low concentrations of 1.5625-6.25 µM and longer time incubations A-MG seemed to increase cell viability to up to 40% for MCF-7 and MCF-7-CR as well as around 20% for MDA-MB-231 cells. A-MG resulted in 50% cell death in cancer cells starting at concentration ranges of 12.5-25 µM for 24h, 48h, and 72h incubation, where in MCF-7 the concentrations were at the higher spectrum, in MCF-7-CR the concentrations were at the lower spectrum, and in MDA-MB-231 the concentrations were around the middle of the concentration ranges. Based on the dose-dependent curves in the figures, A-MG was most potent on MDR cancer cells MCF-7-CR and MDA-MB-231 on longer time incubation and higher concentration.

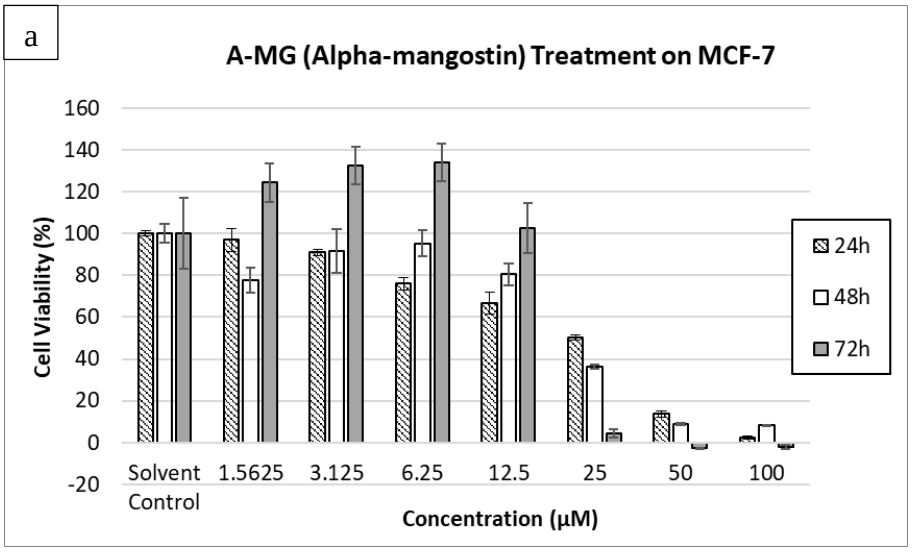

Figure 4.3. Dose-dependent effects of Alpha-Mangostin (A-MG) treatment on breast cancer cells (a) MCF-7, (b) MCF-7-CR, and (c) MDA-MB-231 under different exposure times.

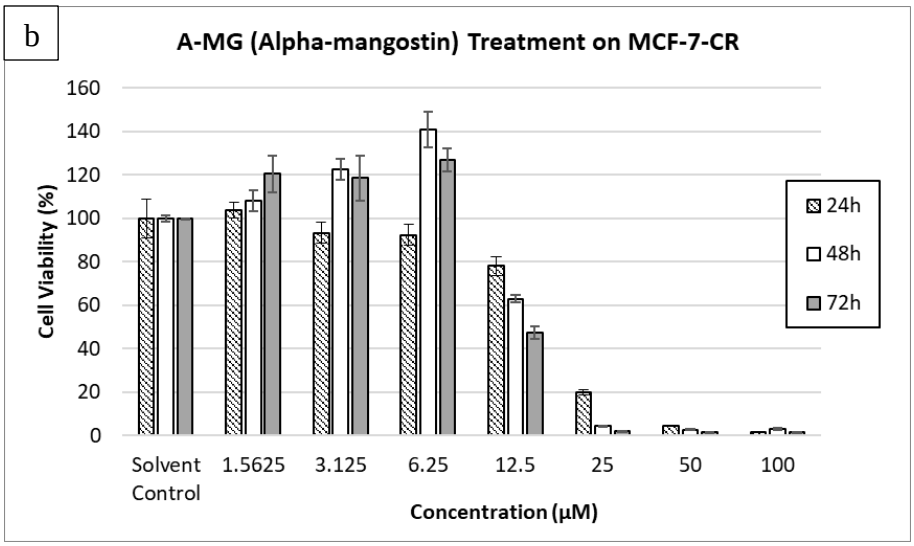

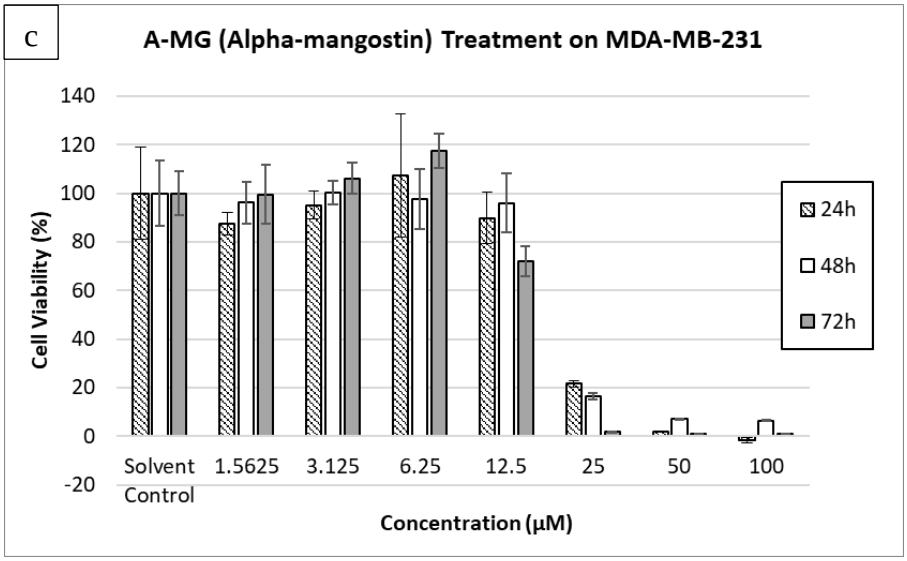

Figure 4.3., Continued, Dose-dependent effects of Alpha-Mangostin (A-MG) treatment on breast cancer cells (a) MCF-7, (b) MCF-7-CR, and (c) MDA-MB-231 under different exposure times.

4.1.4. Breast cancer cell lines against Andrographolide (Andr-G)

Similar to A-MG, Andr-G was found to cause cell death in MCF-7, MCF-7-CR, and MDA-MB-231 cells for all incubation times. At 24h incubation, low concentrations of Andr-G on 1.5625-6.25 µM resulted in a small increase in cell viability as seen with A-MG treatment for longer incubations. It was also found that Andr-G was less effective in reducing the viability of MCF-7 cells when compared with MDR cancer cells (Figures 4.4a, 4.4b, and 4.4c). Even at the highest concentration of 100 µM, treatment of MCF-7

in 24h incubation time did not result in viability lower than 70%, while viability was reduced to up to 40% in MCF-7-CR and MDA-MB-231 cells. At longer time incubation such as 48h and 72h, Andr-G induced high cytotoxicity in MCF-7-CR and MDA-MB-231 cells as seen in Figures 3.4b and 3.4c, where 50% viability was reached at range 6.25-12.5 µM for MCF-7-CR and 25 µM for MDA-MB-231 cells. When compared to Figure 11a, 50% MCF-7 viability in 48h and 72h was only achievable using more than 25 µM concentration treatment. This suggested that Andr-G was more effective against MDR cancer cells as also seen in the case of A-MG treatment.

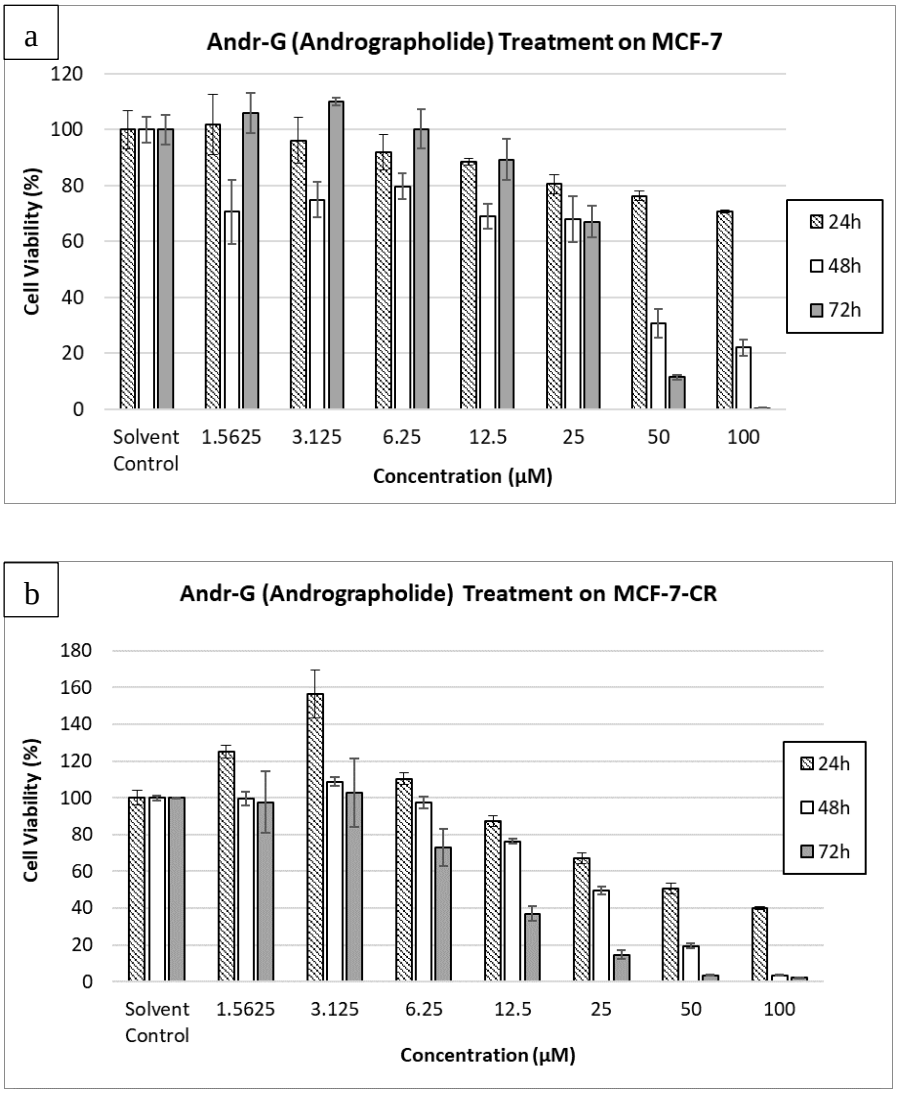

Figure 4.4. Dose-dependent effects of Andrographolide (Andr-G) treatment on breast cancer cells (a) MCF-7, (b) MCF-7-CR, and (c) MDA-MB-231 under different exposure times.

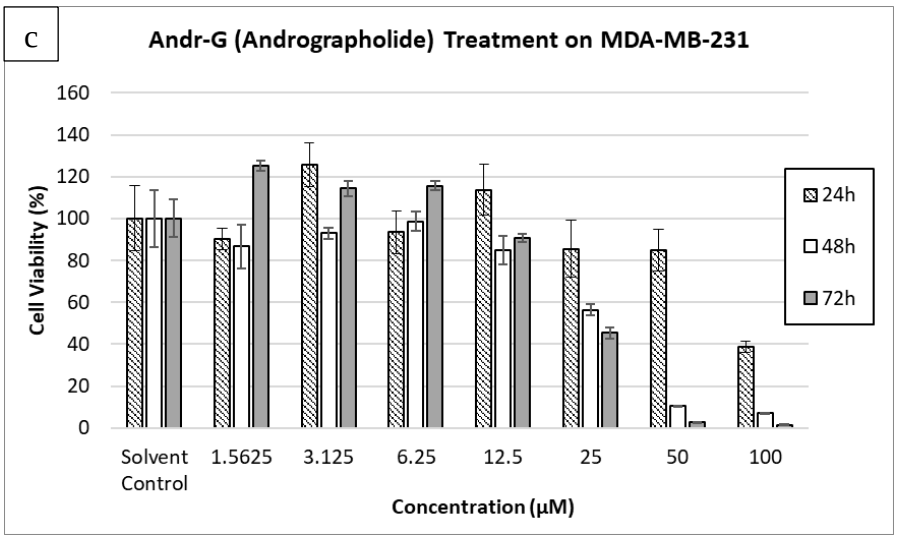

Figure 4.4., Continued, Dose-dependent effects of Andrographolide (Andr-G) treatment on breast cancer cells (a) MCF-7, (b) MCF-7-CR, and (c) MDA-MB-231 under different exposure times.

4.2.Characterization of gold nanoparticles (AuNP) and silver nanoparticles (AgNP) for metallic nanoparticle-based therapeutics

Inorganic nanoparticles were synthesized using noble metals in the form of gold nanoparticles (AuNPs) and silver nanoparticles (AgNPs). Nanoparticle synthesis was done by chemical reduction, with reducing agents hydrazine hydrate, ascorbic acid, as well as sodium borohydride ($NaBH_4$). Synthesized nanoparticles were characterized using UV-vis spectroscopy, with UV-vis spectra for AuNP found at around 520nm (Figure 4.5a) whereas UV-vis spectra AgNPs were found at around 400nm (Figure 4.5b). AuNP synthesized using ascorbic acid was more stable compared with other reducing agents, while AgNPs were more stable when synthesized in the presence of reducing agent $NaBH_4$. In both AuNPs and AgNPs instances, syntheses in the presence of hydrazine hydrate were highly unstable and did not result in a well-dispersed colloid, with a large number of aggregates forming within several seconds of mixing. This resulted in noise-heavy spectra recorded in AgNPs UV-vis (Figure 4.5a) and no detectable plasmonic

bands in AuNPs UV-vis (Figure 4.5b). Hydrazine hydrate was hence not used for subsequent experiments due to its inability to form stable enough nanoparticles.

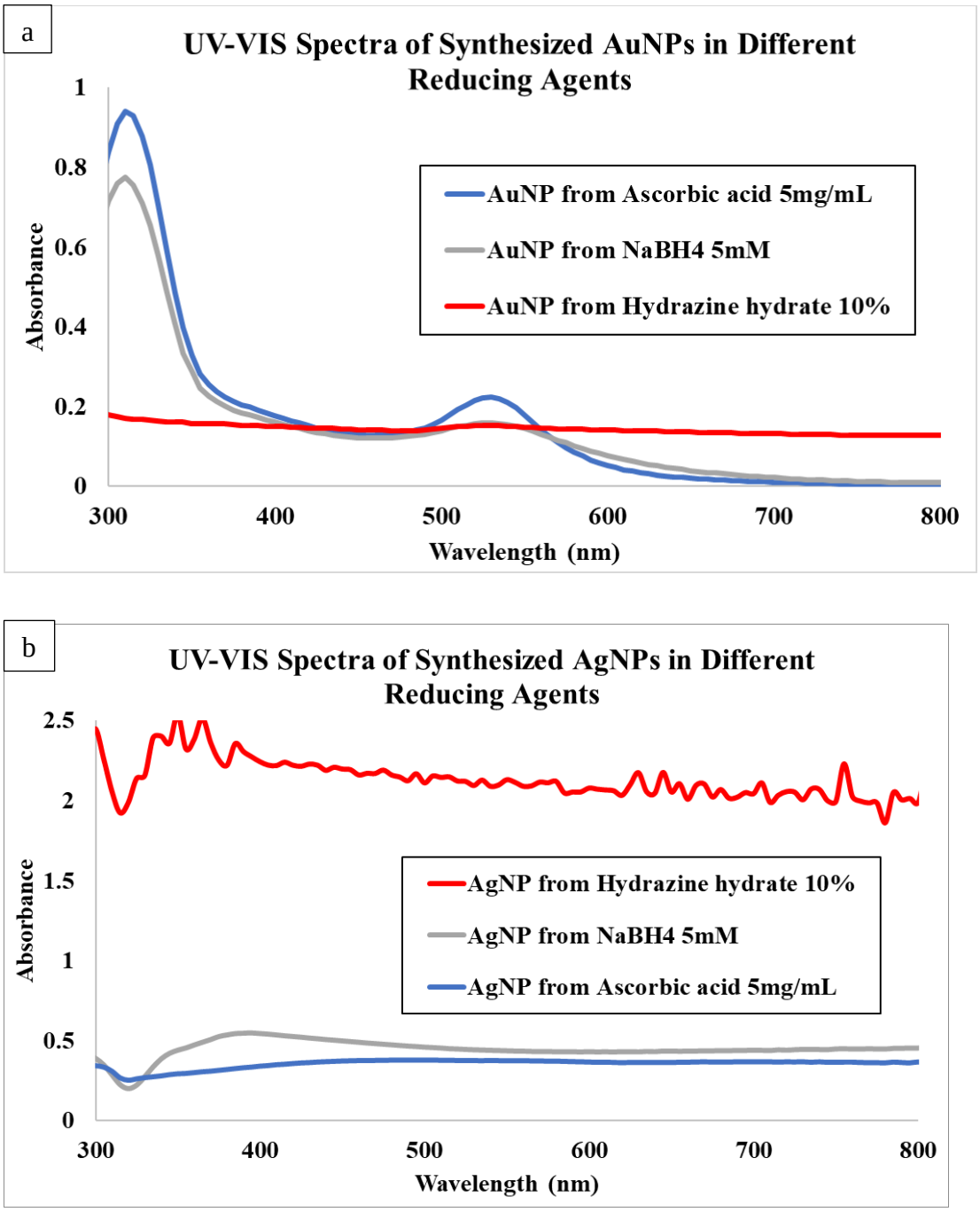

Figure 4.5 Synthesized metallic nanoparticles UV-vis spectra characterization, with (a) AuNPs and (b) AgNPs synthesized using reducing agents $NaBH_4$, hydrazine hydrate, as well as ascorbic acid.

By comparing the general spectral peaks and stability in Figures 4.5a and 4.5b, the most stable and highest SPR peaks between each nanoparticle were found to be AuNPs

synthesized in Ascorbic acid 5 mg/mL and AgNPs synthesized in $NaBH_4$ 5mM. Therefore, both aforementioned nanoparticles were selected for further measurement such as in Fourier Transform Infra-Red (FTIR) Spectroscopy, Scanning Electron Microscopy (SEM) observation, and Dynamic Light Scattering (DLS) as they had higher nanoparticle presence and overall synthesis yield. The spectral results for the AuNPs and AgNPs in FTIR spectroscopy could be seen in Figures 4.6a and 4.6b respectively. Figure 4.6a showed the spectral peaks for synthesized AuNPs at 3340, 1723, 1620, 1421, 1054, 508, and 441 cm^{-1}. The strong and broad peak at 3,340 cm^{-1} confirmed O–H stretching of hydroxyl groups which signified traces of hydrates from gold (III) chloride. Other peaks were found to be traces of ascorbic acid such as peaks on 1723 cm^{-1} and 1620 cm^{-1} which were confirmed to be C=O stretching, the small peak at 1421 cm^{-1} which was C–H bending, and C–O–C stretching on 1054 cm^{-1} (Panicker *et al.*, 2006). Figure 4.6b showed the spectral peaks for synthesized AgNPs at 2669, 2354, 2042, 1753, 1283, 800, and 732 cm^{-1}. The strong peaks at 1283 cm^{-1}, 800 cm^{-1}, and 732 cm^{-1} corresponded surface chemical fingerprint of nanoparticles, which was confirmed to be highly similar to peaks for silver nitrate (Oves *et al.*, 2013). Another small peak at 2354 cm^{-1} also corresponded to B-H stretching, signifying traces of $NaBH_4$ found in the surface of AgNPs (Mao *et al.*, 2015). Both IR spectra for AuNPs and AgNPs were compared to the FTIR reference of H_2O for background noise and control, with only one peak corresponding to O–H stretching for AuNPs which was confirmed to be traces of hydrates in the salt precursors (Coblentz Society, 2023).

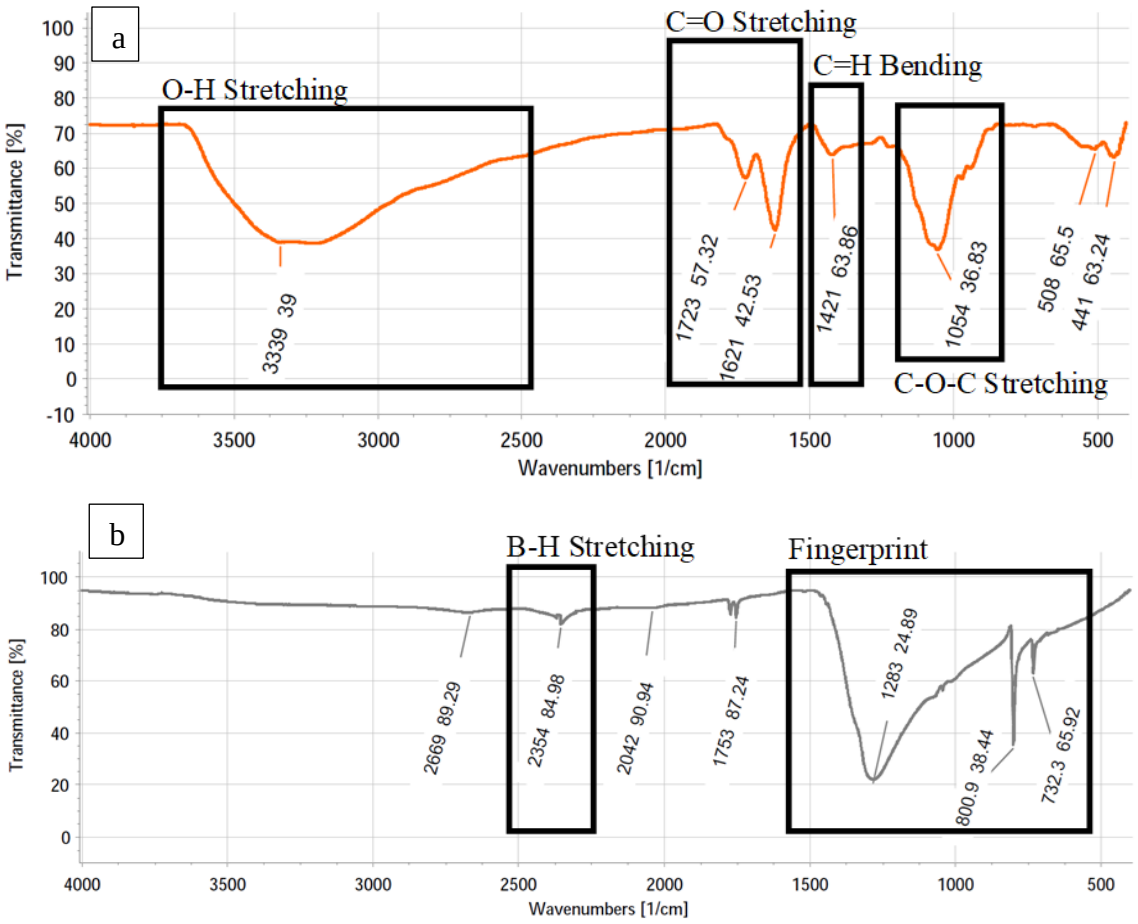

Figure 4.6. Synthesized metallic nanoparticles FTIR spectroscopy characterization, with (a) AuNPs synthesized using reducing agent ascorbic acid and (b) AgNPs synthesized using reducing agent $NaBH_4$.

Figures 4.7a and 4.7b showed ascorbic acid-reduced synthesized AuNPs and $NaBH_4$-reduced synthesized AgNPs observed at 15000x magnification using SEM. AuNPs were observed to be successfully synthesized at an observed mean size of 171 ± 53 nm using ImageJ Analyzer (Figure 4.7a), with clear spherical morphology. While AgNPs were also observed to be synthesized, morphology was determined to be highly irregular and the observed mean size was 680 ± 188 nm (Figure 4.7b). Flocculation was seen throughout the AuNPs particulates and was more apparent in AgNPs, with most quasi-spheres forming connections with the surrounding nanoparticles, resulting in an irregular mesh of AgNPs.

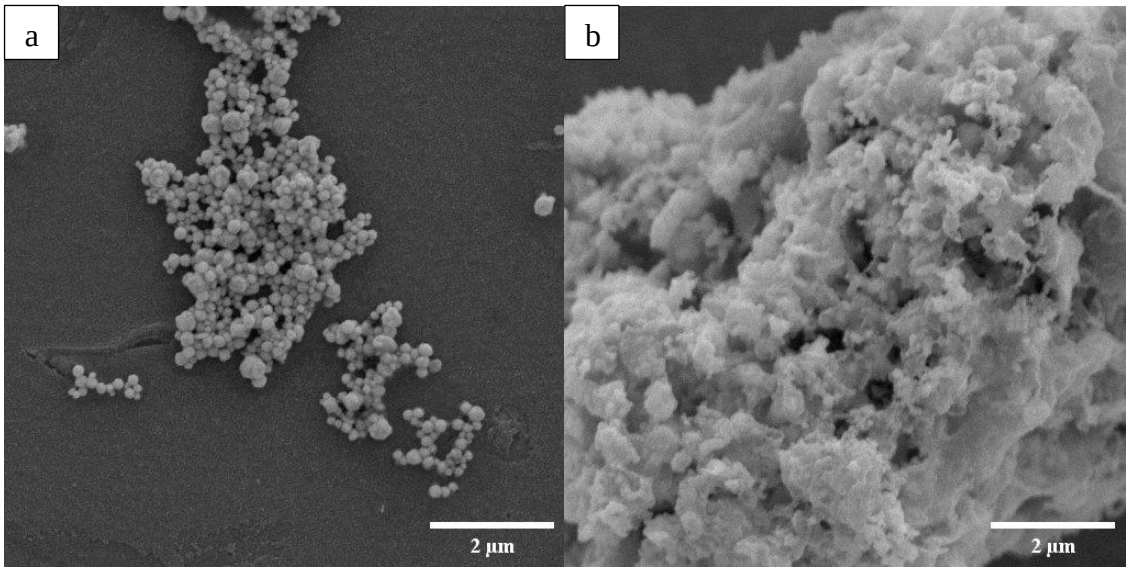

Figure 4.7. Synthesized metallic nanoparticles SEM characterization at 15000x magnification, with (a) AuNPs synthesized using reducing agent ascorbic acid and (b) AgNPs synthesized using reducing agent $NaBH_4$.

Particle analysis was performed using dynamic light scattering (DLS) to measure the zeta potential of selected AuNPs and AgNPs. The zeta potential and polydispersity of AuNPs and AgNPs were found to be low, with the zeta potential of AgNPs only about -21 mV and the polydispersity index as low as 15% (Table 4.1). Coupled with the SEM images, synthesized AgNPs were suggested to be unstable and easily react with surrounding nanoparticles; whereas synthesized AuNPs were able to maintain stable nanospheres but were indicated to be prone to coagulation due to polarity attraction.

Table 4.1 Synthesized metallic nanoparticle size and zeta potential characterization for AuNPs synthesized using reducing agent ascorbic acid and AgNPs synthesized using reducing agent $NaBH_4$. Mean Observed Size was calculated from Figures 4.7a-b and was analyzed in ImageJ.

Samples	Polydispersity index (%)	Mean Observed Size (nm)	Mean Zeta Potential (mV)
AuNP-Ascorbic	17.91 ± 0.90	171 ± 53	-36.08 ± 0.77
AgNP-$NaBH_4$	15.24 ± 3.86	680 ± 188	-21.35 ± 0.20

4.3.Cytotoxicity of gold nanoparticles (AuNPs) and silver nanoparticles (AgNPs) against breast cancer cell lines

Inorganic metal nanoparticles synthesized in different reducing agents were then tested for toxicity in different cancer cells. Ascorbic acid-reduced and $NaBH_4$-reduced synthesized AuNPs were found to exhibit toxicity to MCF-7, MCF-7-CR, and MDA-MB-231 cells (Figures 4.8a and 4.8b). $NaBH_4$-reduced AuNPs were found to be slightly more toxic than ascorbic acid-reduced AuNPs. Both AuNPs were more toxic in MCF-7 and MDA-MB-231 cells when compared with MCF-7-CR, with cell viability on MCF-7 and MDA-MB-231 for 10 µM $NaBH_4$-reduced reaching about 75% and 80% while ascorbic acid-reduced reaching about 80% and 90%. However, the viability of MCF-7-CR was seen to be reduced significantly in both instances of ascorbic and $NaBH_4$-reduced AuNPs to about 20% reduction on the lowest concentration.

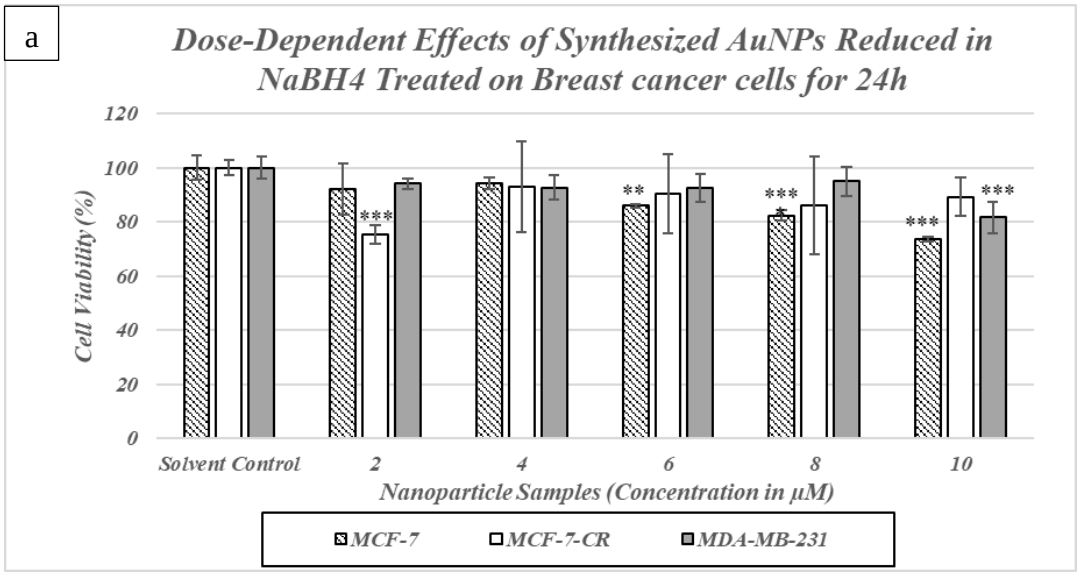

Figure 4.8. Dose-dependent effects of synthesized AuNPs treatment on MCF-7, MCF-7-CR, and MDA-MB-231 with AuNPs synthesized using reducing agents (a) $NaBH_4$ and (b) ascorbic acid. Student's *t*-test was performed for AuNPs concentrations compared to the solvent control for p-value $\alpha < 0.05$, $\alpha < 0.01$, and $\alpha < 0.005$ (* is partially significant, ** is significant, and *** is highly significant).

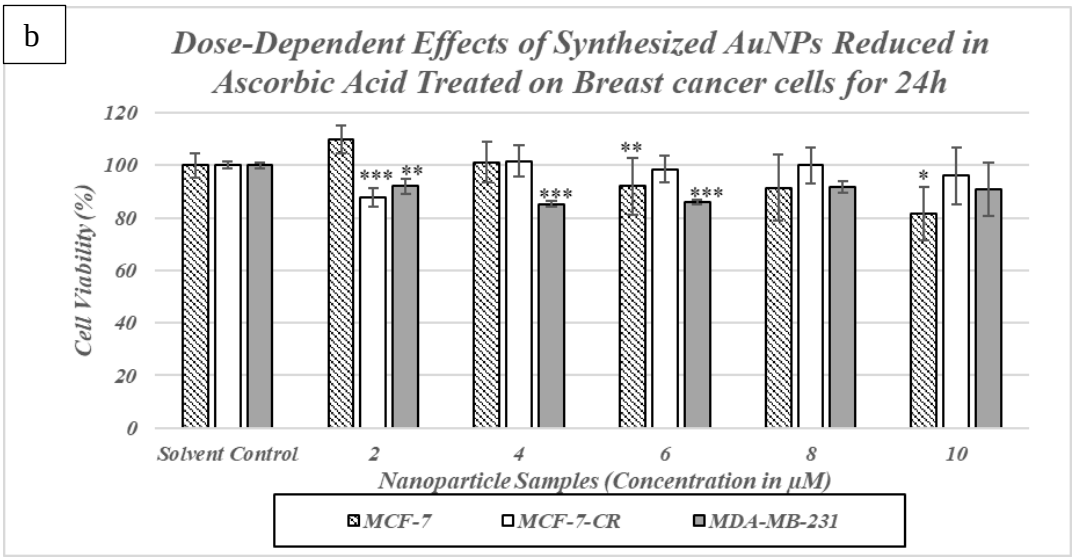

Figure 4.8., Continued, Dose-dependent effects of synthesized AuNPs treatment on MCF-7, MCF-7-CR, and MDA-MB-231 with AuNPs synthesized using reducing agents (a) $NaBH_4$ and (b) ascorbic acid. Student's *t*-test was performed for AuNPs concentrations compared to the solvent control for p-value $\alpha < 0.05$, $\alpha < 0.01$, and $\alpha < 0.005$ (* is partially significant, ** is significant, and *** is highly significant).

Synthesized AgNPs were also tested in breast cancer and MDR breast cancer cell lines (Figures 4.9a and 4.9b). It was found that all synthesized AgNPs samples were able to induce cytotoxic effects in MCF-7 cells, with the strongest viability reduction seen in the highest concentration of ascorbic acid-reduced synthesized AgNPs at 50% cell viability. In terms of MCF-7-CR, ascorbic acid-reduced AgNPs had slightly stronger cytotoxic effects than $NaBH_4$-reduced AgNPs, however, both AgNPs samples at the highest concentration only resulted in around 15% cell death. Interestingly, only $NaBH_4$-reduced AgNPs were found to be toxic to MDA-MB-231 cells among the AgNPs samples, albeit still less potent than in MCF-7 and MCF-7-CR cells.

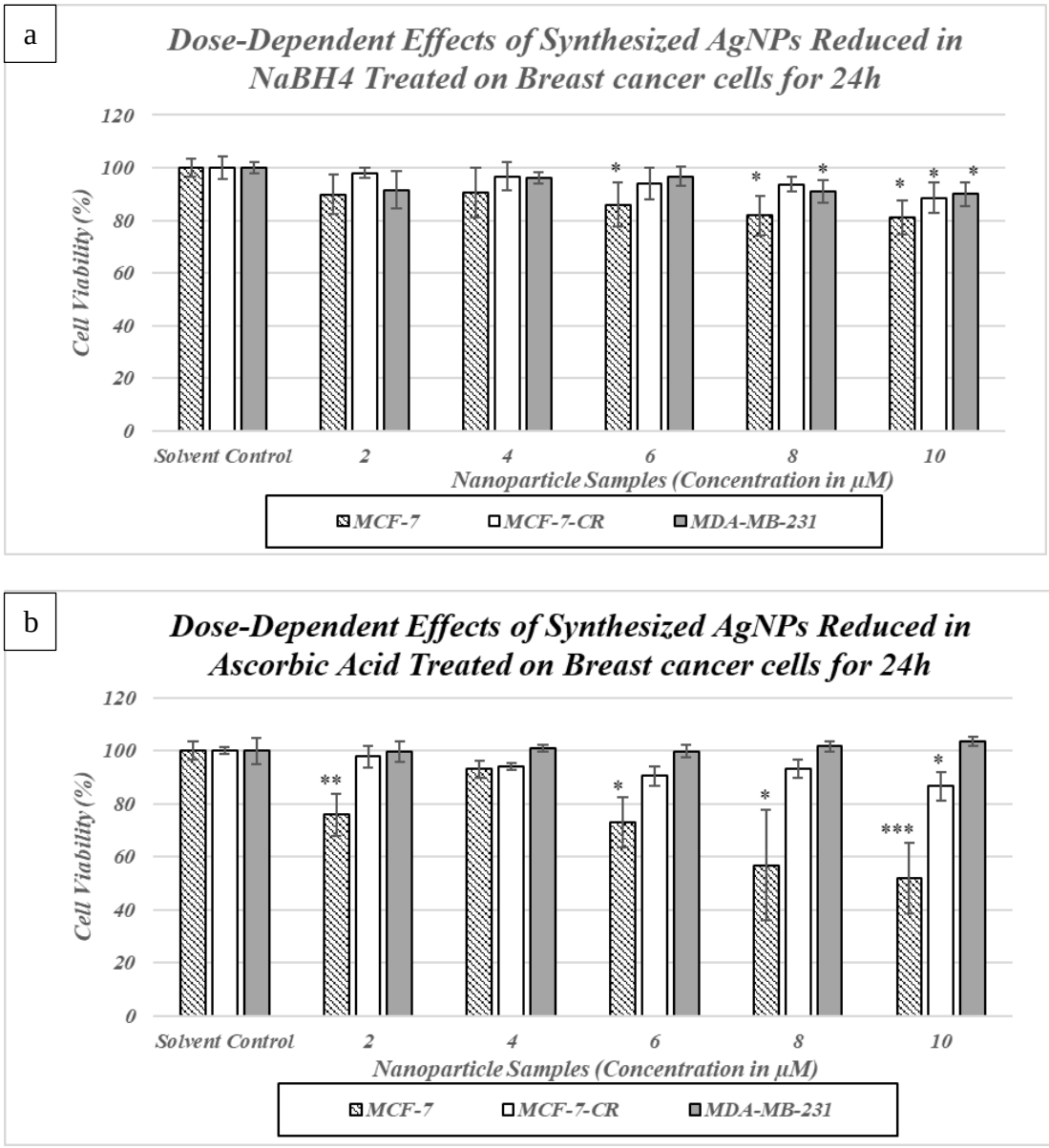

Figure 4.9. Dose-dependent effects of synthesized AuNPs treatment on MCF-7, MCF-7-CR, and MDA-MB-231 with AgNPs synthesized using reducing agents (a) $NaBH_4$ and (b) ascorbic acid. Student's *t*-test was performed for AgNPs concentrations compared to the solvent control for p-value $\alpha < 0.05$, $\alpha < 0.01$, and $\alpha < 0.005$ (* is partially significant, ** is significant, and *** is highly significant).

When comparing with the cytotoxicity results for AgNPs and AuNPs (Figures 4.8a, 4.8b, 4.9a, and 4.9b), ascorbic acid-reduced AgNPs were found to have the strongest cytotoxicity compared to most nanoparticles against MCF-7 and MCF-7-CR. However, in terms of cytotoxicity against MDR breast cancer cells such as MCF-7-CR and MDA-

MB-231, $NaBH_4$-reduced AuNPs were the more potent nanoparticles, indicating a higher potential for both inorganic metallic nanoparticles to be used as the basis for therapeutics on MDR breast cancer cells.

4.4.Cytotoxicity of graphene oxide (GO) nanoparticles as organic nanoparticle-based therapeutics against breast cancer cell lines

Graphene Oxide (GO) nanoparticles were used as the organic nanoparticle-based therapeutics to contrast against the metallic inorganic nanoparticles. GO samples were synthesized and provided by Prof. Khalid's team (Simon *et al.*, 2021), where GO samples were characterized by UV-vis spectroscopy, FTIR spectroscopy, Raman spectroscopy, and FESEM analysis.

To characterize GO suitability as an organic nanoparticle-based therapeutic, GO nanoparticles were first screened for toxicity against breast cancer cells. Breast MDR cancer cell lines were also tested to see whether GO as a treatment could affect the viability of MDR phenotype-exhibiting cancer cells. DI H_2O-dissolved GO, further diluted in PBS solvent was used for the treatment of breast cell line MCF-7 as well as on MDR cancer cells MCF-7-CR and MDA-MB-231 (Figure 4.10). While the treatment resulted in cell viability reduction in both MCF-7 and MDA-MB-231 cells, the treatment did not result in cell death for MCF-7-CR. Student's *t*-test was also performed for the highest GO concentration treatment against solvent control to determine the significance of cell viability reduction or treatment in cells, with the GO treatment at the highest concentration in MCF-7 deemed to be significant at $\alpha < 0.05$ and MDA-MB-231 to not be significant ($\alpha < 0.05$). At lower concentrations, GO treatment on both cells was found to not be potent, with the cytotoxic threshold noted to start around 25 µg/mL. Interestingly, GO increased the viability of MCF-7-CR even with only PBS solvent treatment at 3h incubation.

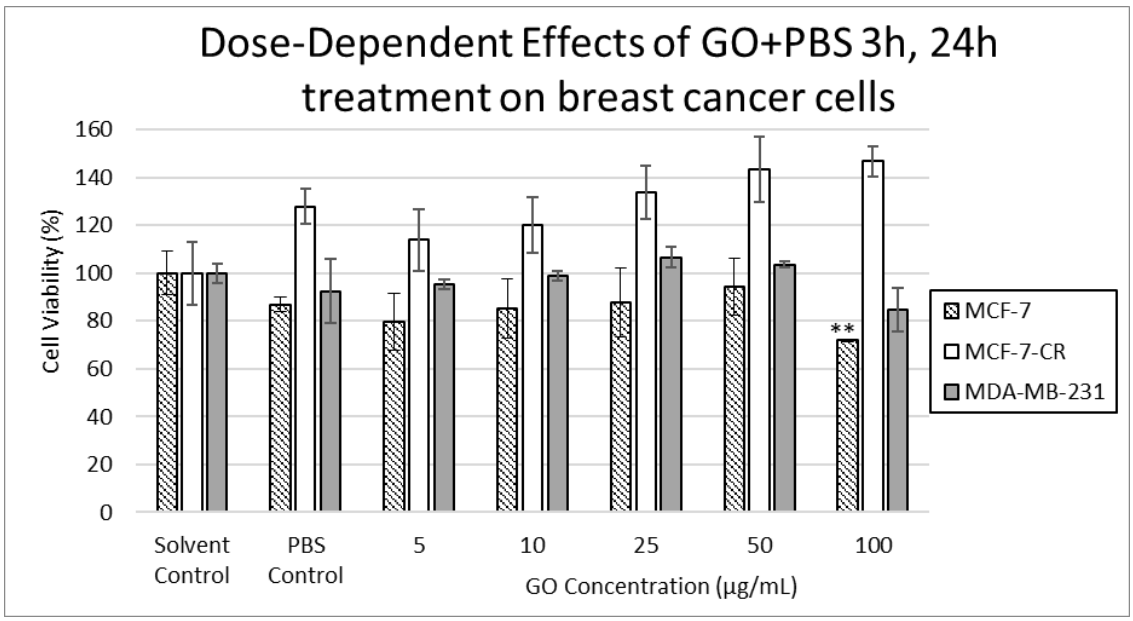

Figure 4.10 Dose-dependent effect of DI H_2O-dissolved GO on MCF-7, MCF-7-CR, and MDA-MB-231. Cells were treated in GO diluted in PBS for 3h before being added with completed DMEM media for additional incubation of 24h. Student's *t*-test was performed for GO concentration compared to the solvent control for p-value $\alpha < 0.05$, $\alpha < 0.01$, and $\alpha < 0.005$ (* is partially significant, ** is significant, and *** is highly significant).

Based on Figure 4.10, GO was more cytotoxic in MCF-7 instead of the other chemo-drug-resistant cancer cells. To determine whether the toxicity of GO was influenced by different solvent treatments, GO was further tested against the standard breast cancer cell line non-chemo-drug-resistant MCF-7 instead of the other cell lines. One sample revolved around treatment by DI H_2O-dissolved GO dilution in PBS for 3h incubation treatment before supplemented with completed DMEM media for an additional 24h, while another sample worked with DI H_2O-dissolved GO dilution in 10% completed DMEM for 24h incubation treatment. Based on Figure 4.11a, 3h treatment of PBS+GO reduced viability to about 85% at 25 µg/mL but did not result in further reduction of cell viability on increasing concentration. In the other experiment (Figure 4.11b), 24h incubation treatment of DMEM+GO was confirmed to have dose-dependent effects on MCF-7 with cell viability reduced to up to 60% at the highest concentration.

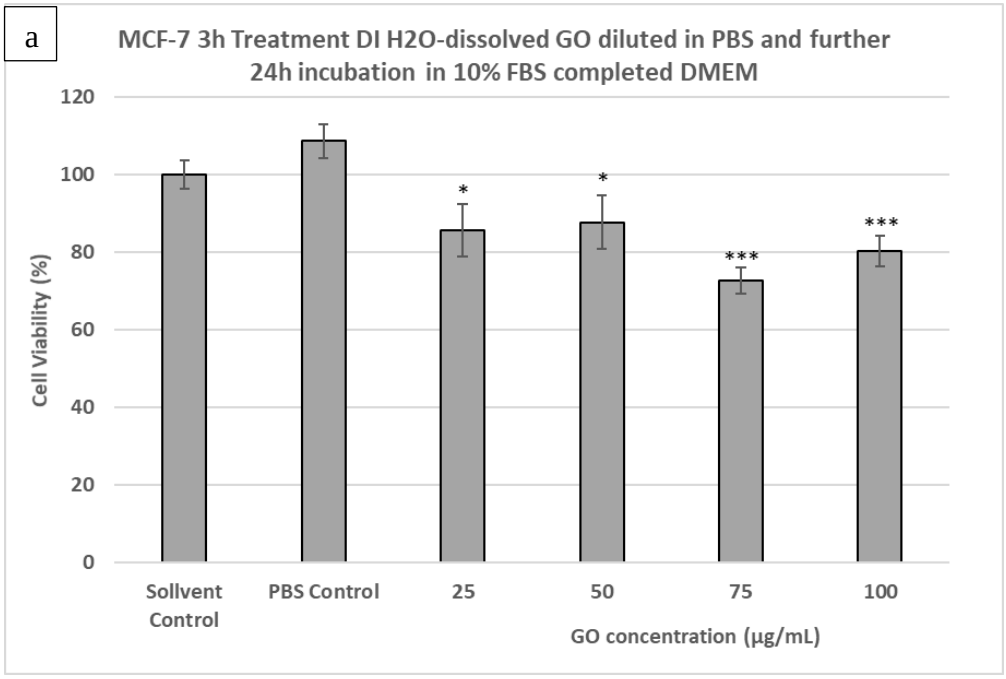

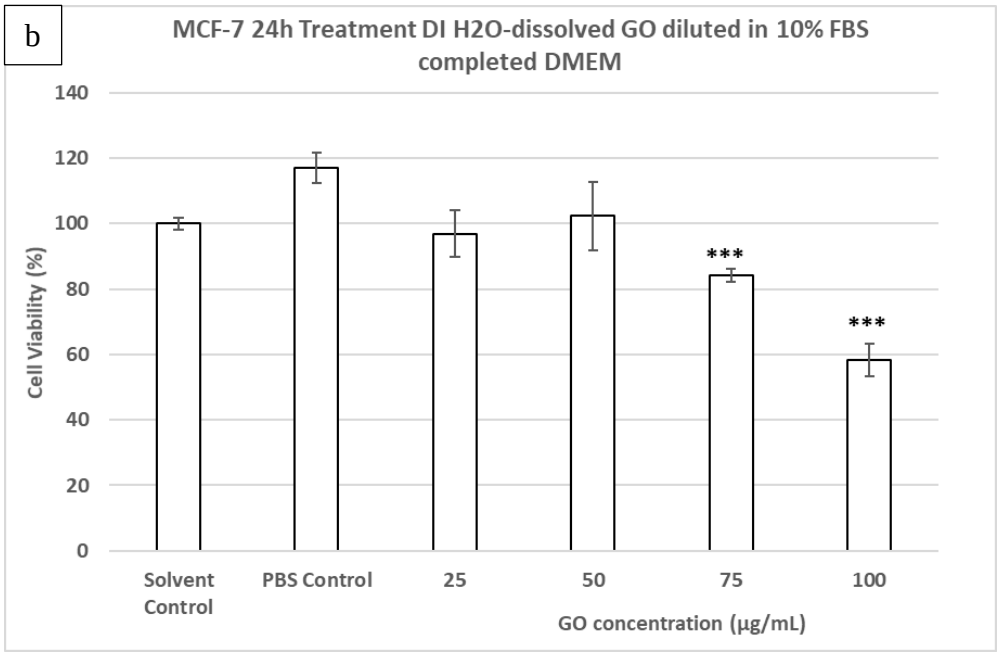

Figure 4.11 Dose-dependent effect of DI H_2O-dissolved GO treatments on MCF-7, where (a) cells were treated in GO diluted in PBS for 3h before being added with completed DMEM media incubation for 24h and (b) GO diluted in completed DMEM media for 24h incubation treatment. Student's *t*-test was performed for samples GO concentration compared to the respective solvent control for p-value $\alpha < 0.05$, $\alpha < 0.01$, and $\alpha < 0.005$ (* is partially significant, ** is significant, and *** is highly significant).

To determine whether UV-B irradiation could modulate the cytotoxicity of GO and further reduce cell viability, UV-B irradiation experiment on PBS+GO treatment was conducted (Figures 4.12a and 4.12b). DI H_2O-dissolved GO diluted in PBS were treated to cells for at least 3h and 6h before exposure to UV-B irradiation and subsequent incubation in culture media for an additional 24h. As seen in Figure 4.12a, samples would have GO dose-dependent effects as well as UV dose-dependent effects on MCF-7, where a higher concentration of GO and UV-B exposure energy would increase cell death. At 3h incubation using GO 50 µg/mL, viability was reduced to around 50% for UV-B at 10 mJ/cm^2 which was 30% and 20% lower than 0 and 5 mJ/cm^2. The results suggested some indication of synergistic or possible additive toxicity from both UV-B and GO treatment. In Figure 4.12b, the same GO dose-dependent effect was seen for 6h GO incubation but not entirely for UV dose-dependent effect as the cell viability of UV-B exposure at 10 mJ/cm^2 for 50 µg/mL was not lower than 0 and 5 mJ/cm^2. While additive toxicity effects were indeed seen on both occasions of 3h and 6h incubation on 0 and 5 mJ/cm^2, the resulting cell viability discrepancy was not too high. Another thing to note was the cytotoxicity on 6h of PBS treatment, where all MCF-7 viability was seen to be reduced by 20%, which suggested that PBS may attenuate GO incubation at lower duration incubation but would become more toxic as time progresses.

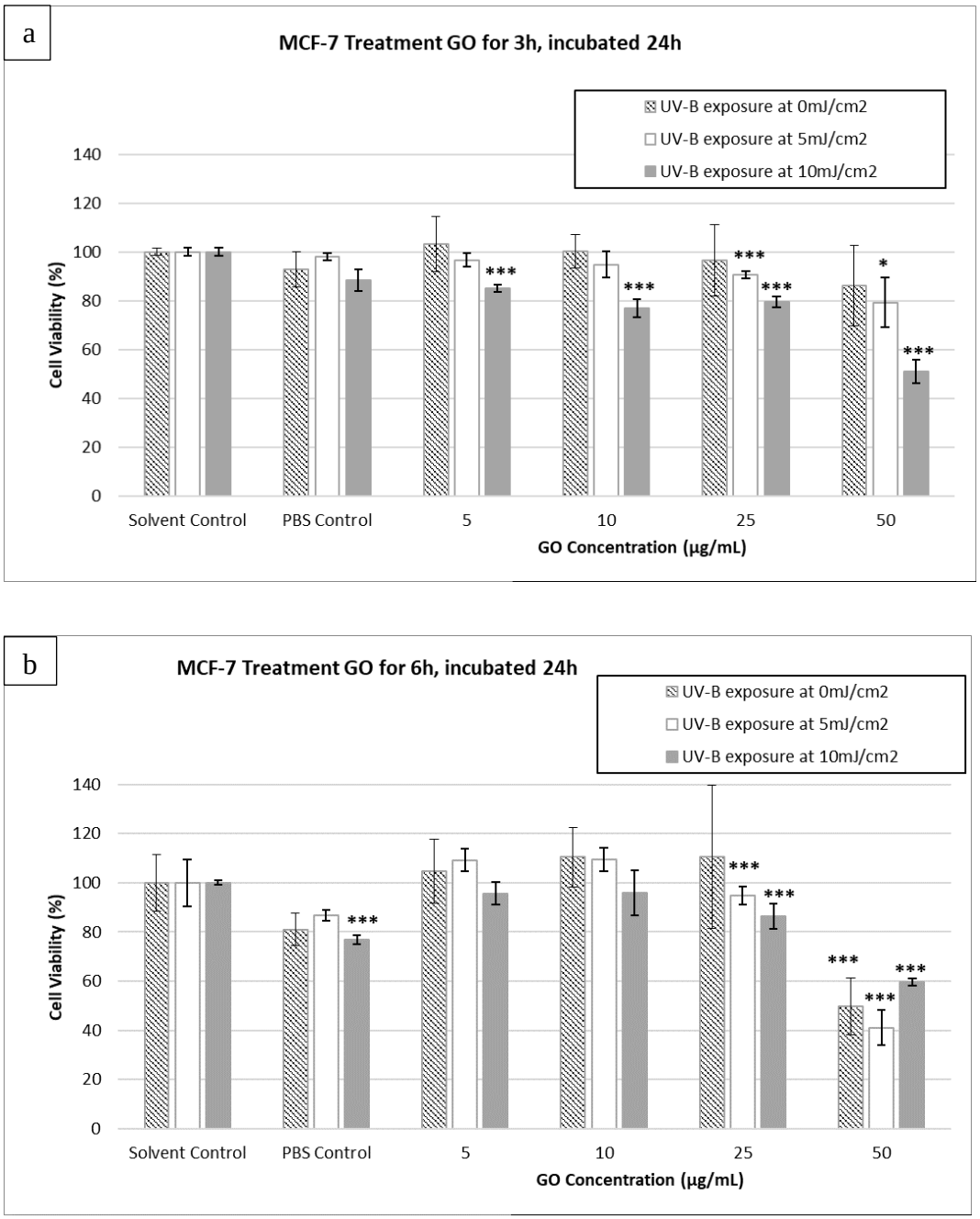

Figure 4.12 Dose-dependent effect of DI H_2O-dissolved GO coupled with UV-B irradiation exposure on MCF-7. Cells were treated in GO diluted in PBS for (a) 3h and (b) 6h before being irradiated in UV-B at 0 mJ/cm^2, 5 mJ/cm^2, and 10 mJ/cm^2. Cells were then added with completed DMEM media for 24h incubation. Student's *t*-test was performed for samples GO concentration compared to the respective solvent control for p-value $\alpha < 0.05$, $\alpha < 0.01$, and $\alpha < 0.005$ (* is partially significant, ** is significant, and *** is highly significant).

CHAPTER 5 - DISCUSSION

5.1.Cytotoxicity of breast cancer cell lines against various antineoplastic agents

Cisplatin (CDDP) treatment effects on cell viability revealed that while initially, all cell lines did not die in response to different drug doses, cells eventually were affected by CDDP and were shown to die in higher concentrations starting from MCF-7, MDA-MB-231, and MCF-7-CR (Figures 4.1a, 41b, and 4.1c). MCF-7-CR and MDA-MB-231 were known to be breast cancer cell lines with chemoresistance against specific drugs, with MCF-7-CR being resistant to CDDP; while the MDA-MB-231 cell line was nonresponsive against hormonal-related drugs due to their lack of hormone receptors (Theodossiou *et al.*, 2019). As a DNA-alkylating agent, CDDP has been widely used as a treatment for metastatic breast cancer mainly due to how it can force apoptosis, DNA damage, and intracellular Ca^{2+} gradient imbalance due to ROS generation. However, prolonged exposure to CDDP resulted in heightened resistance for MCF-7 in the form of MCF-7-CR cells (Al-Taweel *et al.*, 2014; Ajabnoor *et al.*, 2012) as well as in TNBCs such as in MDA-MB-231 cells (Koh *et al.*, 2021; Wawruszak *et al.*, 2015).

Intriguingly, results for CDDP cytotoxicity in MCF-7-CR were not dissimilar to MCF-7 even at 48h and 72h (Figures 4.1a and 4.1b), unlike the results reported by Al-Taweel *et al*. (2014), Ruiz-Silvestre *et al*. (2024), as well as Watson *et al*. (2007) where even at 24h significant resistance were seen at about two-fold compared from MCF-7 and MCF-7-CR. In the procedures performed by Al-Taweel *et al*., Ruiz-Silvestre *et al*., and implied performed by Watson *et al*., the MCF-7 cells were initially subjected to sublethal doses of CDDP and the remaining surviving cells were treated with increasing CDDP dosage until their final differing concentrations at about 1 or 50 µM. Using the highest concentration, MCF-7-CR cells were further treated up to 7 times to maintain the artificially conferred MDR phenotype in the cells. While the low-dose resistance could be explained by how MCF-7 cells are highly prone to mutation and short-term MDR

phenotype expression (Comşa *et al.*, 2015; Lee *et al.*, 2015); it was highly speculated that the MCF-7-CR cells generated in this study was not as stable or had not expressed enough MDR-associated proteins and genes as the ones reported in the other studies due to technicalities such drug degradation which would also explain the inconsistent and unremarkable cytotoxicity results on MCF-7 and MDA-MB-231 in Figures 4.1a-c. CDDP was not freshly prepared upon treatment and was roughly used in the study for about 7-8 months in 4°C storage, which may have resulted in further degradation for each drug to the extent of reduced lethality. For CDDP, it was reported that while DMF solvent coupled with 4°C temperature was a highly appropriate environment for storage, cytotoxicity was found to be slightly reduced in A2780 ovarian cancer cells after cold-stored for 57 days (Yi and Bae, 2011). Sub-culture issues may also be another factor that resulted in lower MCF-7-CR stability, as MCF-7 cells are generally known to be genotypically unstable and can morph into variants rapidly, resulting in more finicky situations on sub-culturing MCF-7 cells even in lower cell passages (Comșa *et al.*, 2015). Therefore, the results for most MCF-7-CR cells as well as CDDP cytotoxicity in this study should not be taken at face value and may need to be appropriately retested to confirm whether such technical errors had occurred.

Similar to CDDP, treatment of paclitaxel (PTX) resulted in increased cell death percentage proportional to increased concentration and exposure time, albeit reaching stagnation at a faster rate than CDDP in most cell lines (Figures 4.2a, 4.2b, and 4.2c). In terms of mechanism of action, the key cytotoxic principle of PTX is through the stabilization of microtubules, thereby resulting in mitotic arrest (Kim *et al.*, 2015) as well as subsequent apoptosis due to the disruption of mitochondrial ionic homeostasis (Saunders *et al.*, 1997; Martins *et al.*, 2020). Treatment of PTX was studied to result in high apoptosis in MCF-7, yet apoptosis and necrosis were not induced in MDA-MB-231 cells (Calaf *et al.*, 2018). Prolonged exposure to PTX in breast cancer was recorded and

reviewed to result in MDR phenotype acquisition, with MCF-7 cells recorded to produce MDR1 protein thereby increasing PTX efflux, whereas expression of key proteins and RNAs resulted associated with some cancer hallmarks were upregulated in MDA-MB-231 cells after prolonged exposure to PTX (Zhao *et al.*, 2022; Samaan *et al.*, 2019).

In all cell lines, alpha-mangostin (A-MG) and andrographolide (Andr-G) resulted in cell death reduction starting from 24h (Figures 4.3a and 4.3a), especially MDR phenotype cell lines MCF-7-CR and MDA-MB-231 where cells were found to be more sensitized compared to non-MDR MCF-7 (Figures 4.3b, 4.3c, 4.4b, and 4.4c). Both A-MG and Andr-G are considered antineoplastic-behaving phytochemical compounds which can induce apoptosis signaling as well as cell cycle arrest in breast cancer cells, despite not yet being designated as FDA-approved anticancer drugs (National Center for Biotechnology Information **B** and **C**, 2023; Zhu *et al.*, 2021; Tohkayomatee *et al.*, 2022). It was reported by Simon *et al.* (2022) that A-MG was able to inhibit MCF-7 and MCF-7-CR growth by regulating certain apoptotic-related proteins, with prolonged exposure resulting in highly increased cell death. A-MG was also further studied to treat MDA-MB-231 cells by inhibiting the important FAS pathways that were related to the metabolism of intracellular free fatty acids and cell membrane lipids (Li *et al.*, 2014). Andr-G was confirmed to be effective as a cytotoxic agent as shown and discussed by Tohkayomatee *et al.* (2022). It was reported that the compound was able to specifically target Luminal A-subtype breast cancer cells such as MCF-7 due to possessing an anti-estrogenic activity against the ERα receptors in MCF-7 cells and interestingly inhibited the already low-leveled ERβ estrogenic receptor in MDA-MB-231 cells. Besides MDA-MB-231 (Peng *et al.*, 2018), Andr-G was also found to suppress cell metastasis and proliferation in MCF-7 by inhibiting NF-κB and VEGF signaling (Li *et al.*, 2021).

By comparing the cytotoxicity of each antineoplastic agent on multiple cell lines, PTX was still the strongest even among the more novel compounds in terms of used

concentration at the nM scale. In the higher concentration µM scale, A-MG was more toxic than Andr-G and CDDP, with the least cytotoxic inducing drug being Andr-G on MCF-7 cells (Figure 4.4a). However, in terms of cell sensitization over treatment duration, A-MG and Andr-G were the most potent, with the least potent being PTX where both drug-resistant cancer cells were shown to become more desensitized over time (Figures 4.2b and 4.2c). As seen with PTX treatment in MCF-7-CR and MDA-MB-231, toxicity was not enough as the criterion for selecting antineoplastic drugs. Besides inherent cytotoxic activity, anticancer drugs need to have high cancer sensitization and low resistivity capability for use in MDR breast cancer cases, which may be able to be evaluated by noting the effects of drug treatments on various cancer parameters over periods such as cell viability or proliferation. Novel targeted drugs can bypass the MDR mechanisms in cancer (Bukowski *et al.*, 2020), as in the case of the A-MG and Andr-G which are still not much studied against cancer cells. The results on each antineoplastic agent cytotoxicity against MCF-7-CR and MDA-MB-231 showed that despite breast cancer cells becoming more resistant to two commonly used FDA-approved anticancer drugs in the long run, there are still many novel potential anticancer drugs that are highly sensitive and can be found throughout nature as in the case for A-MG and Andr-G.

5.2.Synthesis and characterization of gold nanoparticles (AuNPs) and silver nanoparticles (AgNPs) as metallic nanoparticle-based therapeutics

UV-vis spectroscopy can be used for the measurement or more specifically, the observation of SPR in nanoparticles which enables the determination of various other characteristics such as size-shape morphology, nanoparticle colloidal stability, and nanoparticle purity (Kovacs *et al.*, 2022). This can be achieved by the measurement of changes in plasmonic peak shifts, absorbance amplitude change, and specific changes in certain absorbance ranges. Metallic nanoparticles in the form of gold nanoparticles (AuNPs) and silver nanoparticles (AgNPs) were able to be synthesized using different

types of reducing agents, with different reducing agents resulting in various changes in SPR plasmonic characteristics (Figures 4.5a and 4.5b). As reducing agents, ascorbic acid, $NaBH_4$, and hydrazine hydrate are used in the chemical synthesis of metallic nanoparticles in certain quantities to keep the balance between particle dispersal stability and particle agglomeration. All three reducing agents were confirmed to be able to synthesize AgNPs and AuNPs based on the observed SPR of both nanoparticles. While hydrazine hydrate was able to reduce Ag and Au into solids in higher amounts than $NaBH_4$ and ascorbic acid, the hydrate also increased ionic interactions which caused AgNPs and AuNPs synthesized by hydrazine hydrate to form large precipitates (Figures 4.5a and 4.5b).

Further characterization of AgNPs in strong reducing agent $NaBH_4$ and AuNPs in strong reducing agent ascorbic acid revealed that despite the successful synthesis of nanoparticles as shown in UV-vis spectroscopy with traces of intermolecular surface interaction and surface moieties in FTIR spectroscopy (Figure 4.5a, 4.5b, 4.6a, and 4.6b), SEM showed that dried AuNPs were attracted to others (Figure 4.7a). The Zeta potential and polydispersity of AuNPs synthesized in ascorbic acid (Table 4.1) suggested that the nanoparticles did not have high enough electrokinetic potential to form a shielding layer between Au solid against the ionic solvent. Zeta potential corresponds to colloidal stability and dispersity of nanoparticles, with higher zeta potential associated with higher nanoparticle dispersal (Rasmussen *et al.*, 2020). The surface functional groups also contributed to stability, as the moieties impacted the polarity of the nanoparticle and resulted in changes in the weakly charged outer nanoparticle region. Size-shape morphology also influences colloidal stability due to the inversely proportional relationship between size and zeta potential (Nakatuka *et al.*, 2015; Malvern Instruments, 2015). This was more apparent in SEM analysis and DLS on synthesized AgNPs in $NaBH_4$, where most nanoparticles had combined resulting in an irregular mesh with a

very large diameter (Figure 4.7b and Table 4.1). The surface charge of AgNPs was also far lower than the general zeta potential threshold for electrostatically stable suspension of ±30 mV, which was determined to be highly unstable and easily agglomerated (Gumustas *et al.*, 2017). In some studies, AgNPs were able to be synthesized with similar and lower zeta potential than threshold ±30 mV albeit in the presence of stabilizing agents such as PVA for the spherical $NaBH_4$-AgNPs with zeta potential -11.10 mV and particle size of around 30 nm (Roto *et al.*, 2018) as well as trisodium citrate capping agent for the spherical $NaBH_4$-AgNPs with zeta potential -22.2 mV and particle size of around 50 nm (Kaur *et al.*, 2013).

To regulate particle size-shape formation, surface charge, and aggregation, stabilizing agents such as polymers are an important additive as they control surface contact between the outer nanoparticle crystalline structure and ionic solvent through steric and electrostatic blocking (Javed *et al.*, 2020). Roto *et al.* (2018) reported that AgNPs synthesized with the three aforementioned reducing agents were stabilized with PVA and resulted in plasmonic peak shift as well as particle morphology change.

Aside from SPR peak shift and size-shape morphology change, differences in reducing agents would also result in different characteristics. It was noted that AgNPs synthesized in $NaBH_4$ and ascorbic acid resulted in more negatively charged zeta potential as well as overall more shelf-stable colloids than AgNPs synthesized in hydrazine hydrate even in the presence of stabilizers (Roto *et al.*, 2018), confirming our hypothesis that AuNPs and AgNPs made from hydrazine hydrate (Figure 4.5a and 4.5b) were less stable due to the inherent property of the reducing agent itself. Demchenko *et al.* (2020) investigated changes in electrical, thermomechanical, and morphological properties of AgNP-polymer nanocomposite synthesized in different reducing agents and found that due to the different reducing strengths of each agent, nanoparticles unique from one another were synthesized with different antimicrobial levels.

5.3.Cytotoxicity of gold nanoparticles (AuNPs) and silver nanoparticles (AgNPs) against breast cancer cells

In our study, AuNPs and AuNPs synthesized in ascorbic acid were found to exhibit different levels of cytotoxicity against breast cancer cells MCF-7, MCF-7-CR, and MDA-MB-231 compared with nanoparticles synthesized in $NaBH_4$. In all types of cell models, $NaBH_4$-reduced AuNPs were relatively more toxic than ascorbic acid-reduced AuNP (Figures 4.8a, and 4.8); whereas ascorbic acid-reduced AgNPs were more toxic than $NaBH_4$-reduced AgNPs, except in MDA-MB-231 cells where ascorbic acid-reduced AgNPs did not result in any cell deaths (Figures 4.9a and 4.9b). In terms of cytotoxicity in MCF-7 cells, the most to least cytotoxic nanoparticles were ascorbic acid-reduced AgNPs > $NaBH_4$-reduced AuNPs > $NaBH_4$-reduced AgNPs > ascorbic acid-reduced AuNPs. In terms of cytotoxicity in MCF-7-CR cells, the most to least cytotoxic nanoparticles were $NaBH_4$-reduced AuNPs > ascorbic acid-reduced AgNPs > $NaBH_4$-reduced AgNPs > ascorbic acid-reduced AuNPs. In terms of cytotoxicity in MDA-MB-231 cells, the most to least cytotoxic nanoparticles were $NaBH_4$-reduced AuNPs > ascorbic acid-reduced AuNPs > $NaBH_4$-reduced AgNPs > ascorbic acid-reduced AgNPs. The disparity in different breast cancer cell models was likely due to the size-shape morphology of each nanoparticle, zeta potential, the surface composition of each nanoparticle which contained traces of reducing agents working as capping agents, or even the inherent toxicity of the base metals used for each nanoparticle (Kaur *et al.*, 2013).

While there were conflicting reports on the mechanism of action of ascorbic acid cancer toxicity, ascorbic acid was known to affect breast cancer cells and was also found to synergize with other anticancer drugs (Hong *et al.*, 2007). In one recent study, ascorbic acid was able to induce apoptosis and generate oxidative stresses in TPC-1 thyroid cancer (Tronci *et al.*, 2021). Although meager studies were found on the cytotoxicity of $NaBH_4$, it is regarded as a toxic and corrosive chemical, possibly due to its highly reducing

properties similar to ascorbic acid and how it can decompose into hydrogen gas and sodium hydroxide in the presence of water (Schlesinger *et al.*, 1953; National Center for Biotechnology Information **A**, 2023).

AuNPs made from both reducing agents were indicated to have some cytotoxicity activity against MCF-7 breast cancer (Figure 4.8a and 4.8b), which is supported by Woźniak *et al.* (2017) where spherical AuNPs synthesized in tannic acid were able to kill HeLa cervical cancer within 24h starting from 16 µM of nanoparticles. In a study where $NaBH_4$ was used as both a reducing and capping agent, spherical AuNPs were able to exhibit cytotoxicity comparable with cisplatin to induce apoptosis and DNA damage in A549 lung cancer while not targeting normal cell line HBL100 (Ramalingam *et al.*, 2017). Synthesized AuNPs in our study showed cytotoxic effects in chemo-drug-resistant cancer cell MCF-7-CR (Figures 4.8a and 4.8b), which were in line with a study done by Jiang *et al.* (2020) that used a different chemo-drug-resistant breast cancer derivative MCF-7/ADR that was resistant to adriamycin. Jiang *et al.* (2020) reported that $NaBH_4$-reduced AuNPs induced apoptosis and bypassed MDR efflux receptors in cells due to its larger size than the protein binding pocket at around 5.4 nm, showing that size morphology impacted MDR-related chemotherapy. The cytotoxicity of $NaBH_4$-reduced AuNPs in MDA-MB-231 cells was also supported by a study done by Balakrishnan *et al.* (2017) where the dose-dependent activity of AuNPs was seen on both MCF-7 and MDA-MB-231 treatment. In the highest concentration 125 µM, both treatments resulted in about 75% cell viability and detected apoptotic cell death.

While not as strong as in both chemo-drug-resistant breast cancer cells, AgNPs were confirmed to be more toxic than AuNPs in MCF-7 cells (Figures 4.9a and 4.9b), likely due to the same mechanism of action in AuNPs treatment. $NaBH_4$-reduced AgNPs were found to be toxic to non-MDR cancer cells similar to several reported studies, where Kovacs *et al.* (2020) were able to inhibit MCF-7 growth and reduced viability at IC_{50}

approximately 50 µM AgNPs; while Kaur *et al.* (2013) found that $NaBH_4$-reduced AgNPs were toxic to A431 skin carcinoma despite not as toxic as tannic-acid-reduced AgNPs. In terms of mechanism of action, AgNPs were recorded to be able to induce necrosis and lipid peroxidation; while Ag^+ ions were more capable of inducing apoptosis and DNA damage in cancer cells (Rohde *et al.*, 2021). An investigation in doxorubicin-resistant, drug efflux transporter-overexpressing chemo-drug-resistant breast cancer cell derivative MCF-7/KCR was performed by Gopisetty *et al.* (2019), where it was revealed that cytotoxicity and MDR phenotype attenuation exhibited by $NaBH_4$-reduced AgNPs was size-dependent. Smaller AgNPs were more prone to be removed from cancer cells but were more toxic to cells due to the higher amount of reactive silver, while larger AgNPs were less cytotoxic due to not being well uptaken but caused MDR phenotype attenuation through endoplasmic reticulum stress which increased protein misfolding, including MDR receptor proteins. The cytotoxicity results for both AgNPs on MDA-MB-231 cells were also found to be far less effective than in one study done by Roszak *et al.* (2017), likely due to the multiple reducing agents and stabilizers used which resulted in key characteristics that could induce genotoxicity such as size-shape morphology. Their investigation found that the synthesized AgNPs were more sensitive against MDA-MB-231 cells rather than MCF-7, likely due to some endocytic activity from Ag^+ ions as well as smaller endocytosed AgNPs.

Types of solvents may also have some effects on the cytotoxicity of AgNP and AuNP towards cancer cells, however, the nanoparticles were prepared and constituted in water solvent which is known to be non-toxic even at the tested sample concentration. Investigations on various solvent effects were also not performed in this study. For one, certain solvents influence the size-shape morphology, surface charge, toxicity, as well as stability of synthesized nanoparticles due to polarity, as in the case of the use of organic polar aprotic solvent DMSO in synthesis. In one study performed by Xu and Han (2016),

DMSO was used as a solvent for the synthesis of AgNPs and they noted that DMSO resulted in more stable particle formation and less colloidal aggregation due to the high solvent polarity. Besides AgNPs, the geometric shape of AuNPs was also found to be affected by DMSO solvents as an additional capping agent due to the Au-S partial conjugation bonds (Niu *et al.,* 2017). The use of other solvents was also suggested to influence the cytotoxicity of nanoparticles by changing size-shape morphology as well as additive toxicity effects from the solvents, as reported by Amgoth *et al.* (2019). Amgoth *et al.* (2019) found that AuNPs made from DMF at size 10 nm were more toxic than N-methyl-2-pyrrolidone AuNP at size 40 nm when treated with K562 leukemia cancer cells, likely due to the ease of internalization for smaller AuNP and subsequent accumulation of the more toxic organic solvent DMF.

5.4.Graphene oxide (GO) as organic nanoparticle-based therapeutics

As a type of both organic and ceramic-nanoparticle, Graphene oxide (GOs) and their derivatives or functionalized GOs have been a large interest in the cancer therapeutic field of study, particularly with the toxicity mechanism of action towards various cancer hallmark signaling. The structure of GO and its moieties allow the generation of intracellular ROS, which is a well-known therapeutic means to treat cells as they can induce immune responses, DNA repair mechanism, as well as organelle breakdown (Rhazouani *et al.*, 2021; Ou *et al.*, 2016). In a study performed by Shen *et al.* (2022), GO induced ROS formation inside HCT116 colorectal cancer cells which triggered specific pathways associated with autophagy and apoptosis. GO was also reported to reduce breast cancer cell viability for non-chemo-drug-resistant MCF-7 cells by inducing apoptosis (Simon *et al.*, 2021) and for MDR MDA-MB-231 cells by increasing ROS formation (Wu *et al.*, 2015). Our study also showed that GO exhibited cytotoxicity effects on MCF-7 and MDA-MB-231 cells, likely due to similar apoptotic signaling (Figure 4.10). However, GO did not exhibit toxicity in MCF-7-CR and even increased viability, thus indicating

that the GO had triggered some MDR phenotype signaling in the Luminal A subtype MCF-7-CR that was different from basal-like subtype MDA-MB-231.

Due to its structure and high solubility, GO nanosheets, or more specifically the moieties of GO nanosheets are prone to intermolecular interactions with other charged particles and electrolytes in certain solvents. PBS and cell culture media have been documented to affect GO aggregation and solubility which also impacted cancer cell uptake as well as toxicity, in the form of cell membrane ruffling and shedding without causing damage (Bussy and Kostarelos, 2017). Franqui *et al.* (2019) and Cho *et al.* (2016) suggested that GO nanosheet multi-layered stacking had also contributed to cell uptake and toxicity, as the singular hydrophobic GO sheets would be covered and adsorbed proteins such as FBS from cell culture media which made them highly dispersed and easily exhibit cytotoxicity. However, multi-layered, protein-covered, hydrophobic GO sheets with large hydrophilic edge regions would result in larger GO aggregates which lowered cytotoxicity due to lower cell uptake. Results from our study also showed different cytotoxicity levels between GO in salt-bearing PBS and FBS-impregnated DMEM culture media, which further suggested that the selection of appropriate treatment solvent is crucial (Figures 4.11a and 4.11b).

5.5. Influence of UV-B irradiation on cytotoxicity of Graphene oxide (GO) against non-chemo-drug-resistant MCF-7 breast cancer cell

UV-B irradiation has been long studied as a prospective non-chemotherapy. Prolonged UV-B (280-320nm) exposure can reduce cell viability by increasing ROS generation which damages DNAs as well as disrupting organelles, thereby inducing apoptosis. While cell death was not seen immediately post-irradiation, after 24h a large percentage of HaCaT skin cancer cells were dead (Khalil and Shebaby, 2017). In breast cancer MDA-MB-468 and MCF-7, cell migration and structural motility were reduced with apoptosis seen in cells treated after UV-B irradiation, particularly MDA-MB-231 cells which were

highly sensitized to UV-B irradiation even without additional drugs (Sarkar *et al.*, 2013). This was also seen in our results for the UV-B energy at 5 and 10 mJ/cm^2 albeit not too pronounced, suspected due to the presence of Phenol-Red in some cell culture media which were irradiated by UV-B (Figures 4.12a and 4.12b). Phenol-red is a photoactive estrogen-based hormone that can form ROS and it was primarily known to be controversial concerning how it affects cell proliferation, including MCF-7 (Kuncharoenwirat *et al.*, 2020; Morgan *et al.*, 2019).

Interestingly, the cell viability result for 5 and 10 mJ/cm^2 UV-B irradiation in the presence of GO was lower than only using UV-B as well as only GO, indicating an additive or synergistic activity in terms of cytotoxicity between UV-B irradiation and GO (Figure 4.12a). As both treatments were known to induce intracellular ROS formation and subsequent apoptosis, the coupling of both treatments might synergistically affect treating cells that are more resilient to either cytotoxic mechanism. In one study, UV-A irradiation to GO resulted in structural change, particularly the removal of most hydroxyl and carbonyl functional groups which increased toxicity on monocytes by around 40% for 72h incubated GO 50 µg/mL (Gallegos-Perez *et al.*, 2019). Both UV-B and GO treatments showed proportional time- and dose-dependent toxicity effects to toxicity in MCF-7 cells, with coupled treatment found to increase ROS activity and show proper synergistic effect by calculation in combination index (Simon *et al.*, 2021).

5.6.Cytotoxicity comparison between AuNPs, AgNPs, and GO against various breast cancer cell lines

Toxicity results between the metallic nanoparticles AuNPs, AgNPs, and organic-ceramic nanoparticle GO treatments on the three cancer cell lines were compared with each other (Figures 4.8a, 4.8b, 4.9a, 4.9b, and 4.10). All nanoparticles were seen to exhibit cytotoxicity towards breast cancer cells albeit attenuated in the case of MDR phenotype-behaving cancer cells such as MCF-7-CR and MDA-MB-231. GO was more toxic against

MCF-7 and MDA-MB-231 compared to both metallic nanoparticles, with the cytotoxicity of GO being easily influenced or even increased by UV-B treatment and solvent used. Regardless, AuNPs and most AgNPs were also toxic to all breast cancer cell models tested, as they were also shown to be easily synthesized and versatile in terms of tunability of physicochemical properties. From the results, these nanoparticles show a promising future for use in MDR-related therapy as all three nanoparticles have only been extensively studied in other publications using standard breast cancer cell models in terms of mechanism of action, combinational therapy such as carrier for chemotherapeutic delivery and photothermal therapy, as well as biodistribution study in an *in vivo* model (Zhang *et al.*, 2019; Liu *et al.*, 2021). While the results could not be compared quantitatively with the four antineoplastic agents due to concentration and treatment procedure differences, all seven treatments, especially the three nanoparticles and two novel bio-derived compounds were highly potential for further studies on MDR breast cancer treatment.

Nevertheless, this study still has a major flaw, in which no tests were performed against normal cell models as well as toxicologic experiments. While the three nanoparticles were potent against breast cancer cells, there is still the possibility that the cytotoxicity was non-selective enough and may lead to systemic toxicity when exposed to normal tissue. In a study conducted by Chen *et al.* (2012), GO was treated in multiple models such as cell lines and zebrafish embryos. They found that GO resulted in lower acute cytotoxicity compared to multiwalled-carbon nanotubes due to their structures, with instances of apoptosis locally seen in the forehead and eye region of embryos. While GO was less toxic than carbon nanotubes, GO still resulted in defective morphological phenotypes such as bent spine and stunted growth. In another study, GO-induced autophagy and subsequent apoptotic cell death were found even in non-cancerous endothelial cells due

to increased Ca^{2+} in mitochondria and ER, with upregulation of c-Jun N-terminal kinase and reduced levels of Bcl-xL as well as Bcl-2 detected (Lim *et al.*, 2016).

Even at a mean size range of 20-100 nm, AgNPs purchased from Nanux were also found to induce acute toxicities and accumulate over time in the lungs, liver, kidneys, and immune organs such as spleens when tested on Sprague-Dawley rats (Wen *et al.*, 2017). Multiple intracellular biomarkers were also detected in the bloodstream after single-dose administration, suggesting tissues accumulated with AgNPs had died after internalization. Genomic malignancies were also increased in AgNPs-affected tissues, with the suggested reason being increased ROS formation which disrupted the cell cycle.

In a study done by Fraga *et al.*, (2014), 16 nm-sized polypeptide-capped AuNP nanospheres were administered in single-dose intravenously to Wistar rats to evaluate short- and long-term systemic toxicity. AuNPs were found to leave the bloodstream at a high rate and accumulate around the liver and spleen within 24h, with minimal to no detection in other vital organs. No organ-based local toxicities were seen throughout the monitoring, except for spleen tissue mass plummeting after 28 days, likely due to AuNP agglomeration in splenic blood vessels. Interestingly, systemic toxicity was seen after 28 days post-administration, where hemolytic phenomenon was detected.

CHAPTER 6 – CONCLUSION

The breast cancer MCF-7 cell line is a luminal A subtype cancer cell that is susceptible to anticancer drugs. However, the acquisition of the MDR phenotype in breast cancer and the rise of TNBC such as MDA-MB-231 cell lines made breast cancer cells insensitive to conventional, FDA-approved chemotherapeutic drugs and are becoming harder to treat. The development of novel ways to treat MDR breast cancer is crucial, particularly in the field of chemically synthesized anticancer compounds as well as bio-derived anticancer compounds. With regards to chemically synthesized compounds, nanoparticles can be used therapeutically to target breast cancer cells, especially against MDR phenotype cancer cells by bypassing MDR phenotype-associated key cancer hallmarks and mechanisms.

In this study, we have briefly investigated two novel bio-derived anticancer agents called A-MG and Andr-G alongside FDA-approved anticancer drugs PTX and CDDP to evaluate the cytotoxicity of each drug and the degree of chemo-drug resistivity of breast cancer cell lines against such drugs. We have found that the FDA-approved anticancer drug PTX was still the most potent among all four drugs tested on MCF-7 and MDR breast cancer cell lines, with the least powerful compound being Andr-G. However, PTX was found to be easily desensitized in cancer cells, especially just after 48h and 72h in MCF-7-CR and MDA-MB-231 MDR breast cancer cell lines. A-MG and Andr-G were regarded to be much harder to be desensitized in cancer cells and were able to retain the same levels of cytotoxicity even after 48h and 72h in MDR breast cancer cells.

We have synthesized metallic nanoparticles AgNPs and AuNPs against breast cancer cells. AuNPs and AgNPs were successfully synthesized in $NaBH_4$ and ascorbic acid, while hydrazine hydrate was not able to yield stable nanoparticles. $NaBH_4$-synthesized AgNPs and ascorbic acid-reduced AuNPs were characterized to be present in colloidal forms and were ascertained to have functional groups associated with their metal ion

precursors as well as reducing agents. Ascorbic acid-reduced AuNPs were found to have a low polydispersity index, spherical shape at around 170 nm, and zeta potential -36 mV. Compared with the AuNP, $NaBH_4$-reduced AgNPs were found to have a lower polydispersity index, a highly irregular shape at around 680 nm, and a low zeta potential at -21 mV. While both instances of nanoparticles were successfully synthesized as colloidal, they were highly prone to flocculation and agglomeration

We have also investigated the cytotoxicity of both metallic nanoparticles synthesized in $NaBH_4$ and ascorbic acid. $NaBH_4$ and ascorbic acid-reduced nanoparticles were toxic against non-chemo-drug-resistant MCF-7 breast cancer cells and slightly toxic against the chemo-drug-resistant MCF-7-CR and MDR MDA-MB-231 cells. The most cytotoxic nanoparticles against MCF-7 and MCF-7-CR found were ascorbic acid-reduced AgNPs as well as $NaBH_4$-reduced AuNPs, where the AgNPs tested were able to cause about 50% MCF-7 cell death while AuNPs were found to reduce MCF-7 cell viability to up to 25-30% when using 10 µM concentration. The most cytotoxic nanoparticles against MDA-MB-231 cells were also $NaBH_4$-reduced AuNPs, with AgNPs not as effective against MDA-MB-231 and no toxicity even observed for ascorbic acid-reduced AgNPs.

Organic ceramic-based nanoparticles GO were also studied for toxicity, the influence of UV-B irradiation on toxicity, and synergistic activity between nanoparticles and UV-B irradiation towards breast cancer cells. To summarize our study, GO was revealed to exhibit cytotoxicity to cancer cell lines except for MDR cancer cell line MCF-7-CR, with most cytotoxicity seen on MCF-7 where cell viability was reduced to around 70% when treated in 100 µg/mL GO. Solvents were seen to affect GO cytotoxicity, where the presence of PBS resulted in attenuation of toxicity on all GO concentrations to about 80-90% MCF-7 cell viability. GO incubation time and UV-B irradiation dose were also found to influence the cytotoxicity of GO by increasing toxicity via additive effects in MCF-7 cells, with the highest GO concentration 100 µg/mL in 3h GO incubation and 10

mJ/cm^2 UV-B energy as well as in 6h GO incubation and 5 mJ/cm^2 UV-B energy resulted in 50% and 40% cell viability respectively.

Limitations and Future Perspective

Unfortunately, the nanoparticles tested in this study (GO, AgNPs, and AuNPs) were not assayed on healthy human cell models nor *in vivo* models, which limits the understanding of whether the nanoparticles could off-target to healthy human cells or even cause significant toxicity after administration. Of the three planned MDR phenotype breast cancer cells (including the originally planned paclitaxel-resistant MCF-7-PTR), only two MDR phenotype models were used in this study as the study was subjected to a limited timeframe. The drug-resistant-acquired MCF-7-CR was even found to be limited in being desensitized due to short-term exposure as well as several other factors briefly discussed related to chemical degradation as well as MCF-7 sub-culture heterogeneity.

Hence, more studies for *in vitro* models such as 3D spheroid model, monolayer healthy breast cell models, and incorporation of paclitaxel including other drug-resistant MCF-7 cells, as well as different subtype breast cancer cell lines should be performed. Tests would need to be conducted using nanoparticles with different size-shape morphologies, FTIR spectrum, and SPR to further understand the influence of nanoparticle characteristics changes in the toxicity as well as the mechanism of action on MDR breast cancer cells. Other artificially MDR-induced breast cancer subclone cell models should also be prepared and quality-controlled in a longer drug time exposure to better control the experiments and investigate different arrays of drug resistance in MCF-7-derived MDR phenotype cell lines against nanoparticles and antineoplastic bio-derived agents.

Further studies should also be conducted to better investigate the mechanism of action for each chemotherapeutic agent used as well as the MDR mechanism of each cell against the chemotherapeutic agents, particularly in the subject of drug effluxion, metastasis,

EMT, as well as apoptosis pathway repression. With regards to the cytotoxicity results of antineoplastic agents as well as nanoparticles, another multi-modal-based study should be performed with more therapies such as the addition of previously studied antineoplastic agents A-MG and Andr-G, or gene-targeting treatments. This is to be done on GO, AgNPs, and AuNPs to better capture the application of nanoparticles in combinational therapies to sensitize MDR phenotype breast cancer cells, especially to help increase clinical usage of combined anticancer drugs and nanoparticles for breast cancer cases.

REFERENCES

Agnihotri, S., Mukherji, S., & Mukherji, S. (2014). Size-controlled silver nanoparticles synthesized over the range 5-100 nm using the same protocol and their antibacterial efficacy. *RSC Advances*, *4*, 3974–3983. https://doi.org/10.1039/c3ra44507k

Ahmad, T., Irfan, M., & Bhattacharjee, S. (2016). Parametric Study on Gold Nanoparticle Synthesis Using Aqueous Elaise Guineensis (Oil palm) Leaf Extract: Effect of Precursor Concentration. *Procedia Engineering*, *148*, 1396–1401. https://doi.org/10.1016/j.proeng.2016.06.558

Ahmad, T., Sarwar, R., Iqbal, A., Bashir, U., Farooq, U., Halim, S. A., Khan, A., & Al-Harrasi, A. (2020). Recent advances in combinatorial cancer therapy via multifunctionalized gold nanoparticles. *Nanomedicine*, 17. https://doi.org/10.2217/nnm-2020-0051

Ajabnoor, G. M. A., Crook, T., & Coley, H. M. (2012). Paclitaxel resistance is associated with switch from apoptotic to autophagic cell death in MCF-7 breast cancer cells. *Cell Death and Disease*, *3*(e260), 1–9. https://doi.org/10.1038/cddis.2011.139

Ajnai, G., Chiu, A., Kan, T., Cheng, C.-C., Tsai, T.-H., & Chang, J. (2014). Trends of Gold Nanoparticle-based Drug Delivery System in Cancer Therapy. *Journal of Experimental and Clinical Medicine*, *6*(6), 172–178. https://doi.org/10.1016/j.jecm.2014.10.015

Aliyev, E., Filiz, V., Khan, M. M., Lee, Y. J., Abetz, C., & Abetz, V. (2019). Structural Characterization of Graphene Oxide: Surface Functional Groups and Fractionated Oxidative Debris. *Nanomaterials*, *8*(1180), 1–15.

Alkaraki, A., Alshaer, W., Wehaibi, S., Gharaibeh, L., Abuarqoub, D., Alqudah, D. A., Al-Azzawi, H., Zureigat, H., Souleiman, M., & Awidi, A. (2020). Enhancing chemosensitivity of wild-type and drug-resistant MDA-MB-231 triple-negative breast cancer cell line to doxorubicin by silencing of STAT 3, Notch-1, and β-catenin genes. *Breast Cancer*, *27*(5), 989–998. https://doi.org/10.1007/s12282-020-01098-9

Al-Taweel, N., Varghese, E., Florea, A.-M., & Büsselberg, D. (2014). Cisplatin (CDDP) triggers cell death of mcf-7 cells following disruption of intracellular calcium ([ca2+]i) homeostasis. *Journal of Toxicological Sciences*, *39*(5), 765–774. https://doi.org/10.2131/jts.39.765

Amgoth, C., Singh, A., Santhosh, R., Yumnam, S., Mangla, P., Karthik, R., Guping, T., & Banavoth, M. (2019). Solvent assisted size effect on AuNPs and significant inhibition on K562 cells. *RSC Advances*, *9*(58), 33931–33940. https://doi.org/10.1039/c9ra05484g

Amina, S. J., & Guo, B. (2020). A Review on the Synthesis and Functionalization of Gold Nanoparticles as a Drug Delivery Vehicle. *International Journal of Nanomedicine*, *15*, 9823–9857.

Amreddy, N., Babu, A., Muralidharan, R., Panneerselvam, J., Srivastava, A., Ahmed, R., Mehta, M., Munshi, A., & Ramesh, R. (2018). Recent Advances in Nanoparticle-Based Cancer Drug and Gene Delivery. In *Advances in Cancer Research* (1st ed., Vol. 137). Elsevier Inc. https://doi.org/10.1016/bs.acr.2017.11.003

Anigol, L. B., Charantimath, J. S., & Gurubasavaraj, P. M. (2017). Effect of Concentration and pH on the Size of Silver Nanoparticles Synthesized by Green Chemistry. *Organic and Medicinal Chemistry*, *3*(5), 1–5. https://doi.org/10.19080/OMCIJ.2017.03.555622

Anwar, A., Fung, L. C., Anwar, A., Jagadish, P., Numan, A., Khalid, M., Shahabuddin, S., Siddiqui, R., & Khan, N. A. (2019). Effects of Shape and Size of Cobalt Phosphate Nanoparticles against Acanthamoeba castellanii. *Pathogens*, *8*(260), 1–14.

Anwar, A., Masri, A., Rao, K., Rajendran, K., Khan, N. A., Shah, M. R., & Siddiqui, R. (2019). Antimicrobial activities of green synthesized gums-stabilized nanoparticles loaded with flavonoids. *Scientific Reports*, *9*(3122), 1–12. https://doi.org/10.1038/s41598-019-39528-0

Aqeel, Y., Siddiqui, R., Anwar, A., Shah, R., & Khan, A. (2016). Gold Nanoparticle Conjugation Enhances the Antiacanthamoebic Effects of Chlorhexidine. *Antimicrobial Agents and Chemotherapy*, *60*(3), 3–8. https://doi.org/10.1128/AAC.01123-15.Address

Balakrishnan, S., Mukherjee, S., Das, S., Bhat, F. A., Raja Singh, P., Patra, C. R., & Arunakaran, J. (2017). Gold nanoparticles–conjugated quercetin induces apoptosis via inhibition of EGFR/PI3K/Akt–mediated pathway in breast cancer cell lines (MCF-7 and MDA-MB-231). *Cell Biochemistry and Function*, *35*(4), 217–231. https://doi.org/10.1002/cbf.3266

Banne, S. V, Patil, M. S., Kulkarni, R. M., & Patil, S. J. (2017). ScienceDirect Synthesis and Characterization of Silver Nano Particles for EDM Applications. *Materials Today: Proceedings*, *4*(11), 12054–12060. https://doi.org/10.1016/j.matpr.2017.09.130

Bao, H., Pan, Y., Ping, Y., Sahoo, N. G., Wu, T., Li, L., Li, J., & Gan, L. H. (2011). Chitosan-Functionalized Graphene Oxide as a Nanocarrier for Drug and Gene Delivery. *Small*, *7*(11), 1569–1578. https://doi.org/10.1002/smll.201100191

Basu, A., Ray, S., Chowdhury, S., Sarkar, A., Mandal, D. P., Bhattacharjee, S., & Kundu, S. (2018). Evaluating the antimicrobial, apoptotic, and cancer cell gene delivery properties of protein-capped gold nanoparticles synthesized from the edible mycorrhizal fungus Tricholoma crassum. *Nanoscale Research Letters*, *13*(154), 1–16. https://doi.org/10.1186/s11671-018-2561-y

Boix-Montesinos, P., Soriano-Teruel, P. M., Armiñán, A., Orzáez, M., & Vicent, M. J. (2021). The past, present, and future of breast cancer models for nanomedicine development. *Advanced Drug Delivery Reviews*, *173*, 306–330. https://doi.org/10.1016/j.addr.2021.03.018

Bukowski, K., Kciuk, M., & Kontek, R. (2020). Mechanisms of Multidrug Resistance in Cancer Chemotherapy. *International Journal of Molecular Sciences*, *21*(9). https://doi.org/10.3390/ijms21093233

Bussy, C., & Kostarelos, K. (2017). Culture Media Critically Influence Graphene Oxide Effects on Plasma Membranes. *CHEM*, *2*, 322–323. https://doi.org/10.1016/j.chempr.2017.01.015

Calaf, G. M., Ponce-cusi, R., & Carrión, F. (2018). Curcumin and paclitaxel induce cell death in breast cancer cell lines. *Oncology Reports*, *40*, 2381–2388. https://doi.org/10.3892/or.2018.6603

Carvalho, A., Fernandes, A. R., & Baptista, P. V. (2019). Nanoparticles as Delivery Systems in Cancer Therapy: Focus on Gold Nanoparticles and Drugs. In S. S. Mohapatra, S. Ranjan, N. Dasgupta, R. K. Mishra, & S. Thomas (Eds.), *Applications of Targeted Nano Drugs and Delivery Systems* (1st ed., pp. 257–295). Elsevier Inc. https://doi.org/10.1016/B978-0-12-814029-1.00010-7

Castellanos, G., Valbuena, D. S., Pérez, E., Villegas, V. E., & Rondón-Lagos, M. (2023). Chromosomal Instability as Enabling Feature and Central Hallmark of Breast Cancer. *Breast Cancer: Targets and Therapy*, *15*(March), 189–211. https://doi.org/10.2147/BCTT.S383759

Chakraborty, B., Pal, R., Ali, M., Singh, L. M., Rahman, D. S., Ghosh, S. K., & Sengupta, M. (2015). Immunomodulatory properties of silver nanoparticles contribute to anticancer strategy for murine fibrosarcoma. *Cellular and Molecular Immunology*, *13*, 191–205. https://doi.org/10.1038/cmi.2015.05

Charmi, J., Nosrati, H., Amjad, J. M., Mohammadkhani, R., & Danafar, H. (2019). Polyethylene glycol (PEG) decorated graphene oxide nanosheets for controlled release curcumin delivery. *Heliyon*, *5*. https://doi.org/10.1016/j.heliyon.2019.e01466

Chekhun, V. F., Lukyanova, N. Y., Kovalchuk, O., Tryndyak, V. P., & Pogribny, I. P. (2007). Epigenetic profiling of multidrug-resistant human MCF-7 breast adenocarcinoma cells reveals novel hyper- and hypomethylated targets. *Molecular Cancer Therapeutics*, *6*(3), 1089–1098. https://doi.org/10.1158/1535-7163.MCT-06-0663

Chen, L. Q., Hu, P. P., Zhang, L., Huang, S. Z., Luo, L. F., & Huang, C. Z. (2012). Toxicity of graphene oxide and multi-walled carbon nanotubes against human cells and zebrafish. *Science China Chemistry*, *55*(10), 2209–2216. https://doi.org/10.1007/s11426-012-4620-z

Cho, Y. C., Pak, P. J., Joo, Y. H., Lee, H.-S., & Chung, N. (2016). In vitro and in vivo comparison of the immunotoxicity of single- and multi-layered graphene oxides with or without pluronic F-127. *Scientific Reports*, *6*, 1–13. https://doi.org/10.1038/srep38884

Coblentz Society, Inc. (2023) Evaluated Infrared Reference Spectra. In P. L. Linstrom and W.G. Mallard (Eds.), *NIST Chemistry Webbook, NIST Standard Reference Database Number 69* (1st ed.). National Institute of Standards and Technology. Retrieved April 30, 2023, from https://doi.org/10.18434/T4D303

Comşa, Ş., Cîmpean, A. M., & Raica, M. (2015). The story of MCF-7 breast cancer cell line: 40 Years of experience in research. *Anticancer Research*, *35*(6), 3147–3154.

Daei, S., Ziamajidi, N., Abbasalipourkabir, R., Khanaki, K., & Bahreini, F. (2022). Anticancer Effects of Gold Nanoparticles by Inducing Apoptosis in Bladder Cancer 5637 Cells. *Biological Trace Element Research*, *200*, 2673–2683. https://doi.org/10.1007/s12011-021-02895-9

Dasari, S., & Tchounwou, P. B. (2015). Cisplatin in cancer therapy: molecular mechanisms of action. *European of Journal of Pharmacology*, *740*, 364–378. https://doi.org/10.1016/j.ejphar.2014.07.025.Cisplatin

Demchenko, V., Riabov, S., Kobylinskyi, S., Goncharenko, L., Rybalchenko, N., Kruk, A., Moskalenko, O., & Shut, M. (2020). Effect of the type of reducing agents of silver ions in complexes on the structure , morphology and properties of silver-containing nanocomposites. *Scientific Reports*, *10*(7126), 1–9. https://doi.org/10.1038/s41598-020-64079-0

Dideikin, A. T., & Vul, A. Y. (2019). Graphene Oxide and Derivatives: The Place in Graphene Family. *Frontiers in Physics*, *6*(149). https://doi.org/10.3389/fphy.2018.00149

Ding, Y., Jiang, Z., Saha, K., Kim, C. S., Kim, S. T., Landis, R. F., & Rotello, V. M. (2014). Gold Nanoparticles for Nucleic Acid Delivery. *Molecular Therapy*, *22*(6), 1075–1083. https://doi.org/10.1038/mt.2014.30

Dreaden, E. C., El-sayed, I. H., & El-sayed, M. A. (2014). Chapter 14 – Structure-Activity Relationships for Tumor-Targeting Gold Nanoparticles. In V. Torchilin (Ed.), *Handbook of Nanobiomedical Research: Fundamentals, Applications, and Recent Development* (1st ed., pp. 519–563). World Scientific.

El-Nour, K. M. M. A., Eftaiha, A., Al-Warthan, A., & Ammar, R. A. A. (2010). Synthesis and applications of silver nanoparticles. *Arabian Journal of Chemistry*, *3*(3), 135–140. https://doi.org/10.1016/j.arabjc.2010.04.008

Emiru, T. F., & Ayele, D. W. (2017). Controlled synthesis, characterization and reduction of graphene oxide: A convenient method for large scale production. *Egyptian Journal of Basic and Applied Sciences*, *4*, 74–79. https://doi.org/10.1016/j.ejbas.2016.11.002

Espinosa, E., Zamora, P., Feliu, J., & Barón, M. G. (2003). Classification of anticancer drugs — a new system based on therapeutic targets. *Cancer Treatment Reviews*, *29*, 515–523. https://doi.org/10.1016/S0305-7372(03)00116-6

Ferreira, D., Fontinha, D., Martins, C., Pires, D., Fernandes, A. R., & Baptista, P. V. (2020). Gold Nanoparticles for Vectorization of Nucleic Acids for Cancer Therapeutics. *Molecules*, *25*(3489), 1–23.

Fraga, S., Brandão, A., Soares, M. E., Morais, T., Duarte, J. A., Pereira, L., Soares, L., Neves, C., Pereira, E., Bastos, M. de L., & Carmo, H. (2014). Short- and long-term distribution and toxicity of gold nanoparticles in the rat after a single-dose intravenous administration. *Nanomedicine: Nanotechnology, Biology, and Medicine*, *10*(8), 1757–1766. https://doi.org/10.1016/j.nano.2014.06.005

Franqui, L. S., De Farias, M. A., Costa, C. A. R., Domingues, R. R., Filho, A. G. S., Coluci, V. R., Leme, A. F. P., & Martinez, D. S. T. (2019). Interaction of graphene oxide with cell culture medium: Evaluating the fetal bovine serum protein corona formation towards in vitro nanotoxicity assessment and nanobiointeractions. *Materials Science & Engineering C*, *100*, 363–377. https://doi.org/10.1016/j.msec.2019.02.066

Franchi, M., Piperigkou, Z., Karamanos, K. A., Franchi, L., & Masola, V. (2020). Extracellular matrix-mediated breast cancer cells morphological alterations, invasiveness, and microvesicles/exosomes release. *Cells*, *9*(9), 1–16. https://doi.org/10.3390/cells9092031

Fröhlich, E. (2023). The Variety of 3D Breast Cancer Models for the Study of Tumor Physiology and Drug Screening. *International Journal of Molecular Sciences*, *24*(8). https://doi.org/10.3390/ijms24087116

Fu, L.-M., Hsu, J.-H., Shih, M.-K., Hsieh, C.-W., Ju, W.-J., Chen, Y.-W., Lee, B.-H., & Hou, C.-Y. (2021). Process optimization of silver nanoparticle synthesis and its application in mercury detection. *Micromachines*, *12*(9), 1–16. https://doi.org/10.3390/mi12091123

Galatage, S. T., Hebalkar, A. S., Dhobale, S. V, Mali, O. R., Kumbhar, P. S., Nikade, S. V, & Killedar, S. G. (2021). Silver Nanoparticles: Properties, Synthesis, Characterization, Applications and Future Trends. In S. Kumar, P. Kumar, & C. S. Pathak (Eds.), *Silver Micro-Nanoparticles - Properties, Synthesis, Characterization, and Applications* (1st ed.). IntechOpen.

Gallegos-Perez, W. R., Reynosa-Martinez, A. C., Soto-Ortiz, C., Alvarez-Lemus, M. A., Barroso-Flores, J., Montalvo, V. G., & Lopez-Honorato, E. (2020). Effect of UV radiation on the structure of graphene oxide in water and its impact on cytotoxicity and As (III) adsorption. *Chemosphere*, *249*, 1–15.

Gamboa, S. M., Rojas, E. R., Martinez, V. V., & Vega-Baudrit, J. (2019). Synthesis and characterization of silver nanoparticles and their application as an antibacterial agent. *International Journal of Biosensors & Bioelectronics*, *5*(5), 166–173. https://doi.org/10.15406/ijbsbe.2019.05.00172

Gao H., Li, H., Liu, W., Mishra, S. K., & Li, C. (2021). Andrographolide Induces Apoptosis in Gastric Cancer Cells through Reactivation of p53 and Inhibition of Mdm-2. *Doklady Biochemistry and Biophysics*, *500*(1), 393-401. https://doi.org/10.1134/S1607672921050070

Goklany, S., Lu, P., Godeshala, S., Hall, A., Garrett-Mayer, E., Voelkel-Johnson, C., & Rege, K. (2019). Delivery of TRAIL-expressing plasmid DNA to cancer cells: In vitro and in vivo using aminoglycoside-derived polymers. *Journal of Materials Chemistry B*, *7*(44), 7014–7025. https://doi.org/10.1039/c9tb01286a

Gomes, H. I. O., Martins, C. S. M., & Prior, J. A. V. (2021). Silver Nanoparticles as Carriers of Anticancer Drugs for Efficient Target Treatment of Cancer Cells. *Nanomaterials*, *11*(964), 1–31. https://doi.org/10.3390/nano11040964

Gopisetty, M. K., Kovács, D., Igaz, N., Rónavári, A., Bélteky, P., Rázga, Z., Venglovecz, V., Csoboz, B., Boros, I. M., Kónya, Z., & Kiricsi, M. (2019).

Endoplasmic reticulum stress: major player in size-dependent inhibition of P-glycoprotein by silver nanoparticles in multidrug-resistant breast cancer cells. *Journal of Nanobiotechnology*, *17*(9), 1–15. https://doi.org/10.1186/s12951-019-0448-4

Gumustas, M., Sengel-Turk, C. T., Gumustas, A., Ozkan, S. A., & Uslu, B. (2017). Effect of Polymer-Based Nanoparticles on the Assay of Antimicrobial Drug Delivery Systems. In A. M. Grumezescu (Ed.), *Multifunctional Systems for Combined Delivery, Biosensing and Diagnostics* (1st ed., pp. 67–108). Elsevier Inc. https://doi.org/10.1016/B978-0-323-52725-5.00005-8

Guo, J., Armstrong, M. J., O'Driscoll, C. M., Holmes, J. D., & Rahme, K. (2015). Positively charged, surfactant-free gold nanoparticles for nucleic acid delivery. *RSC Advances*, *5*, 17862–17871. https://doi.org/10.1039/c4ra16294c

Guo, S., Huang, Y., Jiang, Q., Sun, Y., Deng, L., Liang, Z., Du, Q., Xing, J., Zhao, Y., Wang, P. C., Dong, A., & Liang, X.-J. (2010). Enhanced Gene Delivery and siRNA by Gold Nanoparticles Coated with Charge-Reversal Polyelectrolyte. *ACS Nano*, *4*(9), 5505–5511.

Gupta, N., Gupta, P., & Srivastava, S. K. (2019). Penfluridol overcomes paclitaxel resistance in metastatic breast cancer. *Scientific Reports*, *9*(1), 1–14. https://doi.org/10.1038/s41598-019-41632-0

Gurusamy, V., Krishnamoorthy, R., Gopal, B., Veeraravagan, V., Periyasamy, & Neelamegam, P. (2017). Systematic investigation on hydrazine hydrate assisted reduction of silver nanoparticles and its antibacterial properties. *Inorganic and Nano-Metal Chemistry*, *47*(5), 761–767. https://doi.org/10.1080/15533174.2015.1137074

Haghnavaz, N., Asghari, F., Komi, D. E. A., Shanehbandi, D., Baradaran, B., & Kazemi, T. (2019). HER2 positivity may confer resistance to therapy with paclitaxel in breast cancer cell lines. *Artificial Cells, Nanomedicine, and Biotechnology*. https://doi.org/10.1080/21691401.2017.1326927

Hamouda, R. A., Hussein, M. H., Abo-elmagd, R. A., & Bawazir, S. S. (2019). Synthesis and biological characterization of silver nanoparticles derived from the cyanobacterium Oscillatoria limnetica. *Scientific Reports*, *9*(13071), 1–17. https://doi.org/10.1038/s41598-019-49444-y

Hanahan, D. (2022). Hallmarks of Cancer: New Dimensions. *Cancer Discovery*, *12*, 31–46. https://doi.org/10.1158/2159-8290.CD-21-1059

Hanahan, D., & Weinberg, R. A. (2017). Biological Hallmarks of Cancer. In R. C. Bast Jr., C. M. Croce, W. N. Hait, W. K. Hong, D. W. Kufe, M. Piccart-Gebhard, R. E. Pollock, R. R. Weichselbaum, H. Wang, & J. F. Holland (Eds.), *Holland-Frei Cancer Medicine* (9th ed., pp. 1–10). John Wiley & Sons, Inc. https://doi.org/10.1002/9781119000822.hfcm002

Han, J., Lim, W., You, D., Jeong, Y., Kim, S., Lee, J. E., Shin, T. H., Lee, G., & Park, S. (2019). Chemoresistance in the Human Triple-Negative Breast Cancer Cell Line MDA-MB-231 Induced by Doxorubicin Gradient Is Associated with Epigenetic

Alterations in Histone Deacetylase. *Journal of Oncology*, 1–12. https://doi.org/10.1155/2019/1345026

Her, S., Jaffray, D. A., & Allen, C. (2017). Gold nanoparticles for applications in cancer radiotherapy: Mechanisms and recent advancements. *Advanced Drug Delivery Reviews*, *109*, 84–101. https://doi.org/10.1016/j.addr.2015.12.012

Holliday, D. L., & Speirs, V. (2011). Choosing the right cell line for breast cancer research. *Breast Cancer Research*, *13*(215), 1–7.

Hong, S.-W., Jin, D.-H., Hahm, E.-S., Yim, S.-H., Lim, J.-S., Kim, K.-I., Yang, Y., Lee, S.-S., Kang, J.-S., Lee, W.-J., Lee, W.-K., & Lee, M.-S. (2007). Ascorbate (vitamin C) induces cell death through the apoptosis-inducing factor in human breast cancer cells. *Oncology Reports*, *18*(4), 811–815. https://doi.org/10.3892/or.18.4.811

Housman, G., Byler, S., Heerboth, S., Lapinska, K., Longacre, M., Snyder, N., & Sarkar, S. (2014). Drug Resistance in Cancer: An Overview. *Cancers*, *6*(3), 1769–1792. https://doi.org/10.3390/cancers6031769

Hu, J. L., Wang, W., Lan, X. L., Zeng, Z. C., Liang, Y. S., Yan, Y. R., Song, F. Y., Wang, F. F., Zhu, X. H., Liao, W. J., Liao, W. T., Ding, Y. Q., & Liang, L. (2019). CAFs secreted exosomes promote metastasis and chemotherapy resistance by enhancing cell stemness and epithelial-mesenchymal transition in colorectal cancer. *Molecular Cancer*, *18*(91), 1–15.

Huang, Z., Yu, P., & Tang, J. (2020). Characterization of triple-negative breast cancer MDA-MB-231 cell spheroid model. *OncoTargets and Therapy*, *13*, 5395–5405. https://doi.org/10.2147/OTT.S249756

Hung, H.-S., Chang, K.-B., Tang, C.-M., Ku, T.-R., Kung, M.-L., Yu, A. Y. H., Shen, C.-C., Yang, Y.-C., Hsieh, H.-H., & Hsu, S.-H. (2021). Anti-inflammatory fibronectin-agnp for regulation of biological performance and endothelial differentiation ability of mesenchymal stem cells. *International Journal of Molecular Sciences*, *22*(17). https://doi.org/10.3390/ijms22179262

Ielo, I., Rando, G., Giacobello, F., Sfameni, S., Castellano, A., Galletta, M., Drommi, D., Rosace, G., & Plutino, M. R. (2021). Applications of Functional Gold Nanoparticles: A Review. *Molecules*, *26*(5683), 1–40.

Iqbal, J., Abbasi, B. A., Mahmood, T., Kanwal, S., Ali, B., Shah, S. A., & Khalil, A. T. (2017). Plant-derived anticancer agents: A green anticancer approach. *Asian Pacific Journal of Tropical Biomedicine*, *7*(12), 1129–1150. https://doi.org/10.1016/j.apjtb.2017.10.016

Iriarte-Mesa, C., Lopez, Y. C., Matos-Peralta, Y., de la Vega-Hernandez, K., & Antuch, M. (2020). Gold, Silver and Iron Oxide Nanoparticles: Synthesis and Bionanoconjugation Strategies Aimed at Electrochemical Applications. *Topics in Current Chemistry*, *378*(12), 1–40. https://doi.org/10.1007/s41061-019-0275-y

Ivanova, N., Gugleva, V., Dobreva, M., Pehlivanov, I., Stefanov, S., & Andonova, V. (2019). Silver Nanoparticles as Multi-Functional Drug Delivery System. In M.

A. Farrukh & R. Koprowski (Eds.), *Nanomedicines* (1st ed.). IntechOpen. https://doi.org/10.5772/intechopen.80238 89

Javed, R., Zia, M., Naz, S., Aisida, S. O., ul Ain, N., & Ao, Q. (2020). Role of capping agents in the application of nanoparticles in biomedicine and environmental remediation: recent trends and future prospects. *Journal of Nanobiotechnology*, *18*(172), 1–15. https://doi.org/10.1186/s12951-020-00704-4

Jaworski, S., Sawosz, E., Kutwin, M., Wierzbicki, M., Hinzmann, M., Grodzik, M., Winnicka, A., Lipinska, L., Wlodyga, K., & Chawlibog, A. (2015). In vitro and in vivo effects of graphene oxide and reduced graphene oxide on glioblastoma. *International Journal of Nanomedicine*, *10*, 1585–1596.

Jiang, P., Xie, S., Yao, J., He, S., Zhang, H., Shi, D., Pang, S., & Gao, H. (2001). Two-dimensional self-organization of 1-nonanethiol- capped gold nanoparticles. *Chinese Science Bulletin*, *46*(12), 996–998. https://doi.org/10.1007/BF03183543

Jiang, Y., Wang, Z., Duan, W., Liu, L., Si, M., Chen, X., & Fang, C.-J. (2020). The critical size of gold nanoparticles for overcoming P-gp mediated multidrug resistance. *Nanoscale*, *12*(31), 16451–16461. https://doi.org/10.1039/D0NR03226C

Kathryn, J. C., Sireesha V, G., & Stanley, L. (2012). Triple Negative Breast Cancer Cell Lines: One Tool in the Search for Better Treatment of Triple Negative Breast Cancer. *Breast Diseases*, *32*, 35–48. https://doi.org/10.3233/BD-2010-0307.Triple

Kaur, J., & Tikoo, K. (2013). Evaluating cell specific cytotoxicity of differentially charged silver nanoparticles. *Food and Chemical Toxicology*, *51*, 1–14. https://doi.org/10.1016/j.fct.2012.08.044

Ke, S., Zhou, T., Yang, P., Wang, Y., Zhang, P., Chen, K., Ren, L., & Ye, S. (2017). Gold nanoparticles enhance TRAIL sensitivity through Drp1-mediated apoptotic and autophagic mitochondrial fission in NSCLC cells. *International Journal of Nanomedicine*, *12*, 2531–2551. https://doi.org/10.2147/IJN.S129274

Khalil, C., & Shebaby, W. (2017). UVB damage onset and progression 24 h post exposure in human-derived skin cells. *Toxicology Reports*, *4*, 441–449. https://doi.org/10.1016/j.toxrep.2017.07.008

Khan, I., Saeed, K., & Khan, I. (2019). Nanoparticles: Properties, applications and toxicities. *Arabian Journal of Chemistry*, *12*(7), 908–931. https://doi.org/10.1016/j.arabjc.2017.05.011

Khutale, G. V., & Casey, A. (2017). Synthesis and characterization of a multifunctional gold-doxorubicin nanoparticle system for pH triggered intracellular anticancer drug release. *European Journal of Pharmaceutics and Biopharmaceutics*, *119*, 372–380. https://doi.org/10.1016/j.ejpb.2017.07.009

Koh, M. Z., Ho, W. Y., Yeap, S. K., Ali, N. M., Boo, L., & Alitheen, N. B. (2021). Regulation of Cellular and Cancer Stem Cell-Related Putative Gene Expression of Parental and CD44+ CD24− Sorted MDA-MB-231 Cells by Cisplatin. *Pharmaceuticals*, *14*(391).

Kovács, D., Igaz, N., Gopisetty, M. K., & Kiricsi, M. (2022). Cancer Therapy by Silver Nanoparticles: Fiction or Reality? *International Journal of Molecular Medicine*, *23*(839).

Kovács, D., Igaz, N., Marton, A., Rónavári, A., Bélteky, P., Bodai, L., Spengler, G., Tiszlavicz, L., Rázga, Z., Hegyi, P., Vizler, C., Boros, I. M., Konya, Z., & Kiricsi, M. (2020). Core-shell nanoparticles suppress metastasis and modify the tumour-supportive activity of cancer-associated fibroblasts. *Journal of Nanobiotechnology*, *18*(18), 1–20. https://doi.org/10.1186/s12951-020-0576-x

Kunchaorenwirat, N., Chatuphonprasert, W., & Jarukamjorn, K. (2021). Effect of phenol red on cell cultures. *International Journal of Property Sciences*, *17*(1), 13–23.

Kwon, Y. S., Chun, S. Y., Nam, K. S., & Kim, S. (2015). Lapatinib sensitizes quiescent MDA-MB-231 breast cancer cells to doxorubicin by inhibiting the expression of multidrug resistance-associated protein-1. *Oncology Reports*, *34*(2), 884–890. https://doi.org/10.3892/or.2015.4047

Lai, Q., Zhu, S., Luo, X., Zou, M., & Huang, S. (2012). Ultraviolet-visible spectroscopy of graphene oxides. *AIP Advances*, *2*(032146).

Lee, A. V., Oesterreich, S., & Davidson, N. E. (2015). MCF-7 Cells - Changing the Course of Breast Cancer Research and Care for 45 Years. *Journal of the National Cancer Institute*, *107*(7), 1–4. https://doi.org/10.1093/jnci/djv073

Lee, S. H., & Jun, B. (2019). Silver Nanoparticles: Synthesis and Application for Nanomedicine. *International Journal of Molecular Sciences*, *20*(865). https://doi.org/10.3390/ijms20040865

Lee, S. K., Han, M. S., Asokan, S., & Tung, C.-H. (2011). Effective Gene Silencing by Multilayered siRNA-Coated Gold Nanoparticles. *Small*, *7*(3), 364–370. https://doi.org/10.1002/smll.201001314

Lei, Z., Tian, Q., Teng, Q., Wurpel, J. N. D., Zeng, L., Pan, Y., & Chen, Z. (2023). Understanding and targeting resistance mechanisms in cancer. *MedComm*, *4*(3), 1–38. https://doi.org/10.1002/mco2.265

Lepeltier, E., Rijo, P., Rizzolio, F., Popovtzer, R., Petrikaite, V., Assaraf, Y. G., & Passirani, C. (2020). Nanomedicine to target multidrug resistant tumors. *Drug Resistance Updates*, *52*(100704), 1–15. https://doi.org/10.1016/j.drup.2020.100704

Li, J., Huang, L., He, Z., Chen, M., Ding, Y., Yao, Y., Duan, Y., Li, Z., Qi, C., Zheng, L., Li, J., Zhang, R., Li, X., Dai, J., Wang, L., & Zhang, Q.-Q. (2021). Andrographolide Suppresses the Growth and Metastasis of Luminal-Like Breast Cancer by Inhibiting the NF-κB / miR-21-5p / PDCD4 Signaling Pathway. *Frontiers in Cell and Developmental Biology*, *9*(643525), 1–12. https://doi.org/10.3389/fcell.2021.643525

Li, P., Tian, W., & Ma, X. (2014). Alpha-mangostin inhibits intracellular fatty acid synthase and induces apoptosis in breast cancer cells. *Molecular Cancer*, *13*(138), 1–11.

Li, S., Li, Q., Lü, J., Zhao, Q., Li, D., Shen, L., Wang, Z., Liu, J., Xie, D., Cho, W. C., Xu, S., & Yu, Z. (2020). Targeted Inhibition of miR-221/222 Promotes Cell Sensitivity to Cisplatin in Triple-Negative Breast Cancer MDA-MB-231 Cells. *Frontiers in Genetics*, *10*, 1–11. https://doi.org/10.3389/fgene.2019.01278

Li, Y. J., Lei, Y.-H., Yao, N., Wang, C.-R., Hu, N., Ye, W.-C., Zhang, D.-M., & Chen, Z.-S. (2017). Autophagy and multidrug resistance in cancer. *Chinese Journal of Cancer*, *36*(52), 1–10. https://doi.org/10.1186/s40880-017-0219-2

Lim, M., Jeung, I. C., Jeong, J., Yoon, S., Lee, S., Park, J., Kang, Y.-S., Lee, H., Park, Y.-J., Lee, H. G., Lee, S.-J., Han, B. S., Song, N. W., Lee, S. C., Kim, J., Bae, K., & Min, J.-K. (2016). Graphene oxide induces apoptotic cell death in endothelial cells by activating autophagy via calcium-dependent phosphorylation of c-Jun N- terminal kinases. *Acta Biomater*, *46*, 191–203. https://doi.org/10.2147/IJN.S112030.

Liu, F., Mahmood, M., Xu, Y., Watanabe, F., Biris, A. S., Hansen, D. K., Inselman, A., Casciano, D., Patterson, T. A., Paule, M. G., Jr, W. S., & Wang, C. (2015). Effects of silver nanoparticles on human and rat embryonic neural stem cells. *Frontiers in Neuroscience*, *9*(115), 1–9. https://doi.org/10.3389/fnins.2015.00115

Liu, J.-L., Yang, Y.-T., Lin, C.-T., Yu, Y.-J., Chen, J.-K., & Chu, L.-K. (2017). Monitoring the Transient Thermal Infrared Emission of Gold Nanoparticles upon Photoexcitation with a Step-Scan Fourier- Transform Spectrometer. *The Journal of Physical Chemistry*, *121*, 878–885. https://doi.org/10.1021/acs.jpcc.6b10044

Liu, X., Shan, K., Shao, X., Shi, X., He, Y., Liu, Z., Jacob, J. A., & Deng, L. (2021). Nanotoxic Effects of Silver Nanoparticles on Normal HEK-293 Cells in Comparison to Cancerous HeLa Cell Line. *International Journal of Nanomedicine*, *16*, 753–761.

Liu, Z., Ding, Y., Ye, N., Wild, C., Chen, H., & Zhou, J. (2016). Direct Activation of Bax Protein for Cancer Therapy. *Medicinal Research Reviews*, *36*(2), 313–341.

LiverTox. (2012). Antineoplastic Agents. In *LiverTox: Clinical and Research Information on Drug-Induced Liver Injury*. National Institute of Diabetes and Digestive and Kidney Diseases. Retrieved 20 September, 2021 from https://www.ncbi.nlm.nih.gov/books/NBK548022/

Lu, B., Huang, X., Mo, J., & Zhao, W. (2016). Drug Delivery Using Nanoparticles for Cancer Stem-Like Cell Targeting. *Frontiers in Pharmacology*, *7*(64), 1–12. https://doi.org/10.3389/fphar.2016.00084

Lukasiewicz, S., Czeczlewski, M., Forma, A., Baj, J., Sitarz, R., & Stanisławek, A. (2021). Breast Cancer—Epidemiology, Risk Factors, Classification, Prognostic Markers, and Current Treatment Strategies— An Updated Review. *Cancers*, *13*(4387), 1–30. https://doi.org/10.3390/cancers13174287

Madani, F., Lindberg, S., Langel, Ü., Futaki, S., & Gräslund, A. (2011). Mechanisms of Cellular Uptake of Cell-Penetrating Peptides. *Journal of Biophysics*, *414729*, 1–10. https://doi.org/10.1155/2011/414729

Malvern Instruments. (2023). *Zeta potential - An introduction in 30 minutes*. Retrieved June 10, 2023 from https://www.malvernpanalytical.com/en/learn/knowledge-center/technical-notes/tn101104zetapotentialintroduction

Mao, J., Gu, Q., Guo, Z., & Liu, H. K. (2015). Sodium borohydride hydrazinates: synthesis, crystal structures, and thermal decomposition behavior. *Journal of Materials Chemistry A*, *3*(21), 11269–11276. https://doi.org/10.1039/c5ta02276b

Martinelli, C., & Biglietti, M. (2020). Nanotechnological approaches for counteracting multidrug resistance in cancer. *Cancer Drug Resistance*, *3*, 1–18. https://doi.org/10.20517/cdr.2020.47

Martins, M. L., Bordallo, H. N., Arrese-Igor, S., Alegr, A., & de Leon, J. C. (2020). Effect of Paclitaxel in the Water Dynamics of MCF-7 Breast Cancer Cells Revealed by Dielectric Spectroscopy. *ACS Omega*, *5*, 18602–18607. https://doi.org/10.1021/acsomega.0c00897

Masui, K., Gini, B., Wykosky, J., Zanca, C., Mischel, P. S., Furnari, F. B., & Cavenee, W. K. (2013). A tale of two approaches: complementary mechanisms of cytotoxic and targeted therapy resistance may inform next-generation cancer treatments. *Carcinogenesis*, *34*(4), 725–738. https://doi.org/10.1093/carcin/bgt086

Matsumoto, C., Gen, M., Matsuki, A., & Seto, T. (2022). Development of spray-drying-based surface-enhanced Raman spectroscopy. *Scientific Reports*, *12*(4511), 1–10. https://doi.org/10.1038/s41598-022-08598-y

Mazzonello, A., Valdramidis, V. V, Farrugia, C., Grima, J. N., & Gatt, R. (2017). Synthesis and characterization of silver nanoparticles. *International Journal of Modern Engineering Research (IJMER)*, *7*(3), 41–47. https://doi.org/10.4028/www.scientific.net/MSF.802.135

Mohd-Zahid, M. H., Mohamud, R., Abdullah, C. A. C., Lim, J. K., Alem, H., Hanaffi, W. N. W., & Alias, I. Z. (2020). Colorectal cancer stem cells: a review of targeted drug delivery by gold nanoparticles. *RSC Advances*, *10*, 973–985. https://doi.org/10.1039/c9ra08192e

Morgan, A., Babu, D., Reiz, B., Whittal, R., Suh, L. Y. K., & Siraki, A. G. (2019). Caution for the routine use of phenol red – It is more than just a pH indicator. *Chemico-Biological Interactions*, *310*. https://doi.org/10.1016/j.cbi.2019.108739

Morris, L. G. T., & Chan, T. A. (2015). Therapeutic Targeting of Tumor Suppressor Genes. *Cancer*, *121*(9), 1357–1368. https://doi.org/10.1002/cncr.29140.Therapeutic

Munoz, R., Singh, D. P., Kumar, R., & Matsuda, A. (2019). Graphene Oxide for Drug Delivery and Cancer Therapy. In S. K. Swain & M. Jawaid (Eds.), *Nanostructured Polymer Composites for Biomedical Application* (pp. 447–488). Elsevier. https://doi.org/10.1016/B978-0-12-816771-7.00023-5

Nakatuka, Y., Yoshida, H., Fukui, K., & Matuzawa, M. (2015). The effect of particle size distribution on effective zeta-potential by use of the sedimentation method. *Advanced Powder Technology*, *26*(2), 650–656. https://doi.org/10.1016/j.apt.2015.01.017

National Center for Biotechnology Information **(A)** (2023). *PubChem Compound Summary for CID 4311764, Sodium borohydride*. Retrieved June 28, 2023 from https://pubchem.ncbi.nlm.nih.gov/compound/Sodium-borohydride

National Center for Biotechnology Information **(B)** (2023). PubChem Compound Summary for CID 5281650, Mangostin. Retrieved September 30, 2023 from https://pubchem.ncbi.nlm.nih.gov/compound/Mangostin

National Center for Biotechnology Information **(C)** (2023). PubChem Compound Summary for CID 5318517, Andrographolide. Retrieved September 30, 2023 from https://pubchem.ncbi.nlm.nih.gov/compound/Andrographolide

Niu, W., Duan, Y., Qing, Z., Huang, H., & Lu, X. (2017). Shaping Gold Nanocrystals in Dimethyl Sulfoxide: Toward Trapezohedral and Bipyramidal Nanocrystals Enclosed by {311} Facets. *Journal of the American Chemical Society*, *139*(16), 5817–5826. https://doi.org/10.1021/jacs.7b00036

Oliveira, C., Chaves, C. R., Bargiela, P., da Rocha, M. da G. C., da Silva, A. F., Chubaci, J. F. D., Bostrom, M., Persson, C., & Malta, M. (2021). Surface studies of the chemical environment in gold nanorods supported by X-ray photoelectron spectroscopy (XPS) and ab initio calculations. *Journal of Materials Research and Technology*, *15*, 768–776. https://doi.org/10.1016/j.jmrt.2021.08.059

Omiecinski, C. J., Vanden Heuvel, J. P., Perdew, G. H., & Peters, J. M. (2011). Xenobiotic Metabolism, Disposition, and Regulation by Receptors: From Biochemical Phenomenon to Predictors of Major Toxicities. *Toxicological Sciences*, *120*(SUPPL.1), S49–S75. https://doi.org/10.1093/toxsci/kfq338

Orrantia-Borunda, E., Anchondo-Nunez, P., Acuna-Aguilar, L. E., Gomez-Valles, F. O., & Ramirez-Valdespino, C. A. (2022). Subtypes of Breast Cancer. In H. N. Mayrovitz (Ed.), *Breast Cancer* (1st ed., pp. 31–42). Exon Publications. https://doi.org/10.36255/exon-publications-breast-cancer

Ou, L., Song, B., Liang, H., Liu, J., Feng, X., Deng, B., Sun, T., & Shao, L. (2016). Toxicity of graphene-family nanoparticles: a general review of the origins and mechanisms. *Particle and Fibre Toxicology*, *13*(57), 1–24. https://doi.org/10.1186/s12989-016-0168-y

Oves, M., Khan, M. S., Zaidi, A., Ahmed, A. S., Ahmed, F., Ahmad, E., Sherwani, A., Owais, M., & Azam, A. (2013). Antibacterial and Cytotoxic Efficacy of Extracellular Silver Nanoparticles Biofabricated from Chromium Reducing Novel OS4 Strain of Stenotrophomonas maltophilia. *PLoS ONE*, *8*(3), 1–14. https://doi.org/10.1371/journal.pone.0059140

Panicker, Y. C., Tresa Varghese, H., & Philip, D. (2006). FT-IR, FT-Raman and SERS spectra of Vitamin C. *Spectrochimica Acta - Part A: Molecular and Biomolecular Spectroscopy*, *65*(3–4), 802–804. https://doi.org/10.1016/j.saa.2005.12.044

Pechyen, C., Ponsanti, K., & Tangnorawich, B. (2022). Biogenic synthesis of gold nanoparticles mediated by Spondias dulcis (Anacardiaceae) peel extract and its cytotoxic activity in human breast cancer cell. *Toxicology Reports*, *9*, 1092–1098. https://doi.org/10.1016/j.toxrep.2022.04.031

Peng, Y., Wang, Y., Tang, N., Sun, D., Lan, Y., Yu, Z., Zhao, X., Feng, L., Zhang, B., Jin, L., Yu, F., Ma, X., & Lv, C. (2018). Andrographolide inhibits breast cancer through suppressing COX-2 expression and angiogenesis via inactivation of p300 signaling and VEGF pathway. *Journal of Experimental & Clinical Cancer Research*, *37*(248), 1–14. https://doi.org/10.1186/s13046-018-0926-9

Pinelli, F., Perale, G., & Rossi, F. (2020). Coating and Functionalization Strategies for Nanogels and Nanoparticles for Selective Drug Delivery. *Gels*, *6*(6), 1–16. https://doi.org/10.3390/gels6010006

Priyadarsini, S., Mohanty, S., Mukherjee, S., Basu, S., & Mishra, M. (2018). Graphene and graphene oxide as nanomaterials for medicine and biology application. *Journal of Nanostructure in Chemistry*, *8*(2), 123–137. https://doi.org/10.1007/s40097-018-0265-6

Qin, Y., Ji, X., Jing, J., Liu, H., Wu, H., & Yang, W. (2010). Size control over spherical silver nanoparticles by ascorbic acid reduction. *Colloids and Surfaces A: Physicochemical and Engineering Aspects*, *372*, 172–176. https://doi.org/10.1016/j.colsurfa.2010.10.013

Rahme, K., & Dagher, N. (2019). Chemistry Routes for Copolymer Synthesis Containing PEG for Targeting, Imaging, and Drug Delivery Purposes. *Pharmaceutics*, *11*(327), 1–23. https://doi.org/10.3390/pharmaceutics11070327

Ramalingam, V., Revathidevi, S., Shanmuganayagam, T. S., Muthulakshmi, L., & Rajaram, R. (2017). Gold nanoparticle induces mitochondria-mediated apoptosis and cell cycle arrest in nonsmall cell lung cancer cells. *Gold Bulletin*, *50*, 177–189. https://doi.org/10.1007/s13404-017-0208-x

Rasmussen, M. K., Pedersen, J. N., & Marie, R. (2020). Size and surface charge characterization of nanoparticles with a salt gradient. *Nature Communications*, *11*(2337), 1–8. https://doi.org/10.1038/s41467-020-15889-3

Rathore, R., McCallum, J. E., Varghese, E., Florea, A.-M., & Büsselberg, D. (2017). Overcoming chemotherapy drug resistance by targeting inhibitors of apoptosis proteins (IAPs). *Apoptosis*, *22*(7), 898–919. https://doi.org/10.1007/s10495-017-1375-1

Repotente Jr, E. C., Carreon, A. J., Devanadera, M. K., Esmalla, M. S., & Santiago-Bautista, M. (2022). Cytotoxic potential on human breast and lung cancer cells of the biosynthesized gold nanoparticles from the reduction of chloroauric acid by lactic acid isolated from Lactobacillus acidophilus. *Frontiers in Materials*, *9*, 1–10. https://doi.org/10.3389/fmats.2022.933749

Rhazouani, A., Gamrani, H., Achaby, M. El, Aziz, K., Gebrati, L., Uddin, M. S., & Aziz, F. (2021). Synthesis and Toxicity of Graphene Oxide Nanoparticles: A Literature Review of In Vitro and In Vivo Studies. *BioMed Research International*, *5518999*.

Rhim, W.-K., Kim, J.-S., & Nam, J.-M. (2008). Lipid-gold-nanoparticle hybrid-based gene delivery. *Small*, *4*(10), 1651–1655. https://doi.org/10.1002/smll.200800628

Roacho-Perez, J. A., Gallardo-Blanco, H. L., Sanchez-Dominguez, M., Garcia-Casillas, P., Chapa-Gonzalez, C., & Sanchez-Dominguez, C. N. (2018). Nanoparticles for

death-induced gene therapy in cancer (Review). *Molecular Medicine Reports*, *17*(1), 1413–1420. https://doi.org/10.3892/mmr.2017.8091

Roduner, E. (2006). Size matters: why nanomaterials are different. *Chemical Society Reviews*, *35*(7), 583–592. https://doi.org/10.1039/b502142c

Rohde, M. M., Snyder, C. M., Sloop, J., Solst, S. R., Donati, G. L., Spitz, D. R., Furdui, C. M., & Singh, R. (2021). The mechanism of cell death induced by silver nanoparticles is distinct from silver cations. *Particle and Fibre Toxicology*, *18*(37), 1–24. https://doi.org/10.1186/s12989-021-00430-1

Roszak, J., Domeradzka-Gajda, K., Smok-Pieniążek, A., Kozajda, A., Spryszyńska, S., Grobelny, J., Tomaszewska, E., Ranoszek-Soliwoda, K., Cieślak, M., Puchowicz, D., & Stępnik, M. (2017). Genotoxic effects in transformed and non-transformed human breast cell lines after exposure to silver nanoparticles in combination with aluminium chloride, butylparaben or di-n-butylphthalate. *Toxicology in Vitro*, *45*, 181–193. https://doi.org/10.1016/j.tiv.2017.09.003

Roto, R., Rasydta, H. P., Suratman, A., & Aprilita, N. H. (2018). Effect of Reducing Agents on Physical and Chemical Properties of Silver Nanoparticles. *Indonesian Journal of Chemistry*, *18*(4), 614–620. https://doi.org/10.22146/ijc.26907

Ruiz-Silvestre, A., Garcia-Venzor, A., Ceballos-Cancino, G., S, M., Vazquez-Santillan, K., Mendoza-Almanza, G., Lizarraga, F., Melendez-Zajgla, J., & Maldonado, V. (2024). Transcriptomic Changes in Cisplatin-Resistant MCF-7 Cells. *International Journal of Molecular Sciences*, *25*(3820), 1–14.

Saha, T., Solomon, J., Samson, A. O., & Gil-Henn, H. (2021). Invasion and metastasis as a central hallmark of breast cancer. *Journal of Clinical Medicine*, *10*(16), 1–12. https://doi.org/10.3390/jcm10163498

Sajjad, H., Imtiaz, S., Noor, T., Siddiqui, Y. H., Sajjad, A., & Zia, M. (2021). Cancer models in preclinical research: A chronicle review of advancement in effective cancer research. *Animal Models and Experimental Medicine*, *4*(2), 87–103. https://doi.org/10.1002/ame2.12165

Salehan, M. R., & Morse, H. R. (2013). DNA damage repair and tolerance: A role in chemotherapeutic drug resistance. *British Journal of Biomedical Science*, *70*(1), 31–40. https://doi.org/10.1080/09674845.2013.11669927

Samaan, T. M. A., Samec, M., Liskova, A., Kubatka, P., & Büsselberg, D. (2019). Paclitaxel' s Mechanistic and Clinical Effects on Breast Cancer. *Biomolecules*, *9*(789), 1–22.

Sani, A., Cao, C., & Cui, D. (2021). Toxicity of gold nanoparticles (AuNPs): A review. *Biochemistry and Biophysics Reports*, *26*(100991). https://doi.org/10.1016/j.bbrep.2021.100991

Sarkar, S., Rajput, S., Tripathi, A. K., & Mandal, M. (2013). Targeted therapy against EGFR and VEGFR using ZD6474 enhances the therapeutic potential of UV-B phototherapy in breast cancer cells. *Molecular Cancer*, *12*(122), 1–18.

Saunders, D. E., Lawrence, W. D., Christensen, C., Wappler, N. L., Ruan, H., & Deppe, G. (1997). PACLITAXEL-INDUCED APOPTOSIS IN MCF-7 BREAST-CANCER CELLS. *International Journal of Cancer*, *70*, 214–220.

Schaeublin, N. M., Braydich-Stolle, L. K., Schrand, A. M., Miller, J. M., Hutchison, J., Schlager, J. J., & Hussain, S. M. (2011). Surface charge of gold nanoparticle mediates mechanism of toxicity. *Nanoscale*, *3*, 410–420. https://doi.org/10.1039/c0nr00478b

Schlesinger, H. I., Brown, H. C., Finholt, A. E., Gilbrbath, J. R., Hoekstra, H. R., & Hyde, E. K. (1953). Sodium Borohydride, Its Hydrolysis and its Use as a Reducing Agent and in the Generation of Hydrogen. *Journal of the American Chemical Society*, *75*(1), 215–219.

Schmid, G., Kreyling, W. G., & Simon, U. (2017). Toxic effects and biodistribution of ultrasmall gold nanoparticles. *Archives of Toxicology*, *91*, 3011–3037. https://doi.org/10.1007/s00204-017-2016-8

Shah, M., Badwaik, V., Kherde, Y., Waghwani, H. K., Modi, T., Aguilar, Z. P., Rodgers, H., Hamilton, W., Marutharaj, T., Webb, C., Lawrenz, M. B., & Dakshinamurthy, R. (2014). Gold nanoparticles: various methods of synthesis and antibacterial applications. *Frontiers in Bioscience*, *19*(8), 1320–1344. https://doi.org/10.2741/4284

Shang, L., Nienhaus, K., & Nienhaus, G. U. (2014). Engineerd nanoparticles interacting with cells: size matters. *Journal of Nanobiotechnology*, *12*(5), 1–11.

Sharma, H., & Mondal, S. (2020). Functionalized Graphene Oxide for Chemotherapeutic Drug Delivery and Cancer Treatment: A Promising Material in Nanomedicine. *International Journal of Molecular Sciences*, *21*(6280).

Shen, J., Dong, J., Shao, F., Zhao, J., Gong, L., Wang, H., Chen, W., Zhang, Y., & Cai, Y. (2022). Graphene oxide induces autophagy and apoptosis via the ROS-dependent AMPK / mTOR / ULK-1 pathway in colorectal cancer cells. *Nanomedicine*, *17*(9), 591–605. https://doi.org/10.2217/nnm-2022-0030

Sherr, C. J. (2004). Principles of Tumor Suppression. *Cell*, *116*(2), 235–246. https://doi.org/10.1016/S0092-8674(03)01075-4

Siegel, R. L., Miller, K. D., Wagle, N. S., & Jemal, A. (2023). Cancer statistics, 2023. *CA: A Cancer Journal for Clinicians*, *73*, 17–48. https://doi.org/10.3322/caac.21763

Simon, S. E., Lim, H. S., Jayakumar, F. A., Tan, E. W., & Tan, K. O. (2022). Alpha-Mangostin Activates MOAP-1 Tumor Suppressor and Mitochondrial Signaling in MCF-7 Human Breast Cancer Cells. *Evidence-Based Complementary and Alternative Medicine*, *2022*(7548191), 1–12. https://doi.org/10.1155/2022/7548191

Simon, S. E., Numan, A., Angelin, F., Khalid, M., & Onn, K. (2021). Investigating the impact of UV irradiated graphene oxide on human breast cancer cells. *Materials Today Communications*, *29*(102830). https://doi.org/10.1016/j.mtcomm.2021.102830

Smith, A. T., Marie, A., Zeng, S., Liu, B., & Sun, L. (2019). Synthesis, properties, and applications of graphene oxide / reduced graphene oxide and their nanocomposites. *Nano Materials Science*, *1*(1), 31–47. https://doi.org/10.1016/j.nanoms.2019.02.004

Sobczak-Kupiec, A., Malina, D., Zimowska, M., & Wzorek, Z. (2011). Characterization of gold nanoparticle for various medical application. *Digest Journal of Nanomaterials and Biostructures*, *6*(2), 803–808.

Steckiewicz, K. P., Barcinska, E., Malankowska, A., Zauszkiewicz–Pawlak, A., Nowaczyk, G., Zaleska-Medynska, A., & Inkielewicz-Stepniak, I. (2019). Impact of gold nanoparticles shape on their cytotoxicity against human osteoblast and osteosarcoma in in vitro model. Evaluation of the safety of use and anti-cancer potential. *Journal of Materials Science: Materials in Medicine*, *30*(2), 1–15. https://doi.org/10.1007/s10856-019-6221-2

Suberu, J. O., Romero-Canelón, I., Sullivan, N., Lapkin, A. A., & Barker, G. C. (2014). Comparative Cytotoxicity of Artemisinin and Cisplatin and Their Interactions with Chlorogenic Acids in MCF7 Breast Cancer Cells. *ChemMedChem*, *9*, 2791–2797. https://doi.org/10.1002/cmdc.201402285

Sung, H., Ferlay, J., Siegel, R. L., Laversanne, M., Soerjomataram, I., Jemal, A., & Bray, F. (2021). Global Cancer Statistics 2020: GLOBOCAN Estimates of Incidence and Mortality Worldwide for 36 Cancers in 185 Countries. *CA: A Cancer Journal for Clinicians*, *71*(3), 209–249. https://doi.org/10.3322/caac.21660

Sung, Y. K., & Kim, S. K. (2019). Recent advances in the development of gene delivery systems. *Biomaterials Research*, *23*(8), 1–7. https://doi.org/10.1186/s40824-019-0156-z

Sztandera, K., Gorzkiewicz, M., & Klajnert-Maculewicz, B. (2019). Gold nanoparticles in cancer treatment. *Molecular Pharmaceutics*, *16*(1), 1–23. https://doi.org/10.1021/acs.molpharmaceut.8b00810

Talarska, P., Boruczkowski, M., & Żurawski, J. (2021). Current Knowledge of Silver and Gold Nanoparticles in Laboratory Research — Application, Toxicity, Cellular Uptake. *Nanomaterials*, *11*(2454), 1–23.

Taşkın-Tok, T., & Gowder, S. (2014). Chapter 9 - Anticancer Drug — Friend or Foe. In S. J. T. Gowder (Ed.), *Pharmacology and Therapeutics* (pp. 255–269). IntechOpen. https://doi.org/dx.doi.org/10.5772/58552

The Global Cancer Observatory. (2020). *Breast*. In *World Heatlh Organization.* Retrieved 20 April, 2023 from https://gco.iarc.fr/today/data/factsheets/cancers/20-Breast-fact-sheet.pdf

The Global Cancer Observatory. (2021). Malaysia. In *World Health Organization*. Retrieved 25 April, 2023 from https://gco.iarc.fr/today/data/factsheets/populations/458-malaysia-fact-sheets.pdf

Theodossiou, T. A., Ali, M., Grigalavicius, M., Grallert, B., Dillard, P., Schink, K. O., Olsen, C. E., Wälchli, S., Inderberg, E. M., Kubin, A., Peng, Q., & Berg, K. (2019). Simultaneous defeat of MCF7 and MDA-MB-231 resistances by a

hypericin PDT–tamoxifen hybrid therapy. *Npj Breast Cancer*, *13*. https://doi.org/10.1038/s41523-019-0108-8

Tohyakomatee, R., Reabroi, S., Tungmunnithum, D., Parichatikanond, W., & Pinthong, D. (2022). Andrographolide Exhibits Anticancer Activity against Breast Cells (MCF-7 and MDA-MB-231 Cells) through Suppressing Cell Proliferation and Inducing Cell Apoptosis via Inactivation of ER-a Receptor and PI3K/AKT/mTOR Signaling. *Molecules*, *27*(3544), 1–20.

Tronci, L., Serreli, G., Piras, C., Frau, D. V., Dettori, T., Deiana, M., Murgia, F., Santoru, M. L., Spada, M., Leoni, V. P., Griffin, J. L., Vanni, R., Atzori, L., & Caria, P. (2021). Vitamin C Cytotoxicity and Its Effects in Redox Homeostasis and Energetic Metabolism in Papillary Thyroid Carcinoma Cell Lines. *Antioxidants*, *10*(809), 1–15.

Umair, M., Javed, I., Rehman, M., Madni, A., Javeed, A., Ghafoor, A., Ghafoor, A., & Ashraf, M. (2016). Nanotoxicity of Inert Materials: The Case of Gold, Silver and Iron. *Journal of Pharmacy and Pharmaceutical Sciences*, *19*(3), 161–180. https://doi.org/10.18433/J31021

Umut, E. (2013). Surface Modification of Nanoparticles Used in Biomedical Application. In M. Aliofkhazraei (Ed.), *Modern Surface Engineering Treatments* (1st ed., pp. 185–208). IntechOpen. https://doi.org/10.5772/55746

Vlasceanu, G. M., Marin, S., Tiplea, R. E., Bucur, I. R., Lemnaru, M., Marin, M. M., Grumezescu, A. M., & Andronescu, E. (2016). Silver Nanoparticles in Cancer Therapy. In A. M. Grumezescu (Ed.), *Nanobiomaterials in Cancer Therapy* (1st ed., pp. 29–56). Elsevier Inc. https://doi.org/10.1016/B978-0-323-42863-7.00002-5

Wang, E. C., & Wang, A. Z. (2015). NANOPARTICLES AND THEIR APPLICATIONS IN CELL AND MOLECULAR BIOLOGY. *Integrative Biology*, *6*(1), 9–26. https://doi.org/10.1039/c3ib40165k.NANOPARTICLES

Wang, F., Li, L., Liu, B., Chen, Z., & Li, C. (2017). Hyaluronic acid decorated pluronic P85 solid lipid nanoparticles as a potential carrier to overcome multidrug resistance in cervical and breast cancer. *Biomedicine and Pharmacotherapy*, *86*, 595–604. https://doi.org/10.1016/j.biopha.2016.12.041

Wang, H., Guo, S., Kim, S. J., Shao, F., Kei Ho, J. W., Wong, K. U., Miao, Z., Hao, D., Zhao, M., Xu, J., Zeng, J., Wong, K. H., Di, L., Wong, A. H.-H., Xu, X., & Deng, C. X. (2021). Cisplatin prevents breast cancer metastasis through blocking early EMT and retards cancer growth together with paclitaxel. *Theranostics*, *11*(5), 2442–2459. https://doi.org/10.7150/thno.46460

Wang, K., Zhu, X., Zhang, K., Yin, Y., Chen, Y., & Zhang, T. (2017). Interleukin-6 contributes to chemoresistance in MDA-MB-231 cells via targeting HIF-1α. *Journal of Biochemical and Molecular Toxicology*, *32*(3), 1–7. https://doi.org/10.1002/jbt.22039

Wang, Y., Cui, H., Li, K., Sun, C., Du, W., Cui, J., Zhao, X., & Chen, W. (2014). A magnetic nanoparticle-based multiple-gene delivery system for transfection of

porcine kidney cells. *PLoS ONE*, *9*(7), 1–9. https://doi.org/10.1371/journal.pone.0102886

Wang, Y., Quinsaat, J. E. Q., Ono, T., Maeki, M., Tokeshi, M., Isono, T., Tajima, K., Satoh, T., Sato, S., Miura, Y., & Yamamoto, T. (2020). Enhanced dispersion stability of gold nanoparticles by the physisorption of cyclic poly(ethylene glycol). *Nature Communications*, *11*(6089), 1–12. https://doi.org/10.1038/s41467-020-19947-8

War, A. R. (2018). Curcumin Co-Treatment Sensitizes Multi-Drug Resistant Ht29 Colon Cancer Cell Line. *Journal of Cancer Research and Immuno-Oncology*, *4*(2). https://doi.org/10.35248/2684-1266.18.4.117

Watson, M. B., Lind, M. J., Smith, L., Drew, P. J., & Cawkwell, L. (2007). Expression microarray analysis reveals genes associated with in vitro resistance to cisplatin in a cell line model. *Acta Oncologica*, *46*(5), 651–658. https://doi.org/10.1080/02841860601156157

Wawruszak, A., Luszczki, J. J., Grabarska, A., Gumbarewicz, E., Dmoszynska-Graniczka, M., Polberg, K., & Stepulak, A. (2015). Assessment of Interactions between Cisplatin and Two Histone Deacetylase Inhibitors in MCF7, T47D and MDA-MB-231 Human Breast Cancer Cell Lines – An Isobolographic Analysis. *PLoS One*, 1–19. https://doi.org/10.1371/journal.pone.0143013

Weinberg, R. A. (2023). The Nature of Cancer. In R. A. Weinberg (Ed.), *The Biology of Cancer* (3rd ed., pp. 30–64). W.W. Norton.

Wen, H., Dan, M., Yang, Y., Lyu, J., Shao, A., Cheng, X., Chen, L., & Xu, L. (2017). Acute toxicity and genotoxicity of silver nanoparticle in rats. *PLoS ONE*, *12*(9), 1–16. https://doi.org/10.1371/journal.pone.0185554

Wozniak, A., Malankowska, A., Nowaczyk, G., Grzeskowiak, B. F., Tusnio, K., Ryszard, S., Zaleska-Medynska, A., & Jurga, S. (2017). Size and shape-dependent cytotoxicity profile of gold nanoparticles for biomedical applications. *Journal of Materials Science: Materials in Medicine*, *28*(92), 1–11. https://doi.org/10.1007/s10856-017-5902-y

Wu, J., Yang, R., Zhang, L., Fan, Z., & Liu, S. (2015). Cytotoxicity effect of graphene oxide on human MDA-MB-231 cells. *Toxicology Mechanisms and Methods*, 1–8. https://doi.org/10.3109/15376516.2015.1031415

Wyman, P. (2012). Chapter 1 - Hydrophilic coatings for biomedical applications in and ex vivo. In M. Driver (Ed.), *Coatings for Biomedical Applications* (1st ed., p. 40). Woodhead Publishing. https://doi.org/10.1533/9780857093677.1.3

Xu, K., & Han, Q. (2016). DMSO as a solvent/ligand to monodisperse CdS spherical nanoparticles. *Journal of Nanoparticle Research*, *18*(1), 1–10. https://doi.org/10.1007/s11051-016-3323-3

Xuan, L., Hu, J.-H., Bi, R., Liu, S.-Q., & Wang, C.-X. (2022). Andrographolide Inhibits Proliferation and Promotes Apoptosis in Bladder Cancer Cells by Interfering with NF-κB and PI3K/AKT Signaling *In Vitro* and *In Vivo*. *Chinese Journal of Integrative Medicine*, *28*, 249-356.

Yan, J., Chen, Y., He, C., Yang, Z. Z., Lü, C., & Chen, X. S. (2012). Andrographolide induces cell cycle arrest and apoptosis in human rheumatoid arthritis fibroblast-like synoviocytes. *Cell Biology and Toxicology*, *28*(1), 47–56. https://doi.org/10.1007/s10565-011-9204-8

Yang, J., Zhao, X., Tang, M., Li, L., Lei, Y., Cheng, P., Guo, W., Zheng, Y., Wang, W., Luo, N., Peng, Y., Tong, A., Wei, Y., Nie, C., & Yuan, Z. (2017). The role of ROS and subsequent DNA-damage response in PUMA-induced apoptosis of ovarian cancer cells. *Oncotarget*, *8*(14), 23492–23506.

Yang, T., Yao, Q., Cao, F., Liu, Q., Liu, B., & Wang, X.-H. (2016). Silver nanoparticles inhibit the function of hypoxia-inducible factor-1 and target genes: insight into the cytotoxicity and antiangiogenesis. *International Journal of Nan*, *11*, 6679–6692.

Yang, W., Wang, L., Mettenbrink, E. M., DeAngelis, P. L., & Wilhelm, S. (2021). Nanoparticle Toxicology. *Annual Review of Pharmacology and Toxicology*, *61*, 269–289. https://doi.org/10.1146/annurev-pharmtox-032320-110338

Ye, L., Chen, Y., Mao, J., Lei, X., Yang, Q., & Cui, C. (2021). Dendrimer-modified gold nanorods as a platform for combinational gene therapy and photothermal therapy of tumors. *Journal of Experimental and Clinical Cancer Research*, *40*(303), 1–16. https://doi.org/10.1186/s13046-021-02105-3

Yesilot, S., & Aydin, C. (2019). Silver Nanoparticles; A New Hope In Cancer Therapy? *Eastern Journal of Medicine*, *24*(1), 111–116. https://doi.org/10.5505/ejm.2019.66487

Yin, L.-L., Wen, X.-M., Lai, Q.-H., Li, J., & Wang, X.-W. (2018). Lenalidomide improvement of cisplatin antitumor efficacy on triple-negative breast cancer cells in vitro. *Oncology Letters*, *15*, 6469–6474. https://doi.org/10.3892/ol.2018.8120

Yi, Y. W., & Bae, I. (2011). Effects of solvents on in vitro potencies of platinum compounds [Letter to the Editor]. *DNA Repair*, *10*(11), 1084–1085. https://doi.org/10.1016/j.dnarep.2011.09.008

Zamora-Justo, J. A., Abrica-González, P., Vázquez-Martínez, G. R., Muñoz-Diosdado, A., Balderas-López, J. A., & Ibáñez-Hernández, M. (2019). Polyethylene Glycol-Coated Gold Nanoparticles as DNA and Atorvastatin Delivery Systems and Cytotoxicity Evaluation. *Journal of Nanomaterials*, *2019*(5982047). https://doi.org/10.1155/2019/5982047

Zhang, I., Gu, F. X., M, C. J., Wang, A. Z., Langer, R. S., & Farokhzad, O. C. (2008). Nanoparticles in Medicine: Therapeutic Applications and Developments. *Translational Medicine*, *83*(5), 761–769. https://doi.org/10.1038/sj.clp

Zhang, J., Zhao, T., Han, F., Hu, Y., & Li, Y. (2019). Photothermal and gene therapy combined with immunotherapy to gastric cancer by the gold nanoshell-based system. *Journal of Nanobiotechnology*, *17*(1), 1–11. https://doi.org/10.1186/s12951-019-0515-x

Zhang, L., Xia, J., Zhao, Q., Liu, L., & Zhang, Z. (2010). Functional Graphene Oxide as a Nanocarrier for Controlled Loading and Targeted Delivery of Mixed Anticancer Drugs. *Small*, *6*(4), 537–544. https://doi.org/10.1002/smll.200901680

Zhang, W., Cai, J., Chen, S., Zheng, X., Hu, S., Dong, W., Lu, J., Xing, J., & Dong, Y. (2015). Paclitaxel resistance in MCF-7/PTX cells is reversed by paeonol through suppression of the SET/phosphatidylinositol 3-kinase/Akt pathway. *Molecular Medicine Reports*, *12*, 1506–1514. https://doi.org/10.3892/mmr.2015.3468

Zhang, X. F. **(A)**, Shen, W., & Gurunathan, S. (2016). Silver nanoparticle-mediated cellular responses in various cell lines: An in vitro model. *International Journal of Molecular Sciences*, *17*(10), 1–26. https://doi.org/10.3390/ijms17101603

Zhang, X.-F. **(B)**, Liu, Z.-G., Shen, W., & Gurunathan, S. (2016). Silver nanoparticles: Synthesis, characterization, properties, applications, and therapeutic approaches. *International Journal of Molecular Sciences*, *17*(9). https://doi.org/10.3390/ijms17091534

Zhao, T., Zhang, T., Zhang, Y., Zhou, B., & Lu, X. (2022). Paclitaxel Resistance Modulated by the Interaction between TRPS1 and AF178030.2 in Triple-Negative Breast Cancer. *Evidence-Based Complementary and Alternative Medicine*, *6019975.*

Zhu, L., & Chen, L. (2019). Progress in research on paclitaxel and tumor immunotherapy. *Cellular and Molecular Biology Letters*, *24*(40), 1–11.

Zhu, X., Li, J., Ning, H., Yuan, Z., Zhong, Y., Wu, S., & Zeng, J.-Z. (2021). α-Mangostin Induces Apoptosis and Inhibits Metastasis of Breast Cancer Cells via Regulating RXR α-AKT Signaling Pathway. *Frontiers in Pharmacology*, *12*(739658), 1–11. https://doi.org/10.3389/fphar.2021.739658

SUPPLEMENTARY

List of Publications and Papers Presented:

Darmadi, J., Anwar, A., & Anuar, N. A. binti S. (2024). Current Progress on Gold Nanoparticle-Mediated Gene Delivery for Human Cancer Treatment. *E3S Web of Conferences - AMSET2023*, *488*, 1–13. https://doi.org/10.1051/e3sconf/202448803020

Darmadi, J., Anwar, A., & Anuar, N. A. binti S. (2024). Cytotoxicity of synthesized silver nanoparticles on breast cancer cells. *E3S Web of Conferences - AMSET2023*, *488*, 1-7. https://doi.org/10.1051/e3sconf/202448803022

E3S Web of Conferences **488**, 03020 (2024) https://doi.org/10.1051/e3sconf/202448803020
AMSET2023

Current Progress on Gold Nanoparticle-Mediated Gene Delivery for Human Cancer Treatment

Jason Darmadi[1*], *Ayaz* Anwar[1], and *Nurshafida Adzlin* binti Shamsul Anuar[2]

[1]Department of Biological Science, School of Medical and Life Sciences, Sunway University, 47500 Petaling Jaya, Malaysia
[2]Department of Medical Science, School of Medical and Life Sciences, Sunway University, 47500 Petaling Jaya, Malaysia

Abstract. Cancer treatments have become less effective in recent years, with cancer cells mutating into more non-sensitive against a plethora of chemotherapeutics. While gene therapy can lead to cancer cell sensitization and effective treatment, gene-related drugs are prone to degradation and highly unstable. Nanoparticles can thus be used for the delivery of genes as well as other therapeutic compounds into cancer cells. Gold nanoparticles (AuNPs) have been used in cancer therapy especially for drug delivery due to their ease of synthesis and modification. AuNPs were also considered versatile nanoparticles as their characteristics could be easily customized and modulated for therapy, monitoring, or delivery. Another important characteristic that made AuNPs viable for cancer therapy is surface plasmonic resonance (SPR) which enables hyperthermia-based therapy and imaging. Therefore, utilizing AuNPs novel approaches in multi-modal therapies is achievable, where targeted gene and chemotherapy coupled with other modalities such as hyperthermia-based therapy could be performed. This article reviews several reported cases of AuNPs-based gene therapy as well as notable theranostic therapy that includes SPR characteristic utilization for therapy as well as cancer imaging.

1 Introduction

Cancers are cells that have grown uncontrollably and become a malignancy in an organism. There are several causes for the cancer emergence which could be attributed to immune, metabolic, or genetic disorders [1]. However, cancers are most commonly caused by accumulations of mutations and other alterations in the genome which affect cell metabolism and structure. Aside from the internal disorders, cancer formation may also be induced externally by microbiota metabolites, carcinogenic chemicals, radioactive agents, or even oncogenic viruses that are capable of disrupting gene regulations [2, 3].

Despite the myriad of therapeutic interventions, cancer is still deemed a large medical problem. Over time cancer has become more resistant to conventional treatment like chemotherapy, mostly due to the biochemical cellular factor signaling that promotes immortality and unlimited self-replication [4]. In addition, cancer desensitization to multiple

* Corresponding author: jason.d3@imail.sunway.edu.my

E3S Web of Conferences **488**, 03022 (2024) https://doi.org/10.1051/e3sconf/202448803022
AMSET2023

Cytotoxicity of synthesized silver nanoparticles on breast cancer cells

Jason Darmadi[1*], *Ayaz* Anwar[1], and *Nurshafida Adzlin* binti Shamsul Anuar[2]

[1]Department of Biological Science, School of Medical and Life Sciences, Sunway University, 47500 Petaling Jaya, Malaysia
[2]Department of Medical Science, School of Medical and Life Sciences, Sunway University, 47500 Petaling Jaya, Malaysia

Abstract. Breast cancers are becoming harder to treat due to the acquisition of chemo-drug resistance. In this study, silver nanoparticles (AgNPs) were synthesized using reducing agent $NaBH_4$, where resulting nanoparticles were characterized using UV-vis spectroscopy, FTIR spectroscopy, SEM, and DLS. Cytotoxicity of synthesized AgNPs was evaluated against MCF-7, MCF-7-CR, and MDA-MB-231 using MTT assays. $NaBH_4$-reduced AgNPs were unstable as a colloidal system, with zeta potential noted to be around -21 mV and a polydispersity index of around 15%, making them highly prone to aggregation. However, AgNPs significantly reduced the cell viability of MCF-7 breast cancer cell lines, while slight toxicity was seen in multi-drug resistant breast cancer cells MCF-7-CR and MDA-MB-231 at 10 μM.

1 Introduction

Multi-drug resistance (MDR) is a major problem in cancer, especially breast cancer chemotherapy as it makes administering single or multiple drugs harder. Most anticancer drugs also have a non-specific cytotoxic activity towards surrounding normal cells, which can cause further complications [1].

Metallic nanoparticles have been used in cancer research and are documented to induce toxicity against MDR cancer cells [1]. Among them, silver nanoparticles (AgNPs) can induce cytotoxicity in cancer cells via a "Trojan-horse" type mechanism, where internalized AgNPs induce cell death [2]. AgNPs localize in the cytosol, mitochondria, and endoplasmic reticulum, resulting in enzymes and growth factor inhibition related to angiogenesis and cell proliferation [3, 4] AgNPs were also associated with apoptosis as oxidative stress generation and DNA damage were seen after administration to cancer cells [5-7].

Cytotoxic AgNPs can be synthesized chemically using a combination of reducing agents to initiate redox reactions between silver ions and stabilizers to stabilize the formation of silver nucleates from degradation [8]. Chemical synthesis can result in high AgNPs yield and ease of parametric customization, however, most reducing agents used can be toxic and have adverse effects [9, 10]. 'Green' chemistry could be applied to chemical synthesis by using

* Corresponding author: jason.d3@imail.sunway.edu.my